

INVESTIGATION OF THE EFFECT OF TURBULENCE ON ENTROPY
GENERATION IN TURBOMACHINERY

A THESIS SUBMITTED TO
THE GRADUATE SCHOOL OF NATURAL AND APPLIED SCIENCES
OF
MIDDLE EAST TECHNICAL UNIVERSITY

BY

ÖMER EMRE ORHAN

IN PARTIAL FULFILLMENT OF THE REQUIREMENTS
FOR
THE DEGREE OF DOCTOR OF PHILOSOPHY
IN
AEROSPACE ENGINEERING

JANUARY 2014

Approval of the thesis:

**INVESTIGATION OF THE EFFECT OF TURBULENCE ON ENTROPY
GENERATION IN TURBOMACHINERY**

submitted by **ÖMER EMRE ORHAN**, in partial fulfillment of the requirements for
the degree of **Doctor of Philosophy in Aerospace Engineering Department**,
Middle East Technical University by,

Prof. Dr. Canan ÖZGEN
Dean, Graduate School of **Natural and Applied Sciences**

Prof. Dr. Ozan TEKİNALP
Head of Department, **Aerospace Engineering**

Assoc. Prof. Dr. Oğuz UZOL
Supervisor, **Aerospace Engineering Dept., METU**

Examining Committee Members:

Prof. Dr. M. Cevdet ÇELENLİGİL
Aerospace Engineering Dept., METU

Assoc. Prof. Dr. Oğuz UZOL
Aerospace Engineering Dept., METU

Assoc. Prof. Dr. Dilek Funda KURTULUŞ
Aerospace Engineering Dept., METU

Assoc. Prof. Dr. Derek BAKER
Mechanical Engineering Dept., METU

Assist. Prof. Dr. Ayşe Gül GÜNGÖR
Astronautical Engineering Dept., ITU

Date: 27.01.2014

I hereby declare that all information in this document has been obtained and presented in accordance with academic rules and ethical conduct. I also declare that, as required by these rules and conduct, I have fully cited and referenced all material and results that are not original to this work.

Name, Last name : Ömer Emre ORHAN

Signature :

ABSTRACT

INVESTIGATION OF THE EFFECT OF TURBULENCE ON ENTROPY GENERATION IN TURBOMACHINERY

ORHAN, Ömer Emre

PhD, Department of Aerospace Engineering

Supervisor: Assoc. Prof. Dr. Oğuz UZOL

January 2014, 138 pages

The aim of this thesis is to apply a newly developed methodology to calculate entropy production. Entropy production calculations have always attracted attention due to its extreme importance in efficiency improvement. Efficiency improvement can be achieved via several optimization techniques and Entropy Generation Minimization (EGM) is one of the most acknowledged ones.

When it comes to the design and analysis of turbomachinery components, the performance deterioration due to various real flow effects such as secondary flows, profile losses or tip-leakage losses is generally represented through semi-empirical loss coefficients. Instead of relying on these coefficients one can use entropy generation rates as a consistent and quantitative measure of lost work due to irreversibilities, which can be calculated globally using the inlet and exit values of calculated pressures and temperatures of a system. However, if complete quantitative descriptions of velocity and temperature fields are available, one can compute field distributions of local viscous and thermal entropy generation rates by post-processing the available data.

Another way of calculating entropy generation is possible using the combination of entropy transport equation with the positive definite entropy generation equation. In this study, a new entropy transport equation has been developed with the turbulence models and calculated using commercial CFD software. This new equation has been

applied for the calculation of entropy generation around a gas turbine stator blade and the results have been compared with the results of the existing calculation methods.

Keywords: Entropy, turbulence, turbomachinery, efficiency, CFD

ÖZ

TURBOMAKİNALARDA ENTROPİ OLUŞUMUNA TÜRBÜLANS ETKİSİNİN İNCELENMESİ

ORHAN, Ömer Emre

Doktora, Havacılık ve Uzay Mühendisliği Bölümü

Tez Yöneticisi: Doç. Dr. Oğuz UZOL

Ocak 2014, 138 sayfa

Bu çalışmanın amacı, yeni geliştirilmiş olan entropi oluşum hesaplama yöntemini uygulamaktır. Entropi oluşum hesaplamaları, verimliliği arttırma üzerindeki çok önemli etkisi nedeniyle her zaman dikkat çekmiştir. Verimlilik iyileştirmesi, çeşitli yöntemlerle hesaplanabilir ve Entropi Oluşum Minimizasyonu (EOM) bunlar arasında en bilinenlerindedir.

Turbomakina parçalarının tasarım ve analizlerinde, ikincil akışlar, profil ve tip akım kayıpları şeklinde ortaya çıkan performans düşüşleri yarı-empirik kayıp katsayıları ile ifade edilmektedir. Bunlara güvenmek yerine, entropi oluşum hızları, sistemin hesaplanan giriş ve çıkış basınç ve sıcaklık değerleri ile tersinmezlikten kaynaklanan kayıp işin tutarlı ve nicel bir oranı olarak hesaplanabilir. Fakat, bütün sistem için hız ve sıcaklık verileri var ise, lokal viskoz ve termal entropi oluşum hızları, bu veriler kullanılarak hesaplanabilir.

Entropi oluşumunu hesaplamının bir diğer yöntemi ise entropi transport denklemi ile mutlak pozitif entropi oluşum denkleminin birleştirilmesidir. Bu çalışmada, türbülans modelleri eklenerek yeni bir entropi transport denklemi geliştirilmiş ve ticari bir HAD yazılımında uygulanmıştır. Bu yeni denklem, bir gaz türbini stator kanadı çevresindeki entropi oluşumunun hesaplanması için kullanılmış ve sonuçlar diğer hesaplama yöntemlerinin sonuçlarıyla karşılaştırılmıştır.

Anahtar Kelimeler: Entropi, türbülans, turbomakina, verimlilik, HAD

ACKNOWLEDGEMENTS

I would like to thank my advisor, Assoc. Prof. Dr. Oğuz UZOL, for all of his support during the thesis. Since we were logistically apart, it would not be possible to complete this thesis without his continuous support.

I am grateful to Dr. Philipp Schlatter from KTH Sweden. He provided his DNS data without question and helped me to understand and implement them for the results obtained here within.

I cannot forget the support that I got from Dr. Ayşe Gül Güngör from İTÜ in İstanbul. When I was confused with many questions on my mind, she was always there for a helping hand.

It was a privilege to visit and discuss some of the problems with Prof. Sciubba from University of Rome and his student Giorgio Giangaspero.

To Prof. Wyngaard who always answered my questions with patience from the other side of the world.

Thanks a lot to my dear friend Emre Öztürk from Anova Engineering for his support in the utilization of Ansys-Fluent.

Last but not the least, Gökhan Ahmet, Bayram Mercan, Özgün Güler and Cem Gözükar were always there when I needed a hand.

And to my family, their contribution to my improvement is invaluable.

TABLE OF CONTENTS

ABSTRACT	v
ÖZ.....	vii
ACKNOWLEDGEMENTS.....	ix
TABLE OF CONTENTS	x
LIST OF FIGURES	xiii
LIST OF SYMBOLS	xvi
 CHAPTERS	
1 INTRODUCTION	1
1.1 Literature Survey and Past Studies	2
1.2 Thesis Motivation and Objectives	5
1.3 Outline of Thesis.....	8
2 ENTROPY GENERATION MODELING.....	9
2.1 Formulization of Entropy Generation.....	9
2.2 The Clasius-Duhem Equality	14
2.3 Effects of Turbulence in Entropy Generation Modeling	15
2.4 Small Thermal Turbulence Assumption Based Modeling.....	16
2.4.1 Model equation for the velocity-entropy correlation $\overline{u_i' s'}$	17
2.4.2 Model equation for temperature fluctuation correlation $\overline{\frac{\partial}{\partial x_i} (\ln T)' \frac{\partial T'}{\partial x_i}}$	18
2.4.3 Model equation for temperature-entropy correlation $T' \frac{\partial s'}{\partial x_i}$	19

2.4.4 Model equation for velocity-temperature-entropy correlation	
$\overline{T' \frac{\partial (\rho u_i' s')}{\partial x_i}}$	20
2.5 Final Form of Entropy Generation Equation	20
3 A-PRIORI TESTING OF MODELS TO BE USED IN THE REYNOLDS AVERAGED ENTROPY TRANSPORT (RAET) EQUATION	25
3.1 Transport Equation Based Modeling of $\overline{u_i' T'^2}$, $\overline{u_i' T'}$ and $\overline{T'^2}$	25
3.1.1 Transport Equation for $\overline{u_i' T'^2}$	25
3.1.2 Transport Equation for $\overline{u_i' T'}$	29
3.1.3 Transport Equation for $\overline{T'^2}$	31
3.2 A-priori Testing Using Direct Numerical Simulation (DNS) Database	32
3.2.1 The DNS Database	32
3.2.2 Reduced Forms of the Model Equations for the Steady State Fully Developed Channel Flow	33
3.2.2.1 Equations for $\overline{u_i' T'^2}$	33
3.2.2.2 Equations for $\overline{u_i' T'}$	34
3.2.2.3 Equations for $\overline{T'^2}$	36
3.2.3 Results of A-priori Testing	37
3.2.3.1 Results for $\overline{u_i' T'^2}$	42
3.2.3.2 Results for $\overline{u_i' T'}$	55
3.2.3.3 Results for $\overline{T'^2}$	61
4 DIRECT AND APPROXIMATE LOCAL ENTROPY CALCULATION FOR A NON-ISOTHERMAL AXIAL TURBINE CASCADE	69
4.1 Cascade Geometry	69
4.2 Boundary Conditions	70
4.3 Results	74

4.3.1	Calculated Velocity and Pressure Field.....	74
4.3.2	Results About Entropy Generation.....	82
5	CONCLUSION AND FUTURE WORK.....	111
	REFERENCES.....	115
	APPENDICES	
A.	USER DEFINED FUNCTION (UDF) USED IN ANSYS FLUENT	123
	CURRICULUM VITAE.....	137

LIST OF FIGURES

FIGURES

Figure 2.1: Second law analysis for an unit volume[17].....	11
Figure 3.1: Schematic representation of the DNS channel flow taken from [28]	32
Figure 3.2: LHS vs. RHS of Eq (3.36) for $C_I=0.15$	38
Figure 3.3: LHS vs. RHS of Eq (3.36) for different values of C_I	39
Figure 3.4: LHS vs. RHS of Eq (3.37) for $C_I=0.15$	40
Figure 3.5: LHS vs. RHS of Eq (3.37) for different values of C_I	41
Figure 3.6: RHS of Eq (3.29) for default values of C_I	43
Figure 3.7: RHS of Eq (3.29) for different values of C_I	44
Figure 3.8: RHS of Eq (3.30) for default values of C_I C_2 and C_3	45
Figure 3.9: RHS of Eq (3.30) for different values of C_I keeping C_2 and C_3 constant....	46
Figure 3.10: RHS of Eq (3.30) for different values of C_2 keeping C_I and C_3 constant	47
Figure 3.11: LHS vs. RHS of Eq (3.38) for default values of C_{II}	49
Figure 3.12: LHS vs. RHS of Eq (3.38) for different values of C_{II}	50
Figure 3.13: LHS vs. RHS of Eq (3.38) for different values of C_{II}	51
Figure 3.14: LHS vs. RHS of Eq (3.39) for default value of C_{II}	52
Figure 3.15: LHS vs. RHS of Eq (3.39) for different values of C_{II}	53
Figure 3.16: RHS of Eq (3.32) for default values of C_6 C_7 and C_8	55
Figure 3.17: RHS of Eq (3.32) for default values of C_7 , C_8 and for $C_6=0.9$	56
Figure 3.18: RHS of Eq (3.32) for different values of C_7 and C_8 and $C_6=1.0$	57
Figure 3.19: RHS of Eq (3.33) for default values of C_7 and C_8	59
Figure 3.20: RHS of Eq (3.33) for different values of C_7 and for $C_8=3.5$	60

Figure 3.21: RHS of Eq (3.35) for default values of C_9 and C_{10}	62
Figure 3.22: RHS of Eq (3.35) for different values of C_9 and for $C_{10}=0.20$	63
Figure 3.23: RHS of Eq (3.35) for different values of C_{10} and for $C_9=4.00$	64
Figure 4.1: Two dimensional cascade geometry in meters	70
Figure 4.2: Boundary conditions applied to the stator blade.....	71
Figure 4.3: Overall view of the mesh generated.....	72
Figure 4.4: Mesh around the blade. upper: no BL, lower: with 20 levels of BL.....	72
Figure 4.5: Velocity profiles on a line at the wake region with respect to number of cells.....	73
Figure 4.6: Axial and vertical velocity contours around the stator blades	75
Figure 4.7: Velocity magnitude contours around the stator blades	76
Figure 4.8: Static pressure contours around the stator blades	77
Figure 4.9: Total pressure and temperature contours around the stator blades	78
Figure 4.10: Bejan number contours around the stator blade	80
Figure 4.11: Detailed view of Bejan number contours around the stator blade	81
Figure 4.12: Reynolds stress contours around the stator blades; $\overline{u'u'}$	84
Figure 4.13: Reynolds stress contours around the stator blades; $\overline{u'v'}$ and $\overline{v'v'}$ respectively	85
Figure 4.14: $\overline{u'T'}$ and $\overline{v'T'}$ contours around the stator blades	87
Figure 4.15: $\overline{T'^2}$ contours around the stator blades	88
Figure 4.16: $\overline{u'T'^2}$ and $\overline{v'T'^2}$ contours around the stator blades.....	89
Figure 4.17: Contours of $\overline{u'u'}$, $\overline{v'v'}$, $\overline{u'T'}$ and $\overline{T'^2}$	91
Figure 4.18: Contours of $\overline{u'v'}$, $\overline{v'T'}$, $\overline{u'T'^2}$ and $\overline{v'T'^2}$	92
Figure 4.19: Contours of $\overline{u'T'}$ and $\overline{v'T'}$ for default and a-priori coefficients	93
Figure 4.20: Contours of $\overline{T'^2}$, $\overline{u'T'^2}$ and $\overline{v'T'^2}$ for default and a-priori coefficients	94
Figure 4.21: Direct and approximate specific entropy contours	97

Figure 4.22: Direct and approximate source terms	98
Figure 4.23: Location of the wake line considered for comparison	99
Figure 4.24: Static pressure and velocity magnitude profiles along the wake line respectively	100
Figure 4.25: $\overline{T'^2}$, $\overline{u'T'}$ and $\overline{v'T'}$ profiles along the wake line respectively	101
Figure 4.26: $\overline{u'T'^2}$ and $\overline{v'T'^2}$ profiles along the wake line respectively	102
Figure 4.27: Specific entropies for direct and approximate solutions on the wake line	103
Figure 4.28: Nondimensional specific entropies for direct and approximate solutions on the wake line	105
Figure 4.29: Source terms for direct and approximate solutions on the wake line .	106
Figure 4.30: Nondimensional source terms for direct and approximate solutions on the wake line.....	107
Figure 4.31: Detailed contours of specific entropies for direct and approximate solutions around the wake line.	108

LIST OF SYMBOLS

\dot{S}_{gen}	entropy generation rate	$W/m^3 K$
Q	heat transfer	J
W	work	J
E	internal energy	J
\dot{m}	mass flow	kg/s
k	thermal conductivity,	$W/m K$
T	temperature	K
T'	fluctuating temperature	K
x	cartesian coordinate	m
u	velocity	m/s
s	specific entropy	$J/kg K$
F_i	flux	
k_t	turbulent thermal conductivity	$W/m K$
ρ	density	kg/m^3
u_i	instantaneous velocity	m/s
\bar{u}_i	mean velocity	m/s
u_i'	fluctuating velocity	m/s
P	pressure	Pa
μ	viscosity	$kg / (ms)$
φ	viscous dissipation	m^2/s^2
k	turbulent kinetic energy	m^2/s^2
τ_{ij}	stress tensor	Pa
C_v, C_p	specific heats	$J/kg K$
R	universal gas constant	$J/mol K$
$\overline{u_i' u_j'}$	Reynolds stress	m^2/s^2
$\overline{u_i' T'}$	Fluctuating velocity-temperature correlation	$m/s K$
$\overline{T'^2}$	Fluctuating temperature squared	K^2

$\overline{u_i' T'^2}$	Fluctuating velocity-temperature squared correlation	$m/s K^2$
δ_{ij}	Kronecker delta	
y^+	Nondimensional y coordinate	

CHAPTER 1

INTRODUCTION

“Entropy”, “Turbulence” and “Turbomachinery” are the three keywords that a researcher would be very cautious and maybe anxious when they appear all together in one sentence. However, at the same time, one can easily feel that they are extremely important and fundamental parameters, especially in the case of turbomachinery flows. This is due to the fact that entropy is considered to be the main cause of inefficiency and losses in thermodynamics; therefore a thorough understanding of entropy is needed to overcome the difficulty of achieving more efficient machines.

The main driver of this thesis comes from the idea of understanding this complex internally connected phenomenon of entropy and how it is affected by turbulence. This relation, when studied analytically with a theoretical background, will then be applied to specific problems, being a 2D turbomachinery flow around a gas turbine stator in this case. But before diving into the details of entropy, one has to understand what entropy is, which is described in the next section.

Equations and definitions about entropy have been discussed by many scientists and entropy is considered as a thermodynamic property of a system. This is later used to quantify the disorder which is closely related with the efficiency of a system. Increasing efficiency and/or decreasing the losses have always been a hot topic for scientists and engineers since efficiency-loss interaction is defining the performance of machines, especially for the turbomachines. Therefore, many studies have been conducted about entropy and turbulence in turbomachines. Some important and relevant studies about these subjects are summarized in the next section.

1.1 Literature Survey and Past Studies

Literature survey and past studies have been evaluated based on two main categories. The first one is related with calculation of entropy generation. Second category is related with turbulence related issues like Direct Numerical Simulations (DNS) to be used for a-priori testing and entropy turbulence entropy interactions.

There are various areas and subjects where entropy generation calculations have been conducted. *Erbay et al.* [33] investigated the two dimensional entropy generation between two parallel plates for a transient convective transfer whereas *Yapıcı et al.* [34] presented the local entropy generation for a suddenly expanding pipe. Both studies utilize the general descriptions of viscous and thermal entropy generations. In [35], Giangaspero and Sciubba, utilized the local entropy generation maps in order to design a LED-based spotlight. Ertesvåg and Kolbu [36], created an entropy production for a turbulent combustion case using CFD. *Naterer et al.* [37] [38], on the other hand, focused on the numerical and experimental aspects of entropy. In their study, Adeyinka and Naterer performed an experiment to measure the entropy production indirectly [39].

Entropy-turbulence interactions attracted attention of many researchers leading to several thesis studies. Among those, the one performed by Kramer-Bevan [24] is important due to its unique approach to turbulence-entropy formulations. In addition to Kramer-Bevan, Hauke [40] and Edward [41] from Stanford University, performed studies showing the importance of entropy in adequate formulation of turbulence.

Loss predictions in turbomachinery could be based on the direct solution of the entropy generation equation. The entropy production actually can be used as a performance parameter if it can be calculated accurately as a part of the flow solution. One of the first ideas of utilizing the so called Entropy Generation Minimization (EGM) technique was developed by Bejan [5]. Bejan indicates that EGM, in addition to the importance of the first law of thermodynamics, shall have an important role in the analysis of systems involving heat transfer and viscous

dissipation phenomena, which are dominant in turbomachinery flows demonstrating the necessity of entropy generation calculation. Bejan also in his study based on relationship between the constructal law and the design of biosphere [32] states that:

“...for a flow system to persist in in time (to live), it must evolve such that it provides easier and easier access to its currents.”

This definition is similar to what one is trying to achieve via EGM methodology.

In the design and analysis of turbomachinery components, the performance deterioration due to various real flow effects such as secondary flows, profile losses or tip-leakage losses is generally represented through semi-empirical loss coefficients. Instead of relying on these coefficients one can use entropy generation rates as a consistent and quantitative measure of lost work due to irreversibilities, which can be calculated globally using the inlet and exit values of calculated pressures and temperatures of a system. However, if complete quantitative descriptions of velocity and temperature fields are available, one can compute field distributions of local viscous and thermal entropy generation rates by post-processing the available data. One such example for an air-cooled gas turbine stator blade can be found in Natalini and Sciubba [6]. The effective loss of work or destruction of exergy (Sciubba [7]) is related to the entropy generation through the Gouy-Stodola theorem as explained in Bejan [5] and Natalini and Sciubba [6]. Sciubba has some more interesting studies related with the utilization of entropy generation in [30] and [31].

Drost and White [8] realized the lack of entropy generation applications to complex problems and pointed out that up to that time there was no integration of the entropy generation equations with the CFD codes. They emphasized that since no analytical formulations of local entropy generation in turbulent flows exist in open literature, that part of the calculation could not be benchmarked for turbulent flows. Kock and Herwig [9], calculated the entropy generation for a heated pipe. In their study, the entropy production mechanisms were divided into four different groups such as the ones due to mean and fluctuating velocity fields and heat flux. The study concluded

that the entropy production can be a parameter to define the efficiency of the system analyzed. McEligot *et al.* [10], on the other hand, performed a calculation of entropy production using the already available DNS data by Abe *et al.* [11] instead of using a CFD code. Their study was mainly concentrated on the near wall region where they compared two different approaches about pointwise calculation of entropy generation.

There are several studies available that applied entropy generation methodologies using CFD approach. Iandoli *et al.* [15] provides some practical examples for the application of entropy generation formulation to turbomachines. In their study thermal entropy generation contours around the stator blades and the hub have been calculated [15]. On the other hand, Alabi *et al.* [16] computed the entropy generation contours around the B747-200 aircraft. This shows that, the entropy generation can also be used to identify the performance on a more macroscopic level instead of a component level.

Entropy generation calculation as part of turbomachinery design is becoming an integral part of turbomachinery calculations like velocity and temperature fields due to the fact that it affects directly the efficiency. Schmitz *et al.* [42], performed a comparison of experimental results and calculations for an axial turbine blade and entropy contours form an important part of this study. Other studies involve the calculations around the supercritical compressor blades by Song [43], multistage flows around transonic gas turbine compressors by Culver [44], transient viscous flow calculations around a turbine stage by Shavalikul [45] and an experimental study about pressure exchange in supersonic flows by Bulusu [46].

It has been emphasized before that entropy and turbulence are closely correlated. In order to understand the details of this correlation; one also needs to go deeply into turbulence. Since complete understanding of turbulence is not possible, several closure strategies involving turbulence models are needed. In order to check the validity of turbulence models a-priori testing using DNS databases is widely used as reference.

Kawamura et al. has many channel flow studies involving DNS solutions for different Reynolds and Prandtl numbers [11] [47] [48] [49] [50] [51]. Another group of useful studies have been performed by *Moin et al.* both for the channel and flat plate cases [52] [53] [54] [55]. In addition, *Iwamoto et al* [56] and Brandt [57] and have similar studies like Kawamura and Moin. On top of DNS studies, Österlund [58] provides experimental results for turbulent boundary layer flow over a flat plate.

Since entropy-generation equation together with the turbulent effects involve some turbulent scalars, a review of studies about turbulent scalar evaluations has been performed. *Na et al* [59] presents the effect of Prandtl number on temperature fluctuations. Pasinato [60] utilized DNS to understand the physics beyond velocity-temperature fluctuations for channel and plane Couette flows. *Donzis et al* in [61] and [62] compare the scalar dissipation rate calculations with the experimental results.

All of the above mentioned studies reveal the importance of calculating the entropy generation as a performance parameter. However, all of them are based on a calculation that requires the solution of the velocity and temperature fields. Adeyinka and Naterer [12] proposed a more direct approach which involves including the Reynolds Averaged Entropy Transport equations, known as the Reynolds Averaged Clausius-Duhem equality, as a part of the solution process in turbulent flows. This technique of course involves a closure problem, similar to the closure of Reynolds stresses in the momentum equation, related to the calculation of mean entropy generation in terms of other mean flow quantities. A closure model was proposed by Adeyinka and Naterer [12] and tested in a turbulent channel flow between two parallel plates using Direct Numerical Simulation (DNS) data obtained by *Moser et al.* [13]. The findings of the study performed by Adeyinka and Naterer [12] are the main drivers of this thesis.

1.2 Thesis Motivation and Objectives

There are two main approaches of calculating the entropy field in general:

The first one can be considered to be a “global” approach such that only the inlet and exit values of mean pressures and temperatures of a system are used to estimate the amount of entropy change that occurs within the system [3]. This method is straightforward and very easy to implement since no additional information related to the flow variations or turbulence is needed.

The second approach is relatively more advanced such that it attempts to obtain the entropy field by integrating locally calculated viscous and thermal entropy generation rates through a transport equation as long as a complete quantitative description of the mean velocity and mean temperature fields is available. This second approach can be considered as a “direct” method and the related Reynolds-Averaged form of the entropy transport equation is first introduced by Adeyinka and Naterer [12]. The right-hand-side of the Reynolds Averaged Entropy Transport equation, which we will represent in short as the RAET equation from now on (and may appropriately be pronounced as “rate”) represents the rate of local entropy generation and involves many correlations related to the fluctuating temperature and velocity fields, which are difficult to model in general. However, an “approximate” solution may be obtained by disregarding all turbulence related terms on the right-hand-side and just keeping the terms related to the mean flow variations.

The potential of using the second approach as described above for better estimating the entropy field constitutes the main motivation for this study.

In this framework, one of the objectives of this thesis is to first apply and extend the entropy production modeling approach by Adeyinka and Naterer [12]. For this purpose, available models from existing literature on various turbulence-temperature correlations have been collected and adopted for modeling all necessary terms on the right-hand-side of the RAET equation. Therefore a complete closed differential equation set is generated that can be integrated in a coupled manner to obtain the mean entropy field. To the author’s knowledge, this is the first study that attempts to implement a model for each one of the turbulence related terms in the right-hand-side of the RAET equation and that comes up with a closed equation set, which can then

work together with a RANS solver. For testing the prediction performance of the implemented models for the turbulence-temperature correlations, Direct Numerical Simulation (DNS) data for a non-isothermal fully developed channel flow are used (Schlatter [14]).

A second objective of the thesis is to develop a working methodology to obtain a solution to the entropy field through the RAET equation system as described above. This of course involves the utilization of a RANS solver, the converged results of which can be used as an input background flow field to solve the RAET equation system. For a steady-state problem, the implementation involves first obtaining a converged solution for the mean flow field by solving RANS equations together with an appropriate turbulence model and then integrating the RAET equation system using the data from the converged mean flow field. If all turbulence related terms in the RAET equation are to be included in the solution through appropriate models, the calculation for the entropy field involves the solution of six coupled transport equations in total.

A third objective of the current study is to apply the developed methodology to a non-isothermal turbomachinery flow field simulation to investigate the differences in the predicted entropy fields with and without the effects of turbulence. For this purpose the axial turbine cascade geometry of Natalini and Sciubba [6] is used and various comparisons are performed as presented in detail in this thesis.

1.3 Outline of Thesis

In Chapter 2, the governing entropy transport equations are developed. First the relationship between the available work and entropy generation is defined using the Gouy-Stodola theorem. Then the general entropy generation equation is derived including the thermal and viscous parts. This equation is combined later with the entropy transport equation and turbulence effects are considered after Reynolds averaging is applied.

Chapter 3 concentrates on the a-priori testing of the models for turbulence-temperature correlations appearing in the right-hand-side of the RAET equation. Model equations for parameters such as, $\overline{u_i'T'^2}$, $\overline{u_i'T'}$ and $\overline{(T')^2}$ are formed to be utilized in the RAET equation and these model equations are evaluated based on the DNS data available.

The methodology developed in Chapter 2 and 3 is applied to the two dimensional cascade problem given in Natalini and Sciubba [6] and the results are presented in Chapter 4.

The study is finalized with the conclusions and comments about future work which are given in Chapter 5.

CHAPTER 2

ENTROPY GENERATION MODELING

In order to cope with Entropy Generation Minimization (EGM), first entropy generation shall be understood. About the close interaction between entropy generation and lost available work Bejan states that [17]:

“Unlike lost available work, which is subject to convention, the entropy generation S_{gen} depends solely on the degree of thermodynamic irreversibility of the system. If engineering systems and their components are to operate such that the destruction of available work is minimized, then the design of such systems and components must begin with the minimization of entropy generation.”

In this section, first the relationship between the available work and entropy generation is defined using the Gouy-Stodola theorem. This theorem is named after the two famous scientists, Gouy [18] and Stodola [19]. Then the general entropy generation equation is derived including the thermal and viscous parts. This equation is combined later with the entropy transport equation and turbulence effects are considered after Reynolds averaging is applied.

2.1 Formulization of Entropy Generation

According to Gouy-Stodola theorem, the relationship between the lost available work and the entropy generation is defined by [17]:

$$\dot{W}_{lost} = T \dot{S}_{gen} \quad (2.1)$$

where T is the absolute temperature of the environment in Kelvin.

As a result of this theorem, lost available work is directly proportional to the entropy generation and is responsible for the inequality sign in the second law of thermodynamics. It also defines the level of irreversibility of a system has and the more irreversible the process, the more it is shifted away from equality.

On the other hand, entropy generation is as well connected with the entropy transport equation with the following equation [20]:

$$\frac{\partial S}{\partial t} + \frac{\partial F_i}{\partial x_i} \equiv \dot{S}_{gen} \geq 0 \quad (2.2)$$

where

$S = \rho s$ is the volumetric entropy, s is the specific entropy of a state.

Entropy flux, F_i can be defined as:

$$F_i = \rho u_i s + \frac{q_i}{T} \quad (2.3)$$

with u_i and q_i being the velocity and heat flux components in the corresponding direction, respectively.

The only remaining part of Eq. (2.2) that is not detailed is the entropy generation term on the right-hand-side (RHS). This term is generally resolved into the thermal and viscous parts through a second law analysis of a unit volume as shown in Figure 2.1.

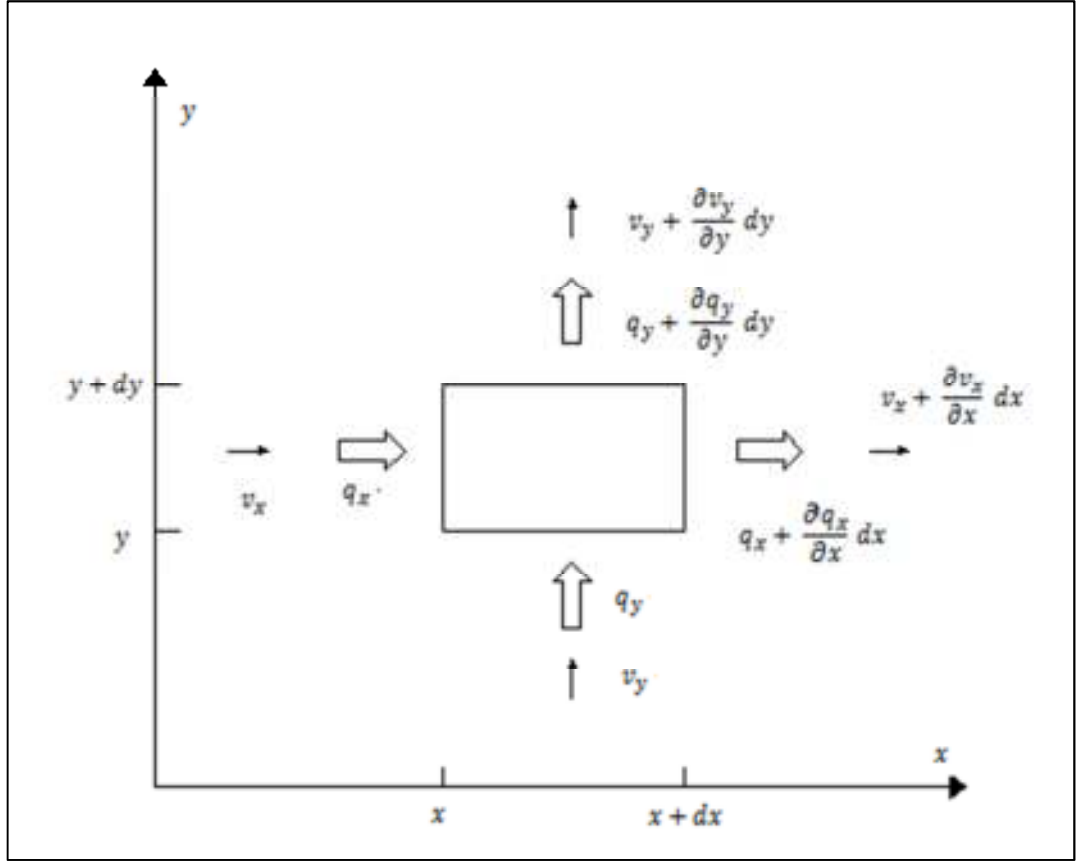


Figure 2.1 Second law analysis for an unit volume [17].

Writing the input-output balance for the RHS of Eq. (2.2) for the unit volume given above yields [17]:

$$\begin{aligned}
 S_{gen} dx dy = & \frac{q_x + \frac{\partial q_x}{\partial x} dx}{T + \frac{\partial T}{\partial x} dx} dy + \frac{q_y + \frac{\partial q_y}{\partial y} dy}{T + \frac{\partial T}{\partial y} dy} dx - \frac{q_x}{T} dy - \frac{q_y}{T} dx + \left(s + \frac{\partial s}{\partial x} dx \right) \left(v_x + \right. \\
 & \left. \frac{\partial v_x}{\partial x} dx \right) \left(\rho + \frac{\partial \rho}{\partial x} dx \right) dy + \left(s + \frac{\partial s}{\partial y} dy \right) \left(v_y + \frac{\partial v_y}{\partial y} dy \right) \left(\rho + \frac{\partial \rho}{\partial y} dy \right) dx - \\
 & s v_x \rho dy - s v_y \rho dx + \frac{\partial(\rho s)}{\partial t} dx dy
 \end{aligned} \tag{2.4}$$

In Eq. (2.4), the first four terms on the RHS are entropy generation terms related with heat transfer; the next four terms are entropy terms which represent the net convection of entropy into the system and the last one is the time rate of entropy

generated inside the control volume.

Rearranging some of the terms and dividing by $dxdy$ gives [17]:

$$S_{gen} \dot{=} \frac{1}{T} \left(\frac{\partial q_x}{\partial x} + \frac{\partial q_y}{\partial y} \right) - \frac{1}{T^2} \left(q_x \frac{\partial T}{\partial x} + q_y \frac{\partial T}{\partial y} \right) + \rho \left(\frac{\partial s}{\partial t} + v_x \frac{\partial s}{\partial x} + v_y \frac{\partial s}{\partial y} \right) + s \left[\frac{\partial \rho}{\partial t} + v_x \frac{\partial \rho}{\partial x} + v_y \frac{\partial \rho}{\partial y} + \rho \left(\frac{\partial v_x}{\partial x} + \frac{\partial v_y}{\partial y} \right) \right] \quad (2.5)$$

Assuming that the flow is incompressible makes the terms in square brackets zero. Eq. (2.5) can be rearranged in order to obtain a more compact form [17]:

$$S_{gen} \dot{=} \frac{1}{T} \nabla q - \frac{1}{T^2} q \nabla T + \rho \frac{Ds}{Dt} \quad (2.6)$$

where $\frac{Ds}{Dt}$ is the substantial derivative of s .

Another way of writing the differential entropy is the Gibbs equation [21]:

$$Tds = de + P d\left(\frac{1}{\rho}\right) \quad (2.7)$$

Since Eq. (2.6) involves the substantial derivative of the entropy, Eq. (2.7) can be converted to the substantial derivative form such as [17]:

$$\rho \frac{Ds}{Dt} = \frac{\rho}{T} \frac{De}{Dt} - \frac{P}{\rho T} \frac{D\rho}{Dt} \quad (2.8)$$

The only remaining unknown is the substantial form of the internal energy, $\rho \frac{De}{Dt}$ which is possible through first law of thermodynamics [17]:

$$\rho \frac{De}{Dt} = -\nabla q - P (\nabla \cdot \mathbf{v}) + \mu \varphi \quad (2.9)$$

where μ and φ are the viscosity and the viscous dissipation function, respectively.

Inserting Eq. (2.9) into Eq. (2.8) and then combining the result with Eq. (2.6) gives:

$$S_{gen} = -\frac{1}{T^2} q \nabla T + \frac{\mu}{T} \varphi \quad (2.10)$$

If Fourier law of conduction is applied for q which is:

$$q = -k \nabla T \quad (2.11)$$

where k is the thermal conductivity of the medium applied, then the final form of the entropy generation equation can be obtained as:

$$S_{gen} = \frac{k}{T^2} (\nabla T)^2 + \frac{\mu}{T} \varphi \quad (2.12)$$

Tensor form of Eq. (2.12) could be needed as well for simplicity of presentation during Reynolds averaging:

$$S_{gen} = \frac{k}{T^2} \left(\frac{\partial T}{\partial x_i} \right)^2 + \frac{\tau_{ij}}{T} \frac{\partial u_i}{\partial x_j} \quad (2.13)$$

where the viscous stress, τ_{ij} is given as [20]:

$$\tau_{ij} = \mu \left[\left(\frac{\partial u_i}{\partial x_j} + \frac{\partial u_j}{\partial x_i} \right) - \frac{2}{3} \frac{\partial u_k}{\partial x_k} \delta_{ij} \right] \quad (2.14)$$

and δ_{ij} is the Kronecker delta that turns the viscous dissipation, φ into:

$$\varphi = \frac{\partial u_i}{\partial x_j} \left[\left(\frac{\partial u_i}{\partial x_j} + \frac{\partial u_j}{\partial x_i} \right) - \frac{2}{3} \frac{\partial u_k}{\partial x_k} \delta_{ij} \right] \quad (2.15)$$

One important feature of Eq. (2.12) is being positive definite meaning that if temperature and velocity gradients exist inside the medium, the result will always be finite and positive. Therefore, it is also called “*positive definite*” form of entropy

generation equation.

At this point, Eq. (2.2) is re-written by combining above results into an overall entropy transport equation that is valid for incompressible flows:

$$\frac{\partial(\rho s)}{\partial t} + \frac{\partial}{\partial x_i} \left(\rho u_i s - \frac{k}{T} \frac{\partial T}{\partial x_i} \right) = \frac{k}{T^2} \left(\frac{\partial T}{\partial x_i} \right)^2 + \frac{\mu}{T} \frac{\partial u_i}{\partial x_j} \left(\frac{\partial u_i}{\partial x_j} + \frac{\partial u_j}{\partial x_i} \right) \quad (2.16)$$

2.2 The Clausius-Duhem Equality

Eq. (2.16) is a general expression for instantaneous entropy generation and transport in incompressible flows. In order to consider the effects of turbulence, Reynolds averaging of this equation can be performed inserting the mean and fluctuating parts for each term to give [20]:

$$\begin{aligned} \frac{\partial(\rho(s+s'))}{\partial t} + \frac{\partial}{\partial x_i} (\rho(u_i + u_i')(s + s')) - \frac{k}{T} \frac{\partial(T+T')}{\partial x_i} = \\ \frac{k}{T^2} \left(\frac{\partial(T+T')}{\partial x_i} \right)^2 + \frac{(\tau_{ij} + \tau_{ij}')}{T} \frac{\partial(u_i + u_i')}{\partial x_j} \end{aligned} \quad (2.17)$$

Taking the Reynolds average of all the terms:

$$\frac{\partial(\overline{\rho(s+s')})}{\partial t} + \frac{\partial}{\partial x_i} (\overline{\rho(u_i + u_i')(s + s')}) - \frac{k}{T} \frac{\partial(\overline{T+T'})}{\partial x_i} = \frac{k}{T^2} \overline{\left(\frac{\partial(T+T')}{\partial x_i} \right)^2} + \frac{\overline{(\tau_{ij} + \tau_{ij}')}}{T} \frac{\partial(\overline{u_i + u_i'})}{\partial x_j} \quad (2.18)$$

As a result of Reynolds averaging, average of a fluctuating component and average of the product of a fluctuating component with a mean component are zero such as [22]:

$$\overline{s'} = 0 \text{ and } \overline{s' \bar{s}} = 0 \quad (2.19)$$

Following the principles of Eq. (2.19), Eq. (2.18) can be rearranged as [23]:

$$\frac{\partial(\rho\bar{s})}{\partial t} + \frac{\partial}{\partial x_i} \left(\rho\bar{u}_i\bar{s} + \overline{\rho u_i' s'} - \frac{\bar{k}}{T} \frac{\partial \bar{T}}{\partial x_i} \right) = \overline{\frac{k}{T^2} \left(\frac{\partial T}{\partial x_i} \right)^2} + \overline{\frac{\tau_{ij}}{T} \frac{\partial u_i}{\partial x_j}} \quad (2.20)$$

This equation is called the Clausius-Duhem equality. It is considered to be highly complex due to the modeling effort that would be needed for various correlations related to velocity, temperature and entropy fluctuations, which would appear after a decomposition of the equation. Following sections focus on such an effort.

2.3 Effects of Turbulence in Entropy Generation Modeling

In this section, modeling of turbulence related terms appearing in the entropy generation is discussed.

If the left hand side of Eq. (2.13) is multiplied by T we obtain,

$$T \dot{S}_{gen} = \frac{k}{T} \left(\frac{\partial T}{\partial x_i} \right)^2 + \tau_{ij} \frac{\partial u_i}{\partial x_j} \quad (2.21)$$

After decomposition, Reynolds averaging and few other manipulations as detailed in [24], this equation can be converted to:

$$\bar{T} \overline{\dot{S}_{gen}} + \overline{T' \dot{S}_{gen}'} = k \frac{\partial}{\partial x_i} (\overline{\ln T}) \frac{\partial \bar{T}}{\partial x_i} + k \frac{\partial}{\partial x_i} (\overline{\ln T})' \frac{\partial T'}{\partial x_i} + \overline{\tau_{ij}} \frac{\partial \bar{u}_i}{\partial x_j} + \overline{\tau_{ij}'} \frac{\partial u_i'}{\partial x_j} \quad (2.22)$$

In order to obtain the correlation for $\overline{T' \dot{S}_{gen}'}$, Eq. (2.2) can be multiplied by T and then time averaged to give [20]:

$$\begin{aligned} \bar{T} \overline{\dot{S}_{gen}} + \overline{T' \dot{S}_{gen}'} &= \bar{T} \left[\frac{\partial(\rho\bar{s})}{\partial t} + \frac{\partial}{\partial x_i} \left(\rho\bar{u}_i\bar{s} + \overline{\rho u_i' s'} - \frac{\bar{k}}{T} \frac{\partial \bar{T}}{\partial x_i} \right) \right] + \overline{T' \frac{\partial}{\partial x_i} (\rho u_i' \bar{s})} + \\ &\overline{T' \frac{\partial}{\partial x_i} (\rho \bar{u}_i s')} + \overline{T' \frac{\partial}{\partial x_i} (\rho u_i' s')} + k \frac{\partial}{\partial x_i} (\overline{\ln T})' \frac{\partial T'}{\partial x_i} \end{aligned} \quad (2.23)$$

If Eq. (2.20) is as well multiplied with T , Reynolds-averaged and then subtracted from Eq. (2.23), correlation equation for $\overline{T' \dot{S}_{gen}'}$ is obtained:

$$\overline{T' \dot{S}_{gen}'} = \overline{T' \frac{\partial}{\partial x_i} (\rho u_i' \bar{s})} + \overline{T' \frac{\partial}{\partial x_i} (\rho \bar{u}_i s')} + \overline{T' \frac{\partial}{\partial x_i} (\rho u_i' s')} - \overline{kT' \frac{\partial}{\partial x_i} (\ln T)} \quad (2.24)$$

Rearranging Eq. (2.24) using chain rule of calculus and incompressible flow assumption gives [20]:

$$\overline{T' \dot{S}_{gen}'} = \rho \overline{T' u_i'} \frac{\partial \bar{s}}{\partial x_i} + \rho \bar{u}_i \overline{T' \frac{\partial s'}{\partial x_i}} + \overline{T' \frac{\partial (\rho u_i' s')}{\partial x_i}} + \overline{kT' \frac{\partial}{\partial x_i} (\ln T)} \quad (2.25)$$

This equation is the new model equation for $\overline{T' \dot{S}_{gen}'}$, which will be useful for the consideration of effects of turbulence in the entropy generation equation.

Overall mean entropy generation equation including the effects of turbulence can be obtained combining Eq.(2.20), Eq.(2.22) and Eq.(2.25) to give [20]:

$$\begin{aligned} \bar{T} \overline{\dot{S}_{gen}} &= \bar{T} \left[\frac{\partial (\rho \bar{s})}{\partial t} + \frac{\partial}{\partial x_i} \left(\rho \bar{u}_i \bar{s} + \rho \overline{u_i' s'} - \frac{k}{T} \frac{\partial \bar{T}}{\partial x_i} \right) \right] = k \frac{\partial}{\partial x_i} (\overline{\ln T}) \frac{\partial \bar{T}}{\partial x_i} + \\ &k \frac{\partial}{\partial x_i} (\overline{\ln T})' \frac{\partial T'}{\partial x_i} + \bar{\tau}_{ij} \frac{\partial \bar{u}_i}{\partial x_j} + \overline{\tau_{ij}' \frac{\partial u_i'}{\partial x_j}} - \left(\rho \overline{T' u_i'} \frac{\partial \bar{s}}{\partial x_i} + \rho \bar{u}_i \overline{T' \frac{\partial s'}{\partial x_i}} + \overline{T' \frac{\partial (\rho u_i' s')}{\partial x_i}} + \right. \\ &\left. \overline{kT' \frac{\partial}{\partial x_i} (\ln T)} \right) \end{aligned} \quad (2.26)$$

2.4 Small Thermal Turbulence Assumption Based Modeling

Eq. (2.26) involves terms like $\overline{u_i' s'}$ and $\frac{\partial}{\partial x_i} (\overline{\ln T})$ that need modeling. For this purpose, a model developed by Kramer-Bevan [24] is implemented. This model is based on a very important assumption, which is called the ‘‘Small Thermal Turbulence Assumption (STTA)’’. This assumption states that the fluctuating component of temperature is small compared to the mean component.

Each term at the RHS of Eq. (2.26) will be treated separately and Eq. (2.26) will be

converted into a more useful form as discussed in the following section.

2.4.1 Model equation for the velocity-entropy correlation $\overline{u_i' s'}$

Kramer-Bevan [24] developed a model for the velocity-entropy correlation following the state equation of entropy for an ideal gas:

$$s = s_0 + \int_{T_0}^T C_v \frac{dT}{T} - \int_{\rho_0}^{\rho} R \frac{d\rho}{\rho} = s_0 + C_v \ln \frac{T}{T_0} - R \ln \frac{\rho}{\rho_0} \quad (2.27)$$

If Eq. (2.27) is time averaged:

$$\bar{s} = \bar{s}_0 + C_v \overline{\ln \frac{T}{T_0}} - R \overline{\ln \frac{\rho}{\rho_0}} \quad (2.28)$$

In order to obtain a model for $\ln T$ term, $\ln T$ can be expressed using a Taylor series expansion around the point $\frac{T'}{\bar{T}} = 0$ leading to [24]:

$$\ln T = \ln \bar{T} + \ln \left(1 + \frac{T'}{\bar{T}} \right) = \ln \bar{T} + \frac{T'}{\bar{T}} - \frac{1}{2} \left(\frac{T'}{\bar{T}} \right)^2 + \dots \quad (2.29)$$

If the higher order terms are neglected and time averaged Eq. (2.29) reduces to;

$$\overline{\ln T} = \overline{\ln \bar{T} + \frac{T'}{\bar{T}}} = \ln \bar{T} \quad (2.30)$$

If this derivation is substituted into Eq. (2.28);

$$\bar{s} = \bar{s}_0 + C_v \ln \frac{\bar{T}}{T_0} - R \ln \frac{\bar{\rho}}{\rho_0} \quad (2.31)$$

If this is subtracted from the instantaneous value to give;

$$s' = s - \bar{s}_0 = s_0 + C_v \ln \frac{T}{T_0} - R \ln \frac{\rho}{\rho_0} - (s_0 + C_v \ln \frac{\bar{T}}{T_0} - R \ln \frac{\bar{\rho}}{\rho_0}) \quad (2.32)$$

$$s' = C_v \ln \frac{T}{\bar{T}} - R \ln \frac{\rho}{\bar{\rho}} = C_v \ln \left(1 + \frac{T'}{\bar{T}} \right) - R \ln \left(1 + \frac{\rho'}{\bar{\rho}} \right) \quad (2.33)$$

Final form of the entropy-velocity correlation is;

$$s' = C_v \frac{T'}{\bar{T}} - R \frac{\rho'}{\bar{\rho}} \quad (2.34)$$

If this new correlation is used in the $\overline{u_i' s'}$ term neglecting the density effects assuming incompressible flow;

$$\overline{u_i' s'} = \frac{C_v}{\bar{T}} \overline{u_i' T'} \quad (2.35)$$

Eq. (2.35) is the new model equation for the velocity-entropy correlation based on STTA.

2.4.2 Model equation for temperature fluctuation correlation $\overline{\frac{\partial}{\partial x_i} (\ln T)' \frac{\partial T'}{\partial x_i}}$

The model equation for $\overline{\frac{\partial}{\partial x_i} (\ln T)' \frac{\partial T'}{\partial x_i}}$ can be obtained using the STTA as well. Using the chain rule of Calculus [24]:

$$\overline{\frac{\partial}{\partial x_i} (\ln T)' \frac{\partial T'}{\partial x_i}} = \frac{1}{\bar{T}} \overline{\frac{\partial T'}{\partial x_i} \frac{\partial T'}{\partial x_i}} + \frac{\partial}{\partial x_i} \left(\frac{1}{\bar{T}} \right) T' \frac{\partial T'}{\partial x_i} \quad (2.36)$$

This equation can be manipulated to give:

$$\overline{\frac{\partial}{\partial x_i} (\ln T)' \frac{\partial T'}{\partial x_i}} = \frac{1}{\bar{T}} \overline{\left(\frac{\partial T'}{\partial x_i} \right)^2} + \frac{\partial}{\partial x_i} \left(\frac{1}{\bar{T}} \right) \frac{1}{2} \overline{\frac{\partial (T'^2)}{\partial x_i}} \quad (2.37)$$

The final form can be written as:

$$\overline{\frac{\partial}{\partial x_i} (\ln T)' \frac{\partial T'}{\partial x_i}} = \frac{1}{\bar{T}} \overline{\left(\frac{\partial T'}{\partial x_i} \right)^2} + \frac{\partial}{\partial x_i} \left(\frac{1}{\bar{T}} \right) \frac{1}{2} \overline{\frac{\partial (T'^2)}{\partial x_i}} \quad (2.38)$$

where

$$\overline{\left(\frac{\partial T'}{\partial x_i}\right)^2} = \frac{1}{2} \frac{\partial}{\partial x_i} \left[\frac{1}{\alpha} \overline{u_i' T'^2} - \frac{\partial \overline{(T'^2)}}{\partial x_i} \right] - \frac{1}{\alpha} \overline{u_i' T'} \frac{\partial \bar{T}}{\partial x_i} - \frac{1}{2\alpha} \bar{u}_i \frac{\partial \overline{(T'^2)}}{\partial x_i} \quad (2.39)$$

and α is the thermal diffusivity [22].

This final form given in Eq. (2.38) will be utilized in the final form of the entropy generation equation.

2.4.3 Model equation for temperature-entropy correlation $\overline{T' \frac{\partial s'}{\partial x_i}}$

Following the STT assumption, $\overline{T' \frac{\partial s'}{\partial x_i}}$ term can be rewritten using Eq. (2.34);

$$T' \frac{\partial s'}{\partial x_i} \cong T' \frac{\partial}{\partial x_i} \left(C_v \frac{T'}{\bar{T}} \right) \quad (2.40)$$

Using the chain rule of Calculus;

$$T' \frac{\partial}{\partial x_i} \left(C_v \frac{T'}{\bar{T}} \right) = C_v (T')^2 \frac{\partial}{\partial x_i} \left(\frac{1}{\bar{T}} \right) + \frac{C_v}{\bar{T}} \left(T' \frac{\partial T'}{\partial x_i} \right) \quad (2.41)$$

When the time averaging is applied;

$$\overline{T' \frac{\partial s'}{\partial x_i}} \cong C_v \overline{(T')^2} \frac{\partial}{\partial x_i} \left(\frac{1}{\bar{T}} \right) + \frac{C_v}{2\bar{T}} \left(\overline{\frac{\partial (T'^2)}{\partial x_i}} \right) \quad (2.42)$$

This form of $\overline{T' \frac{\partial s'}{\partial x_i}}$ will be used in the final form of the entropy generation equation.

2.4.4 Model equation for velocity-temperature-entropy correlation $\overline{T' \frac{\partial (\rho u_i' s')}{\partial x_i}}$

Following the STT assumption, $T' \frac{\partial (\rho u_i' s')}{\partial x_i}$ can be presented using Eq. (2.34) as;

$$T' \frac{\partial (\rho u_i' s')}{\partial x_i} \cong T' \frac{\partial}{\partial x_i} \left(\rho C_v \frac{T'}{\bar{T}} u_i' \right) \quad (2.43)$$

Using the chain rule of Calculus;

$$T' \frac{\partial}{\partial x_i} \left(\rho C_v \frac{T'}{\bar{T}} u_i' \right) = \rho C_v u_i' (T')^2 \frac{\partial}{\partial x_i} \left(\frac{1}{\bar{T}} \right) + \rho C_v \frac{T'}{\bar{T}} \frac{\partial}{\partial x_i} (u_i' T') \quad (2.44)$$

The final term of Eq. (2.44) can be rearranged as;

$$T' \frac{\partial}{\partial x_i} (u_i' T') = T' \left(T' \frac{\partial u_i'}{\partial x_i} + u_i' \frac{\partial T'}{\partial x_i} \right) \quad (2.45)$$

The first term in the parenthesis, $\frac{\partial u_i'}{\partial x_i}$ is zero due to continuity which gives;

$$T' \frac{\partial}{\partial x_i} (u_i' T') = \frac{1}{2} \frac{\partial (u_i' T'^2)}{\partial x_i} \quad (2.46)$$

Substituting this into Eq. (2.44) and Reynolds averaging gives the final form of the

$T' \frac{\partial (\rho u_i' s')}{\partial x_i}$ term;

$$\overline{T' \frac{\partial (\rho u_i' s')}{\partial x_i}} \cong \rho C_v \overline{u_i' (T')^2} \frac{\partial}{\partial x_i} \left(\frac{1}{\bar{T}} \right) + \frac{\rho C_v}{2\bar{T}} \frac{\partial \overline{(u_i' T'^2)}}{\partial x_i} \quad (2.47)$$

2.5 Final Form of Entropy Generation Equation

In Section 2.3, turbulence contribution to entropy generation was obtained as;

$$\overline{T' \dot{S}_{gen}} = \rho \overline{T' u_i'} \frac{\partial \bar{s}}{\partial x_i} + \rho \overline{u_i} \overline{T' \frac{\partial s'}{\partial x_i}} + \overline{T' \frac{\partial(\rho u_i' s')}{\partial x_i}} + \overline{k T' \frac{\partial}{\partial x_i} (\ln T)} \quad (2.25)$$

If the results of Section 2.4.1 to 2.4.4 are combined to give;

$$\begin{aligned} \overline{T' \dot{S}_{gen}} &= \rho \overline{T' u_i'} \frac{\partial \bar{s}}{\partial x_i} + \rho \overline{u_i} C_v \overline{(T')^2} \frac{\partial}{\partial x_i} \left(\frac{1}{\bar{T}} \right) + \frac{C_v}{2\bar{T}} \left(\frac{\partial \overline{(T'^2)}}{\partial x_i} \right) + \rho C_v \overline{u_i' (T')^2} \frac{\partial}{\partial x_i} \left(\frac{1}{\bar{T}} \right) + \\ &\frac{\rho C_v}{2\bar{T}} \frac{\partial \overline{(u_i' T'^2)}}{\partial x_i} \end{aligned} \quad (2.48)$$

The last term in Eq. (2.25) is zero since;

$$\overline{T' \frac{\partial}{\partial x_i} (\ln T)} = \overline{T' \frac{\partial}{\partial x_i} (\ln \bar{T})} = 0 \quad (2.49)$$

If Eq. (2.22) is recalled;

$$\overline{\dot{S}_{gen}} + \overline{T' \dot{S}_{gen}} = k \frac{\partial}{\partial x_i} \overline{(\ln T)} \frac{\partial \bar{T}}{\partial x_i} + k \frac{\partial}{\partial x_i} \overline{(\ln T)'} \frac{\partial T'}{\partial x_i} + \overline{\tau_{ij}} \frac{\partial \overline{u_i}}{\partial x_j} + \overline{\tau_{ij}'} \frac{\partial u_i'}{\partial x_j} \quad (2.22)$$

Revised form of the entropy generation equation including the effects of turbulence can then be obtained after subtracting Eq. (2.48) from Eq. (2.22) and then divided by \bar{T} ;

$$\begin{aligned} \overline{\dot{S}_{gen}} &= \frac{k}{\bar{T}} \frac{\partial}{\partial x_i} \overline{(\ln T)} \frac{\partial \bar{T}}{\partial x_i} + \frac{k}{\bar{T}} \frac{\partial}{\partial x_i} \overline{(\ln T)'} \frac{\partial T'}{\partial x_i} + \frac{\overline{\tau_{ij}}}{\bar{T}} \frac{\partial \overline{u_i}}{\partial x_j} + \frac{1}{\bar{T}} \overline{\tau_{ij}'} \frac{\partial u_i'}{\partial x_j} - \left(\frac{\rho}{\bar{T}} \overline{T' u_i'} \frac{\partial \bar{s}}{\partial x_i} \right) - \\ &\frac{\rho C_v}{\bar{T}} \overline{u_i} \overline{(T')^2} \frac{\partial}{\partial x_i} \left(\frac{1}{\bar{T}} \right) - \frac{C_v}{2\bar{T}^2} \overline{u_i} \left(\frac{\partial \overline{(T'^2)}}{\partial x_i} \right) - \frac{\rho C_v}{\bar{T}} \overline{u_i' (T')^2} \frac{\partial}{\partial x_i} \left(\frac{1}{\bar{T}} \right) - \frac{\rho C_v}{2\bar{T}^2} \frac{\partial \overline{(u_i' T'^2)}}{\partial x_i} \end{aligned} \quad (2.50)$$

Keeping in mind the entropy generation equation is also given in Eq. (2.20);

$$\overline{\dot{S}_{gen}} = \frac{\partial(\rho \bar{s})}{\partial t} + \frac{\partial}{\partial x_i} \left(\rho \overline{u_i} \bar{s} + \rho \overline{u_i' s'} - \frac{k}{\bar{T}} \frac{\partial \bar{T}}{\partial x_i} \right) = \frac{k}{\bar{T}^2} \left(\frac{\partial \bar{T}}{\partial x_i} \right)^2 + \frac{\overline{\tau_{ij}}}{\bar{T}} \frac{\partial \overline{u_i}}{\partial x_j} \quad (2.20)$$

If the left hand sides of Eq. (2.50) and Eq. (2.20) are combined;

$$\begin{aligned}
\frac{\partial(\rho\bar{s})}{\partial t} + \frac{\partial}{\partial x_i} \left(\rho\bar{u}_i\bar{s} + \rho\overline{u_i' s'} - \frac{k}{\bar{T}} \frac{\partial\bar{T}}{\partial x_i} \right) &= \frac{k}{\bar{T}} \frac{\partial}{\partial x_i} (\overline{\ln T}) \frac{\partial\bar{T}}{\partial x_i} + \frac{k}{\bar{T}} \frac{\partial}{\partial x_i} (\overline{\ln T})' \frac{\partial\bar{T}'}{\partial x_i} + \frac{\bar{\tau}_{ij}}{\bar{T}} \frac{\partial\bar{u}_i}{\partial x_j} + \\
\frac{1}{\bar{T}} \overline{\tau_{ij}' \frac{\partial u_i'}{\partial x_j}} - \left(\frac{\rho}{\bar{T}} \overline{T' u_i'} \frac{\partial\bar{s}}{\partial x_i} \right) - \frac{\rho C_v}{\bar{T}} \bar{u}_i \overline{(T')^2} \frac{\partial}{\partial x_i} \left(\frac{1}{\bar{T}} \right) - \frac{C_v}{2\bar{T}^2} \left(\frac{\partial(\overline{T'^2})}{\partial x_i} \right) - \\
\frac{\rho C_v}{\bar{T}} \overline{u_i' (T')^2} \frac{\partial}{\partial x_i} \left(\frac{1}{\bar{T}} \right) - \frac{\rho C_v}{2\bar{T}^2} \frac{\partial(\overline{u_i' T'^2})}{\partial x_i} & \quad (2.51)
\end{aligned}$$

In the meantime, for an arbitrary scalar, ϕ_k , a general transport equation can be written as [29],

$$\frac{\partial(\rho\phi_k)}{\partial t} + \frac{\partial}{\partial x_i} \left(\rho u_i \phi_k - \Gamma_k \frac{\partial\phi_k}{\partial x_i} \right) = S_{\phi_k} \quad (2.52)$$

where

Γ_k and S_{ϕ_k} are the diffusivity and the source terms respectively.

Therefore, Eq. (2.51) can be rearranged in resemblance with Eq. (2.52) to give:

$$\begin{aligned}
\frac{\partial(\rho\bar{s})}{\partial t} + \frac{\partial}{\partial x_i} \left[\rho\bar{u}_i\bar{s} - \left(\frac{k+k_t}{C_v} \right) \frac{\partial\bar{s}}{\partial x_i} \right] &= \frac{k}{\bar{T}^2} \left(\frac{\partial\bar{T}}{\partial x_i} \right)^2 + \frac{k}{\bar{T}^2} \frac{\partial\bar{T}'}{\partial x_i} \frac{\partial\bar{T}'}{\partial x_i} + \frac{k}{2} \frac{\partial}{\partial x_i} \left(\frac{1}{\bar{T}} \right) \frac{\partial(\overline{T'^2})}{\partial x_i} + \frac{\bar{\tau}_{ij}}{\bar{T}} \frac{\partial\bar{u}_i}{\partial x_j} + \\
\frac{\tilde{\epsilon}}{\bar{T}} - \left(\frac{\rho}{\bar{T}} \overline{u_i' T'} \frac{\partial\bar{s}}{\partial x_i} \right) - \frac{\rho C_v}{\bar{T}} \bar{u}_i \overline{(T')^2} \frac{\partial}{\partial x_i} \left(\frac{1}{\bar{T}} \right) - \frac{\rho C_v}{2\bar{T}^2} \left(\frac{\partial(\overline{T'^2})}{\partial x_i} \right) - \frac{\rho C_v}{\bar{T}} \overline{u_i' (T')^2} \frac{\partial}{\partial x_i} \left(\frac{1}{\bar{T}} \right) - \\
\frac{\rho C_v}{2\bar{T}^2} \frac{\partial(\overline{u_i' T'^2})}{\partial x_i} & \quad (2.53)
\end{aligned}$$

Eq. (2.53) is called as ‘‘Reynolds Averaged Entropy Transport (RAET)’’ equation. The terms on the right hand side of Eq. (2.53) are responsible for the entropy production in an incompressible turbulent flow. The first four terms are responsible for entropy production due to irreversible heat transfer. Terms 5 and 6 are production terms due to viscous effects where $\tilde{\epsilon}$ is defined as the true dissipation of turbulent kinetic energy [12]. Remaining terms are scalar fluctuating terms composed of

temperature-velocity correlations.

In the next section detailed evaluation of models for these terms will be done using a-priori testing methodology based on a DNS database.

CHAPTER 3

A-PRIORI TESTING OF MODELS TO BE USED IN THE REYNOLDS AVERAGED ENTROPY TRANSPORT (RAET) EQUATION

In this chapter, model equations for various parameters such as $\overline{u_i'T'^2}$, $\overline{u_i'T'}$ and $\overline{(T')^2}$, which appear in the RAET equation (Eq. 2.53), will be presented and then will be evaluated based on available DNS data from the literature.

There are several modeling approaches already available in the literature, especially for $\overline{u_i'T'}$ and $\overline{(T')^2}$, but literature on modeling of $\overline{u_i'T'^2}$ is very limited. For $\overline{u_i'T'}$ and $\overline{(T')^2}$, Hanjalic [25] provides a thorough approach starting with the transport equations for these terms and ending up with Differential Second Moment (DSM) closure equations. Durbin and Pettersson [26] and Schiestel [65] present some details on the modeling of $\overline{u_i'T'^2}$.

3.1 Transport Equation Based Modeling of $\overline{u_i'T'^2}$, $\overline{u_i'T'}$ and $\overline{(T')^2}$

3.1.1 Transport equation for $\overline{u_i'T'^2}$

Although, it is possible to encounter the evolution equations of $\overline{u_i'T'^2}$ as given in [26] and [65], it has not been possible to find any model transport equation for $\overline{u_i'T'^2}$ parameter. Therefore in this thesis a model equation for $\overline{u_i'T'^2}$ is developed and tested.

The conservation equation for the fluctuating velocity and temperature are given as:

$$\frac{\partial u_i'}{\partial t} + \bar{U}_j \frac{\partial u_i'}{\partial x_j} = -u_j' \frac{\partial \bar{U}_i}{\partial x_j} - \frac{\partial}{\partial x_j} (u_i' u_j' - \overline{u_i' u_j'}) - \frac{1}{\rho} \frac{\partial p'}{\partial x_i} + \vartheta \frac{\partial^2 u_i'}{\partial x_j \partial x_j} \quad (3.1)$$

$$\frac{\partial T'^2}{\partial t} + \bar{U}_j \frac{\partial T'^2}{\partial x_j} = -2u_j' T' \frac{\partial \bar{T}}{\partial x_j} - 2T' \frac{\partial}{\partial x_j} (u_j' T' - \overline{u_j' T'}) + 2\gamma T' \frac{\partial^2 T'}{\partial x_j \partial x_j} \quad (3.2)$$

Multiplying Eq. (3.1) with T'^2 gives,

$$\begin{aligned} T'^2 \frac{\partial u_i'}{\partial t} + T'^2 \bar{U}_j \frac{\partial u_i'}{\partial x_j} &= -T'^2 u_j' \frac{\partial \bar{U}_i}{\partial x_j} - T'^2 \frac{\partial}{\partial x_j} (u_i' u_j' - \overline{u_i' u_j'}) - T'^2 \frac{1}{\rho} \frac{\partial p'}{\partial x_i} + \\ T'^2 \vartheta \frac{\partial^2 u_i'}{\partial x_j \partial x_j} & \end{aligned} \quad (3.3)$$

Multiplying Eq. (3.2) with u_i' gives,

$$u_i' \frac{\partial T'^2}{\partial t} + u_i' \bar{U}_j \frac{\partial T'^2}{\partial x_j} = -2u_i' u_j' T' \frac{\partial \bar{T}}{\partial x_j} - 2u_i' T' \frac{\partial}{\partial x_j} (u_j' T' - \overline{u_j' T'}) + 2\gamma u_i' T' \frac{\partial^2 T'}{\partial x_j \partial x_j} \quad (3.4)$$

Summing Eq. (3.3) and Eq. (3.4) gives the overall transport equation for $u_i' T'^2$

$$\begin{aligned} \left[T'^2 \frac{\partial u_i'}{\partial t} + u_i' \frac{\partial T'^2}{\partial t} \right] + \left[T'^2 \bar{U}_j \frac{\partial u_i'}{\partial x_j} + u_i' \bar{U}_j \frac{\partial T'^2}{\partial x_j} \right] &= \left[-T'^2 u_j' \frac{\partial \bar{U}_i}{\partial x_j} - 2u_i' u_j' T' \frac{\partial \bar{T}}{\partial x_j} \right] + \\ \left[-T'^2 \frac{\partial}{\partial x_j} (u_i' u_j' - \overline{u_i' u_j'}) - 2u_i' T' \frac{\partial}{\partial x_j} (u_j' T' - \overline{u_j' T'}) \right] &+ \left[\vartheta T'^2 \frac{\partial^2 u_i'}{\partial x_j \partial x_j} + \right. \\ \left. 2\gamma u_i' T' \frac{\partial^2 T'}{\partial x_j \partial x_j} \right] - T'^2 \frac{1}{\rho} \frac{\partial p'}{\partial x_i} & \end{aligned} \quad (3.5)$$

Reynolds averaging of this equation gives;

$$\begin{aligned} \frac{\partial \overline{(u_i' T'^2)}}{\partial t} + \bar{U}_j \frac{\partial \overline{(u_i' T'^2)}}{\partial x_j} &= \left[-\overline{u_j' T'^2} \frac{\partial \bar{U}_i}{\partial x_j} - 2\overline{u_i' u_j' T'} \frac{\partial \bar{T}}{\partial x_j} \right] + \left[-\frac{\partial}{\partial x_j} \overline{(u_i' u_j' T'^2)} + \right. \\ \left. \overline{u_j' \frac{\partial}{\partial x_j} (u_i' T'^2)} \right] + \left[\vartheta \overline{T'^2} \frac{\partial^2 \overline{u_i'}}{\partial x_j \partial x_j} + 2\gamma \overline{u_i' T'} \frac{\partial^2 \overline{T'}}{\partial x_j \partial x_j} \right] &+ \overline{T'^2} \frac{\partial}{\partial x_j} \overline{(u_i' u_j')} + \\ 2\overline{u_i' T'} \frac{\partial}{\partial x_j} \overline{(u_j' T')} - \frac{1}{\rho} \overline{T'^2} \frac{\partial \overline{p'}}{\partial x_i} & \end{aligned} \quad (3.6)$$

The fifth and sixth terms on the RHS represent the correlation of the molecular diffusion with the fluctuating temperature and velocity. It is expected that the scales of these terms are relatively small compared to the other terms in Eq. (3.6), so an order of magnitude analysis is performed to verify this assumption [27].

For the order of magnitude analysis, it is assumed that [27]:

- Fluctuating velocities, u scale with $u = \overline{u_i u_i}^{1/2}$
- Conserved scalar fluctuations, s scale with $s = \overline{c^2}^{1/2}$ where c is any scalar variable
- Mean velocity and scalar gradients scale with u/l and s/l

where the scales given above are the scales of the energy containing eddies.

The scales of the molecular diffusion terms can be obtained with the philosophy described above;

$$\overline{\vartheta T'^2 \frac{\partial^2 u_i'}{\partial x_j \partial x_j}} \cong \vartheta s^2 \frac{u}{l^2} \quad (3.7)$$

$$\overline{2\gamma u_i' T' \frac{\partial^2 T'}{\partial x_j \partial x_j}} \cong \gamma s^2 \frac{u}{l^2} \quad (3.8)$$

On the other hand, scales of the first and second term in Eq. (3.6) can be obtained as;

$$\overline{u_j' T'^2 \frac{\partial \overline{U}_i}{\partial x_j}} \cong u s^2 \frac{u}{l} = \frac{s^2 u^2}{l} \quad (3.9)$$

$$\overline{u_i' u_j' T' \frac{\partial \overline{T}}{\partial x_j}} \cong u^2 s \frac{s}{l} = \frac{s^2 u^2}{l} \quad (3.10)$$

If the RHS of Eq.(3.7) is rearranged;

$$\vartheta \frac{s^2 u}{l^2} = \left(\frac{\vartheta}{ul} \right) \frac{s^2 u^2}{l} = \frac{1}{Re_t} \left(\frac{s^2 u^2}{l} \right) \ll \frac{s^2 u^2}{l} \quad (3.11)$$

where Re_t is the turbulent Reynolds number.

Order of magnitude analysis for the diffusion terms reveals that they can be neglected since scales of other terms in Eq. (3.6) are relatively higher than these terms.

As a result, the final form of Eq. (3.6) can be obtained as;

$$\frac{\partial(\overline{u_i' T'^2})}{\partial t} + \bar{U}_j \frac{\partial(\overline{u_i' T'^2})}{\partial x_j} = -\overline{u_j' T'^2} \frac{\partial \bar{U}_i}{\partial x_j} - 2 \overline{u_i' u_j' T'} \frac{\partial \bar{T}}{\partial x_j} - \frac{\partial}{\partial x_j} (\overline{u_i' u_j' T'^2}) - \frac{1}{\rho} \overline{T'^2} \frac{\partial p'}{\partial x_i} \quad (3.12)$$

The correlations appearing on the RHS of Eq. (3.12) need modeling. The following terms together with the proposed modeling terms are [26]:

$$-\overline{u_i' u_j' T'} = C_1 \frac{k}{\varepsilon} \left(\overline{u_j' u_k'} \frac{\partial(\overline{u_i' T'})}{\partial x_k} + \overline{u_i' u_k'} \frac{\partial(\overline{u_j' T'})}{\partial x_k} \right) \quad (3.13)$$

where C_j is an arbitrary constant.

It was not possible to find a suitable modeling approach for the term $\overline{u_i' u_j' T'^2}$ in the literature, therefore it is modeled based on an analogy with the modeling of $\overline{u_i' u_j' T'}$.

$$-\frac{\partial}{\partial x_j} (\overline{u_i' u_j' T'^2}) = C_2 \frac{k}{\varepsilon} \frac{\partial}{\partial x_j} \left[\overline{u_j' u_k'} \frac{\partial(\overline{u_i' T'^2})}{\partial x_k} \right] \quad (3.14)$$

The fluctuating pressure term can be modeled as a slow term and a rapid term [26].

$$\overline{T'^2} \frac{\partial p'}{\partial x_i} = -C_3 \frac{\varepsilon}{k} \overline{u_i' T'} + C_4 \overline{u_k' T'} \frac{\partial \bar{U}_i}{\partial x_k} + C_5 \overline{u_k' T'} \frac{\partial \bar{U}_k}{\partial x_i} \quad (3.15)$$

The first term at the RHS of Eq. (3.15) is the slow part whereas the other terms are the rapid part.

Combining all these terms gives the final model transport equation for $\overline{u_i'T'^2}$:

$$\begin{aligned} \frac{D(\overline{u_i'T'^2})}{Dt} = & -\overline{u_j'T'^2} \frac{\partial \bar{U}_i}{\partial x_j} + 2C_1 \frac{k}{\varepsilon} (\overline{u_j'u_k'} \frac{\partial(\overline{u_i'T'})}{\partial x_k} + \overline{u_i'u_k'} \frac{\partial(\overline{u_j'T'})}{\partial x_k}) \frac{\partial \bar{T}}{\partial x_j} + \\ & C_2 \frac{k}{\varepsilon} \frac{\partial}{\partial x_j} [\overline{u_j'u_k'} \frac{\partial(\overline{u_i'T'^2})}{\partial x_k}] - \frac{1}{\rho} (C_3 \frac{\varepsilon}{k} \overline{u_i'T'^2}) \end{aligned} \quad (3.16)$$

For the sake of simplicity and since it is considered to be sufficient [26] only the first term of the pressure term, i.e. the slow part, is kept in the equation.

In the literature, also an algebraic model for $\overline{u_i'T'^2}$ is proposed by Schiestel [65] :

$$\overline{u_i'T'^2} = -C_{11} \frac{k}{\varepsilon} (\overline{u_i'u_j'} \frac{\partial(\overline{T'^2})}{\partial x_j} + 2 \overline{u_j'T'} \frac{\partial(\overline{u_i'T'})}{\partial x_j}) \quad (3.17)$$

Both the transport equation model (Eq. 3.16) as well as the algebraic model of Schiestel are tested using the available DNS database and the results are presented in the upcoming sections.

3.1.2 Transport equation for $\overline{u_i'T'}$

The conservation equation for the fluctuating velocity and temperature are given as:

$$\frac{\partial u_i'}{\partial t} + \bar{U}_j \frac{\partial u_i'}{\partial x_j} = -u_j' \frac{\partial \bar{U}_i}{\partial x_j} - \frac{\partial}{\partial x_j} (u_i'u_j' - \overline{u_i'u_j'}) - \frac{1}{\rho} \frac{\partial p'}{\partial x_i} + \vartheta \frac{\partial^2 u_i'}{\partial x_j \partial x_j} \quad (3.1)$$

$$\frac{\partial T'}{\partial t} + \bar{U}_j \frac{\partial T'}{\partial x_j} = -u_j' \frac{\partial \bar{T}}{\partial x_j} - \frac{\partial}{\partial x_j} (u_j'T' - \overline{u_j'T'}) - \gamma \frac{\partial^2 T'}{\partial x_j \partial x_j} \quad (3.18)$$

Multiplying Eq. (3.1) with T' gives,

$$T' \frac{\partial u_i'}{\partial t} + T' \bar{U}_j \frac{\partial u_i'}{\partial x_j} = -T' u_j' \frac{\partial \bar{U}_i}{\partial x_j} - T' \frac{\partial}{\partial x_j} (u_i' u_j' - \overline{u_i' u_j'}) - T' \frac{1}{\rho} \frac{\partial p'}{\partial x_i} + T' \vartheta \frac{\partial^2 u_i'}{\partial x_j \partial x_j} \quad (3.19)$$

Multiplying Eq. (3.18) with u_i' gives,

$$u_i' \frac{\partial T'}{\partial t} + u_i' \bar{U}_j \frac{\partial T'}{\partial x_j} = -u_i' u_j' \frac{\partial \bar{T}}{\partial x_j} - u_i' \frac{\partial}{\partial x_j} (u_j' T' - \overline{u_j' T'}) - \gamma u_i' \frac{\partial^2 T'}{\partial x_j \partial x_j} \quad (3.20)$$

Summing Eq. (3.19) and Eq. (3.20) gives the overall transport equation for $u_i' T'$

$$\begin{aligned} & [T' \frac{\partial u_i'}{\partial t} + u_i' \frac{\partial T'}{\partial t}] + [T' \bar{U}_j \frac{\partial u_i'}{\partial x_j} + u_i' \bar{U}_j \frac{\partial T'}{\partial x_j}] = \\ & -u_j' T' \frac{\partial \bar{U}_i}{\partial x_j} - u_i' u_j' \frac{\partial \bar{T}}{\partial x_j} - u_i' \frac{\partial}{\partial x_j} (u_j' T' - \overline{u_j' T'}) - u_i' \frac{\partial}{\partial x_j} (u_j' T' - \overline{u_j' T'}) - T' \frac{1}{\rho} \frac{\partial p'}{\partial x_i} + \\ & \vartheta T' \frac{\partial^2 u_i'}{\partial x_j \partial x_j} - \gamma u_i' \frac{\partial^2 T'}{\partial x_j \partial x_j} \end{aligned} \quad (3.21)$$

Reynolds averaging of Eq. (3.21) gives;

$$\begin{aligned} \frac{\partial \overline{(u_i' T')}}{\partial t} + \bar{U}_j \frac{\partial \overline{(u_i' T')}}{\partial x_j} &= -\overline{u_j' T'} \frac{\partial \bar{U}_i}{\partial x_j} - \overline{u_i' u_j'} \frac{\partial \bar{T}}{\partial x_j} - \overline{T' \frac{\partial}{\partial x_j} (u_i' u_j')} - \overline{u_i' \frac{\partial}{\partial x_j} (u_j' T')} - \\ \frac{1}{\rho} \overline{T' \frac{\partial p'}{\partial x_i}} + \vartheta \overline{T' \frac{\partial^2 u_i'}{\partial x_j \partial x_j}} &- \gamma \overline{u_i' \frac{\partial^2 T'}{\partial x_j \partial x_j}} \end{aligned} \quad (3.22)$$

The sixth and seventh terms at the RHS of Eq. (3.22) are neglected due to smaller scales of turbulence as explained in the previous section. Therefore the final form of the transport equation for $\overline{u_i' T'}$ is;

$$\frac{D \overline{(u_i' T')}}{Dt} = -\overline{u_j' T'} \frac{\partial \bar{U}_i}{\partial x_j} - \overline{u_i' u_j'} \frac{\partial \bar{T}}{\partial x_j} - \frac{\partial}{\partial x_j} \overline{(u_i' u_j' T')} - \frac{1}{\rho} \overline{T' \frac{\partial p'}{\partial x_i}} \quad (3.23)$$

This transport equation can be revised with the modeling principles as explained in

[25] and detailed in the previous section to give;

$$\frac{D(\overline{u_i' T'})}{Dt} = -(1 - C_6) (\overline{u_j' T'}) \frac{\partial \bar{u}_i}{\partial x_j} - \overline{u_i' u_j'} \frac{\partial \bar{T}}{\partial x_j} + C_7 \frac{k}{\varepsilon} \frac{\partial}{\partial x_j} (\overline{u_j' u_k'} \frac{\partial (\overline{u_i' T'})}{\partial x_k}) - C_8 \frac{1}{\rho} \frac{(\overline{u_i' T'})}{k} \varepsilon \quad (3.24)$$

3.1.3 Transport equation for $\overline{T'^2}$

If Eq. (3.18) is recalled for the general transport of the scalar T' ;

$$\frac{\partial T'}{\partial t} + U_j \frac{\partial T'}{\partial x_j} = -u_j' \frac{\partial T}{\partial x_j} - \frac{\partial}{\partial x_j} (u_j' T' - \overline{u_j' T'}) - \gamma \frac{\partial^2 T'}{\partial x_j \partial x_j} \quad (3.18)$$

Multiplying Eq. (3.18) with $2T'$ gives;

$$2T' \frac{\partial T'}{\partial t} + U_j 2T' \frac{\partial T'}{\partial x_j} = -u_j' 2T' \frac{\partial T}{\partial x_j} - \frac{\partial}{\partial x_j} 2T' (u_j' T' - \overline{u_j' T'}) - \gamma 2T' \frac{\partial^2 T'}{\partial x_j \partial x_j} \quad (3.25)$$

Rearranging and Reynolds averaging of Eq. (3.25) gives;

$$\frac{\partial \overline{(T'^2)}}{\partial t} + U_j \frac{\partial \overline{(T'^2)}}{\partial x_j} = -2 \overline{u_j' T'} \frac{\partial \bar{T}}{\partial x_j} - \frac{\partial \overline{(u_j' T'^2)}}{\partial x_j} - 2\gamma \overline{T'} \frac{\partial^2 T'}{\partial x_j \partial x_j} \quad (3.26)$$

The final form of the transport equation for the scalar T'^2 is;

$$\frac{D\overline{T'^2}}{Dt} = -2 \overline{u_j' T'} \frac{\partial \bar{T}}{\partial x_j} - \frac{\partial \overline{(u_j' T'^2)}}{\partial x_j} - 2\gamma \overline{T'} \frac{\partial^2 T'}{\partial x_j \partial x_j} \quad (3.27)$$

Then the model equation for T'^2 can be given as;

$$\frac{D\overline{T'^2}}{Dt} = -2 \overline{(u_i' T')} \frac{\partial \bar{T}}{\partial x_i} - \frac{1}{2C_9} \frac{\overline{T'^2}}{2k} \varepsilon + C_{10} \frac{k}{\varepsilon} \frac{\partial}{\partial x_j} (\overline{u_i' u_j'} \frac{\partial \overline{T'^2}}{\partial x_i}) \quad (3.28)$$

3.2 A-priori Testing Using Direct Numerical Simulation (DNS) Database

3.2.1 The DNS Database

In order to investigate the performance of the model equations described in the previous section a-priori testing methodology is applied using a DNS database. This database is obtained by simulating an incompressible non-isothermal fully developed turbulent channel flow using SIMSON solver (A Pseudo-Spectral Solver for IncoMpreSsible BOuNdary Layer Flows) as described in detail in [14]. The simulations are performed using the for a Re_τ of 180 (Reynolds number based on the friction velocity) which is obtained by fixing the bulk Reynolds number to 2800. The domain size is $4\pi \times 2 \times 2\pi$ measured in channel half heights as illustrated in Figure 3.1. The coordinates x, y and z refer to the streamwise, wall-normal and spanwise directions, respectively. The simulation is performed using $128 \times 128 \times 128$ grid points in physical space together with dealiasing using the $3/2$ rule in the wall-parallel directions. In addition to the velocity field, three passive scalars with Prandtl numbers of 0.2, 0.71 and 2 are advected, as in a previous study in turbulent boundary layers [66]. Time integration is achieved using a combined third order Runge-Kutta/Crank-Nicolson scheme.

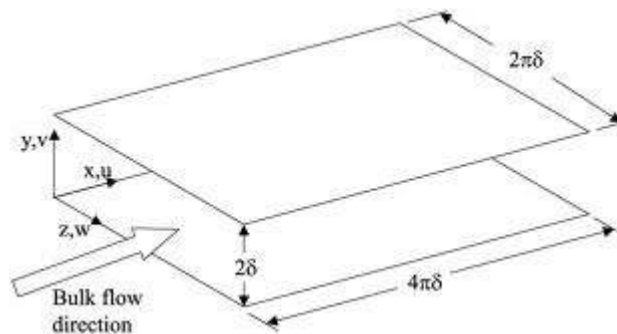


Figure 3.1 Schematic representation of the DNS channel flow taken from [28].

Boundary conditions are periodic in the streamwise and spanwise directions and no

slip boundary conditions are applied for the upper and lower walls. The flow is non-isothermal and this is supplied via two different temperatures for the upper and lower walls [14].

In order to calculate the turbulence statistics, DNS solver called SIMSON (A Pseudo-Spectral Solver for IncoMpreSSible BOuNdary Layer Flows) was used [14]. With the help of the tool, it was possible to get all individual terms given in the equations and then implement the necessary algebra to check the validity of the model equations.

Implementing all the equations for $\overline{u_i'T'^2}$ and $\overline{u_i'T'}$ for the channel case, three different equations are obtained for three different spatial directions whereas for T'^2 , only one equation is developed since it has no correlation component with velocity.

3.2.2 Reduced Forms of the Model Equations for the Steady State Fully Developed Channel Flow

3.2.2.1 Equations for $\overline{u_i'T'^2}$

If the model equation for $\overline{u_i'T'^2}$ is recalled;

$$\begin{aligned} \frac{D(\overline{u_i'T'^2})}{Dt} = & -\overline{u_j'T'^2} \frac{\partial \overline{U_i}}{\partial x_j} + 2C_1 \frac{k}{\varepsilon} \left(\overline{u_j'u_k'} \frac{\partial (\overline{u_i'T'})}{\partial x_k} + \overline{u_i'u_k'} \frac{\partial (\overline{u_j'T'})}{\partial x_k} \right) \frac{\partial \overline{T}}{\partial x_j} + \\ & C_2 \frac{k}{\varepsilon} \frac{\partial}{\partial x_j} \left[\overline{u_j'u_k'} \frac{\partial (\overline{u_i'T'^2})}{\partial x_k} \right] - \frac{1}{\rho} \left(C_3 \frac{\varepsilon}{k} \overline{u_i'T'^2} \right) \end{aligned} \quad (3.16)$$

Components of this equation for three spatial coordinates simplified for the steady state fully developed channel flow case (which makes all LHS's zero) can be written as:

$$0 = -\overline{v'T'^2} \frac{\partial \bar{U}}{\partial y} + 2C_1 \frac{k}{\varepsilon} (\overline{v'v'} \frac{\partial \overline{(u'T')}}{\partial y} + \overline{u'v'} \frac{\partial \overline{(v'T')}}{\partial y}) \frac{\partial \bar{T}}{\partial y} + C_2 \frac{k}{\varepsilon} \frac{\partial}{\partial y} \left(\overline{v'v'} \frac{\partial \overline{(u'T'^2)}}{\partial y} \right) - \frac{C_3 \varepsilon}{\rho k} \overline{(u'T'^2)} \quad (3.29)$$

$$0 = 2C_1 \frac{k}{\varepsilon} (\overline{u'v'} \frac{\partial \overline{(v'T')}}{\partial y} + \overline{v'w'} \frac{\partial \overline{(w'T')}}{\partial y}) \frac{\partial \bar{T}}{\partial y} + C_2 \frac{k}{\varepsilon} \frac{\partial}{\partial y} \left(\overline{v'v'} \frac{\partial \overline{(v'T'^2)}}{\partial y} \right) - \frac{C_3 \varepsilon}{\rho k} \overline{(v'T'^2)} \quad (3.30)$$

$$0 = 2C_1 \frac{k}{\varepsilon} (\overline{u'v'} \frac{\partial \overline{(w'T')}}{\partial y} + \overline{u'v'} \frac{\partial \overline{(w'T')}}{\partial y}) \frac{\partial \bar{T}}{\partial y} + C_2 \frac{k}{\varepsilon} \frac{\partial}{\partial y} \left(\overline{v'v'} \frac{\partial \overline{(w'T'^2)}}{\partial y} \right) - \frac{C_3 \varepsilon}{\rho k} \overline{(w'T'^2)} \quad (3.31)$$

Different model constants for C_1 , C_2 and C_3 are available in the literature but the recommended ones are;

$$0.11 \leq C_1, C_2 \leq 0.2 \text{ and } C_3 = 3.0$$

However, effects of changing these model constants will be evaluated in the upcoming sections of this study.

3.2.2.2 Equations for $\overline{u_i'T'}$

If the model equation for $\overline{u_i'T'}$ is recalled;

$$\frac{D(\overline{u_i'T'})}{Dt} = -(1 - C_6) (\overline{u_j'T'}) \frac{\partial \bar{U}_i}{\partial x_j} - \overline{u_i'u_j'} \frac{\partial \bar{T}}{\partial x_j} + C_7 \frac{k}{\varepsilon} \frac{\partial}{\partial x_j} (\overline{u_j'u_k'} \frac{\partial \overline{(u_i'T')}}{\partial x_k}) - \frac{C_8 \varepsilon}{\rho k} \overline{(u_i'T')} \quad (3.24)$$

Similar to the previous section, components of this equation for three spatial coordinates simplified for the steady state fully developed channel flow case can be written as:

$$0 = -(1 - C_6) (\overline{u'T'}) \frac{\partial \bar{u}}{\partial y} - \overline{u'v'} \frac{\partial \bar{T}}{\partial y} + C_7 \frac{k}{\varepsilon} \frac{\partial}{\partial x_j} (\overline{v'v'} \frac{\partial (\overline{u'T'})}{\partial y}) - \frac{C_8 (\overline{u'T'})}{\rho k} \varepsilon \quad (3.32)$$

$$0 = -\overline{v'v'} \frac{\partial \bar{T}}{\partial y} + C_7 \frac{k}{\varepsilon} \frac{\partial}{\partial x_j} (\overline{v'v'} \frac{\partial (\overline{v'T'})}{\partial y}) - \frac{C_8 (\overline{v'T'})}{\rho k} \varepsilon \quad (3.33)$$

$$0 = -\overline{w'v'} \frac{\partial \bar{T}}{\partial y} + C_7 \frac{k}{\varepsilon} \frac{\partial}{\partial x_j} (\overline{v'v'} \frac{\partial (\overline{w'T'})}{\partial y}) - \frac{C_8 (\overline{w'T'})}{\rho k} \varepsilon \quad (3.34)$$

Recommended model coefficients are [25]:

$$C_6 = 0.55, C_7 = 0.15, C_8 = 3.5$$

3.2.2.3 Equations for $\overline{T'^2}$

If the model equation for $\overline{T'^2}$ is recalled;

$$\frac{D\overline{T'^2}}{Dt} = -2(\overline{u'_i T'}) \frac{\partial \bar{T}}{\partial x_i} - \frac{1}{2C_9} \frac{\overline{T'^2}}{2k} \varepsilon + C_{10} \frac{k}{\varepsilon} \frac{\partial}{\partial x_j} (\overline{u'_i u'_j} \frac{\partial \overline{T'^2}}{\partial x_i}) \quad (3.28)$$

Simplified version of this equation for the steady state fully developed channel flow case can be written as:

$$0 = -2\overline{v' T'} \frac{\partial \bar{T}}{\partial y} - \frac{1}{2C_9} \frac{\overline{T'^2}}{2k} \varepsilon + C_{10} \frac{k}{\varepsilon} \left\{ \frac{\partial}{\partial y} (\overline{v' v'} \frac{\partial \overline{T'^2}}{\partial y}) \right\} \quad (3.35)$$

Recommended coefficients for Eq. (3.35) are given as [25]:

$$C_9 = 0.5, C_{10} = 0.2$$

3.2.3 Results of A-priori Testing

In this section, results for all the turbulent parameters of interest are investigated in more detail for the channel test flow case. Parameters are defined from Eq. (3.28) to Eq. (3.34). LHS of all equations are zero since \bar{V} is zero for this channel flow case. Therefore the performance of all equations is compared through their deviations from zero and all the terms at the RHS are obtained from the DNS solution values.

Before going into the details of the turbulent parameters, a first check will be conducted for Eq. (3.13) which can be recalled as

$$-\overline{u_i' u_j' T'} = C_1 \frac{k}{\varepsilon} \left(\overline{u_j' u_k'} \frac{\partial(\overline{u_i' T'})}{\partial x_k} + \overline{u_i' u_k'} \frac{\partial(\overline{u_j' T'})}{\partial x_k} \right) \quad (3.13)$$

For different values of i, j and k Eq. (3.13) reduces to simple forms.

For $i = 1, j = 1$ and $k = 2$

$$-\overline{u' u' T'} = 2C_1 \frac{k}{\varepsilon} \overline{u' v'} \frac{\partial(\overline{u' T'})}{\partial y} \quad (3.36)$$

For $i = 1, j = 2$ and $k = 2$

$$-\overline{u' v' T'} = C_1 \frac{k}{\varepsilon} \left(\overline{v' v'} \frac{\partial(\overline{u' T'})}{\partial y} + \overline{u' v'} \frac{\partial(\overline{v' T'})}{\partial y} \right) \quad (3.37)$$

Since the flow inside the channel is dominated by the streamwise direction, two parameters given above are selected to be compared. Recommended values for the constant C_1 range between 0.11 and 0.2 whereas a default value is given as 0.15 [26]. Figure 3.2 presents the LHS vs. RHS of Eq. (3.36) for the default value of 0.15 for C_1 as a function of $y^+ (*)$ which is the non-dimensional y coordinate.

(*) $y^+ = \frac{y u_\tau}{\nu}$ where u_τ is the wall shear velocity and ν is the kinematic viscosity.

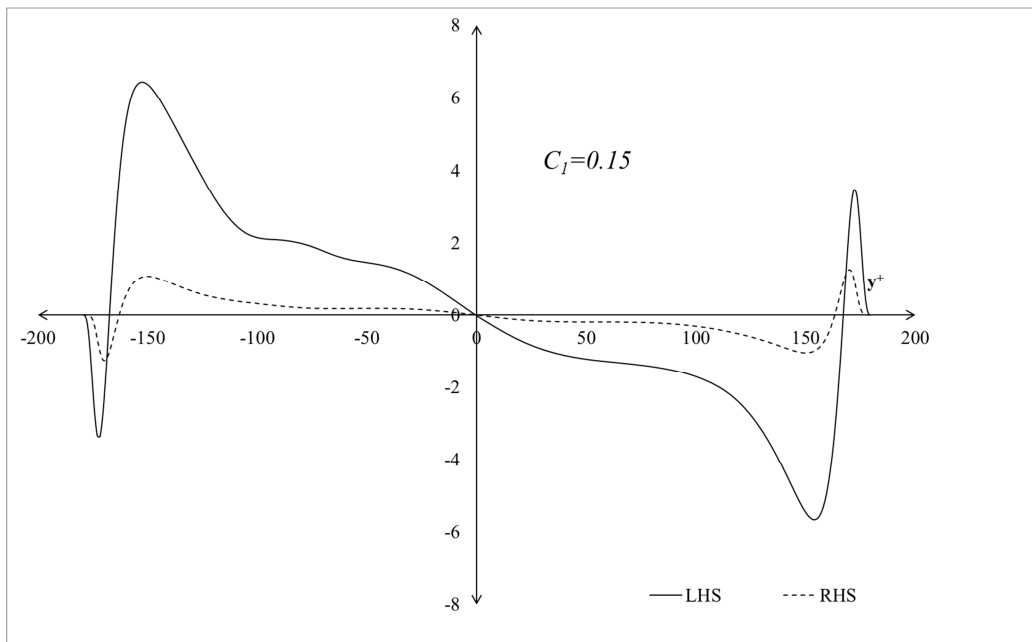


Figure 3.2 LHS vs. RHS of Eq (3.36) for $C_l=0.15$.

It is clear from Figure 3.2 that for the corresponding default coefficient, LHS of Eq. (3.36) does not match well with the RHS. Therefore, the default value for C_l is increased up to a level that a reasonable match is obtained. Figure 3.3 shows the comparison of Eq. (3.36) for different values of C_l . The best fit is observed when $C_l=0.90$.

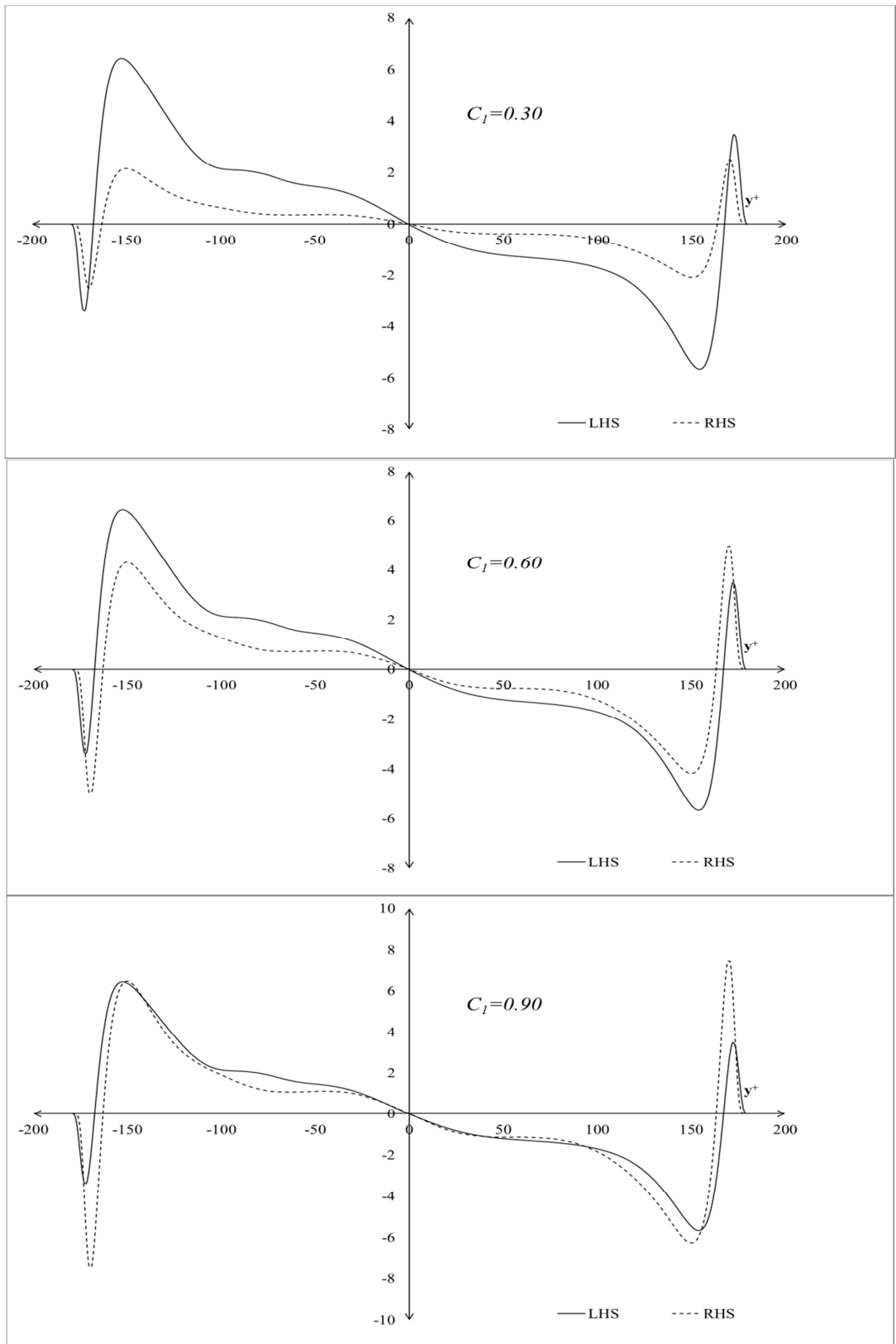


Figure 3.3 LHS vs. RHS of Eq (3.36) for different values of C_l .

Although the matching is quite good in general for the new value of the constant, it is not possible to obtain a perfect match especially in the near wall regions. With a simple model such as the one given in Eq. (3.13), it is not possible to capture the complex near wall phenomena.

The same check can also be performed for $\overline{u'v'T'}$ following the same principle. Figure 3.4 shows LHS and RHS of Eq. (3.37) for the default value of 0.15.

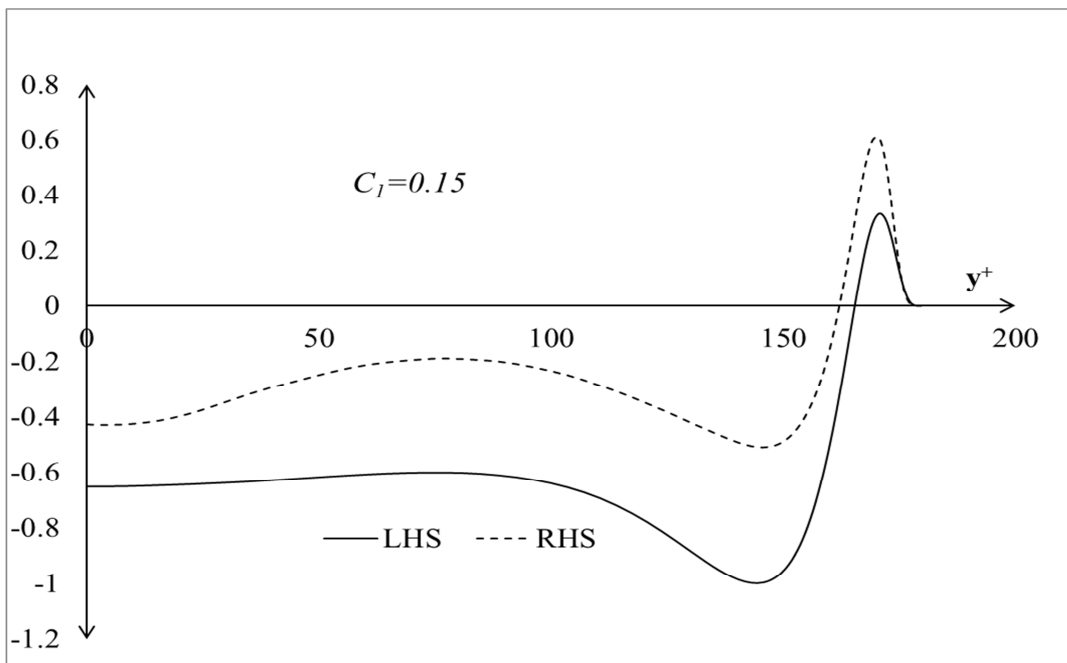


Figure 3.4 LHS vs. RHS of Eq (3.37) for $C_l=0.15$.

The general trend of both curves is similar however the scales are different. Therefore the default value for the constant C_l is changed in Figure 3.5 to have the trends fit in a better manner. As a result of this analysis, the best fit is obtained with $C_l=0.3$. but it is clear that, as in Eq. (3.36), the match is not perfect in the near wall region.

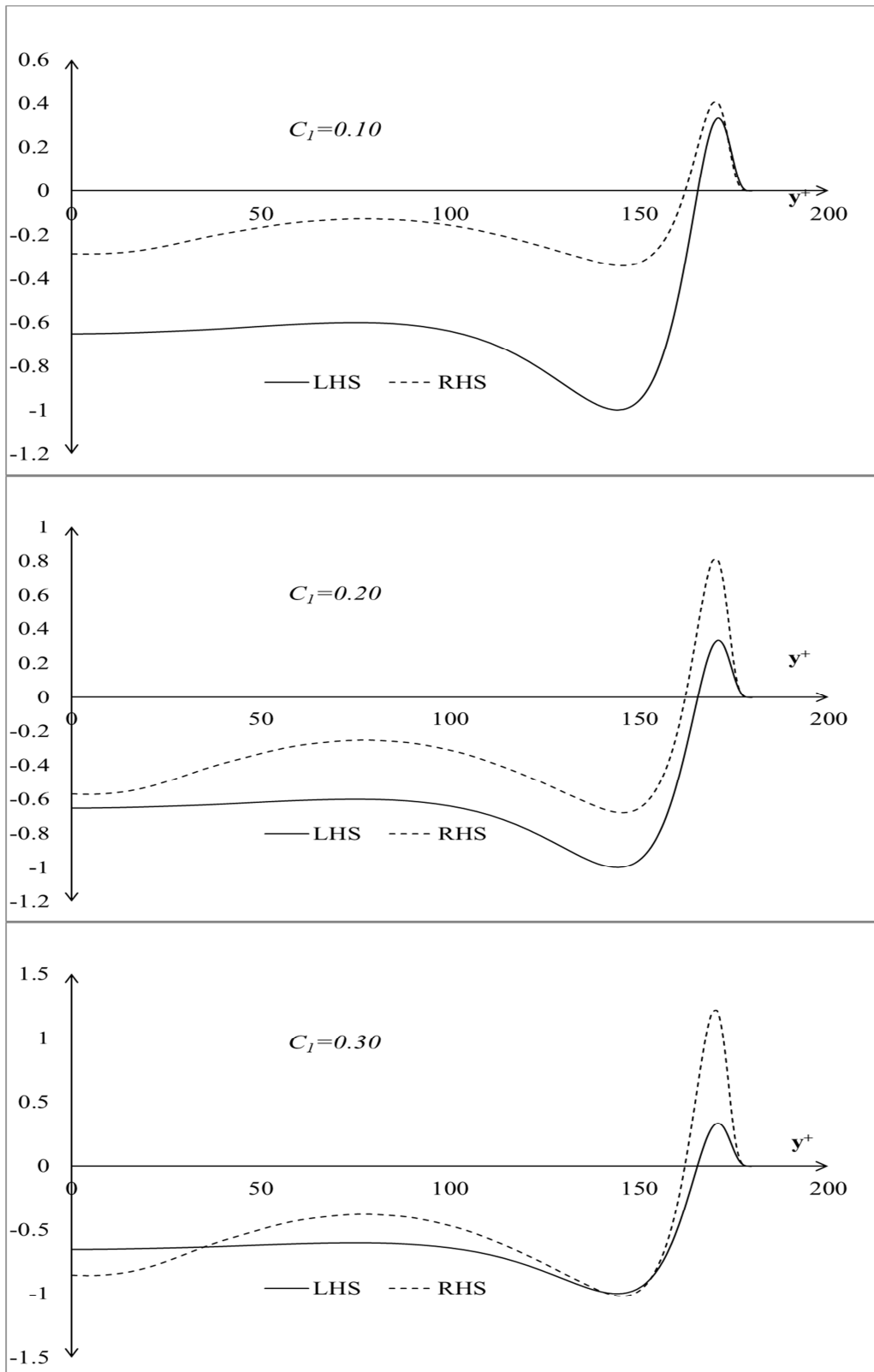


Figure 3.5 LHS vs. RHS of Eq (3.37) for different values of C_1 .

3.2.3.1 Results for $\overline{u_i'T'^2}$

Results for the parameter $\overline{u_i'T'^2}$ are given in Figures 3.6, 3.7 and 3.8. The main characteristic of these figures are that the general trend for the parameter has been obtained for a specific model constant values and these values are all different for different spatial directions. Another observation is that the trends near the wall do not match very well. The model prediction is relatively better compared to the upper wall region. Especially, for the upper wall, there is an overshoot in the modelling although the trend is similar.

After evaluating the performance of Eq. (3.13), governing equations for the turbulent scalars are tested. Eq. (3.16) is the model transport equation for $\overline{u_i'T'^2}$;

$$\begin{aligned} \frac{D(\overline{u_i'T'^2})}{Dt} = & -\overline{u_j'T'^2} \frac{\partial \overline{U_i}}{\partial x_j} + 2C_1 \frac{k}{\varepsilon} \left(\overline{u_j'u_k'} \frac{\partial(\overline{u_i'T'})}{\partial x_k} + \overline{u_i'u_k'} \frac{\partial(\overline{u_j'T'})}{\partial x_k} \right) \frac{\partial \overline{T}}{\partial x_j} + \\ & C_2 \frac{k}{\varepsilon} \frac{\partial}{\partial x_j} \left[\overline{u_j'u_k'} \frac{\partial(\overline{u_i'T'^2})}{\partial x_k} \right] - \frac{1}{\rho} (C_3 \frac{\varepsilon}{k} \overline{u_i'T'^2}) \end{aligned} \quad (3.16)$$

The first term at the RHS is the so called “*mechanical production; mean flow deformation interacting with turbulent heat flux*” [25] or the “*tilting production*” [27]. Second term is the thermal production which is a result of nonuniform temperature field interacting with turbulent stresses [25]. Third term is a modelled term caused by turbulent diffusion transport and the final one is due to fluctuating pressure temperature correlation. The default constants as given in [25] and in [26] are;

$$C_1, C_2 = 0.15 \text{ and } C_3 = 3$$

As explained in the previous sections the LHS of Eq. (3.29) to Eq. (3.31) are zero due to the fact that the y component of the mean velocity is zero in the channel. Therefore, the validity of the model transport equations is evaluated based on the level of their deviation from zero for the sum of RHS terms.

In Figure 3.6, individual terms that constitute Eq. (3.29) which is a simplified form of Eq. (3.16) for y direction, are plotted for the default values as stated above together with their sum. Since all the equations are symmetric around the centerline of the flow, only one side of the plot is shown in order to have a better visualization.

$$0 = -\overline{v'T'^2} \frac{\partial \bar{U}}{\partial y} + 2C_1 \frac{k}{\varepsilon} (\overline{v'v'} \frac{\partial \overline{(u'T')}}{\partial y} + \overline{u'v'} \frac{\partial \overline{(v'T')}}{\partial y}) \frac{\partial \bar{T}}{\partial y} + C_2 \frac{k}{\varepsilon} \frac{\partial}{\partial y} \left(\overline{v'v'} \frac{\partial \overline{(u'T'^2)}}{\partial y} \right) - \frac{C_3 \varepsilon}{\rho k} \overline{(u'T'^2)} \quad (3.29)$$

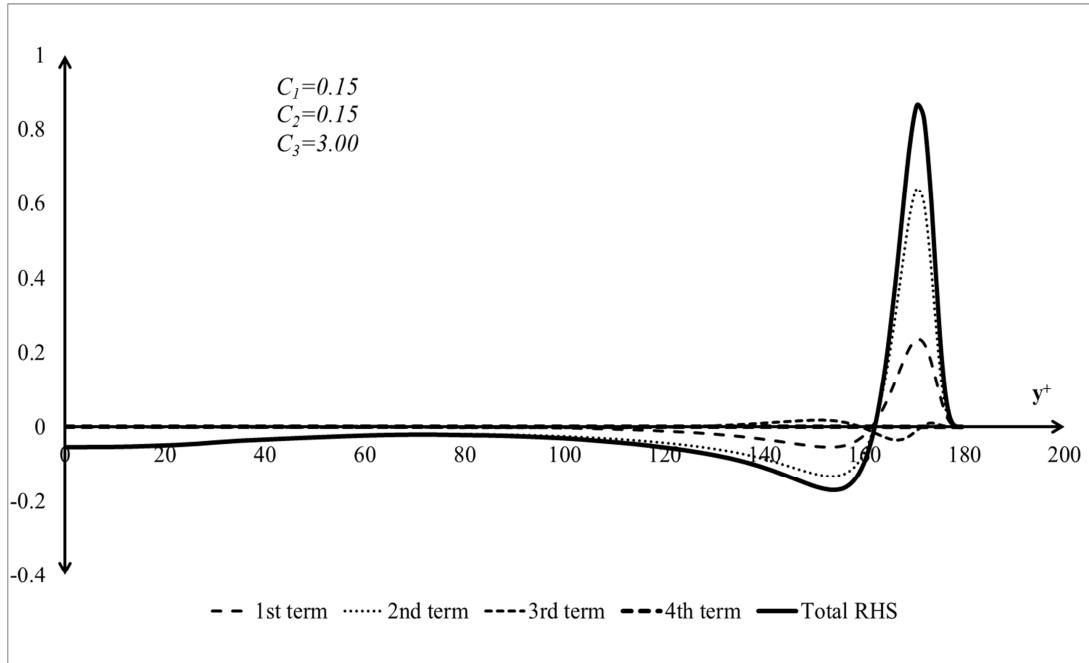


Figure 3.6 RHS of Eq (3.29) for default values of C_I .

Figure 3.6 shows that for the default constants, the general trend of Eq. (3.29) does not deviate much from zero up to a value where the near wall effects are important. It is also clear that, the general trend is defined by the first and second terms which are the production terms.

With the default values of the constants, both production terms are positive. Therefore, the value of the second term has to be opposite of the first one to have almost a zero trend.

Change in the general trend can be observed in the following figure.

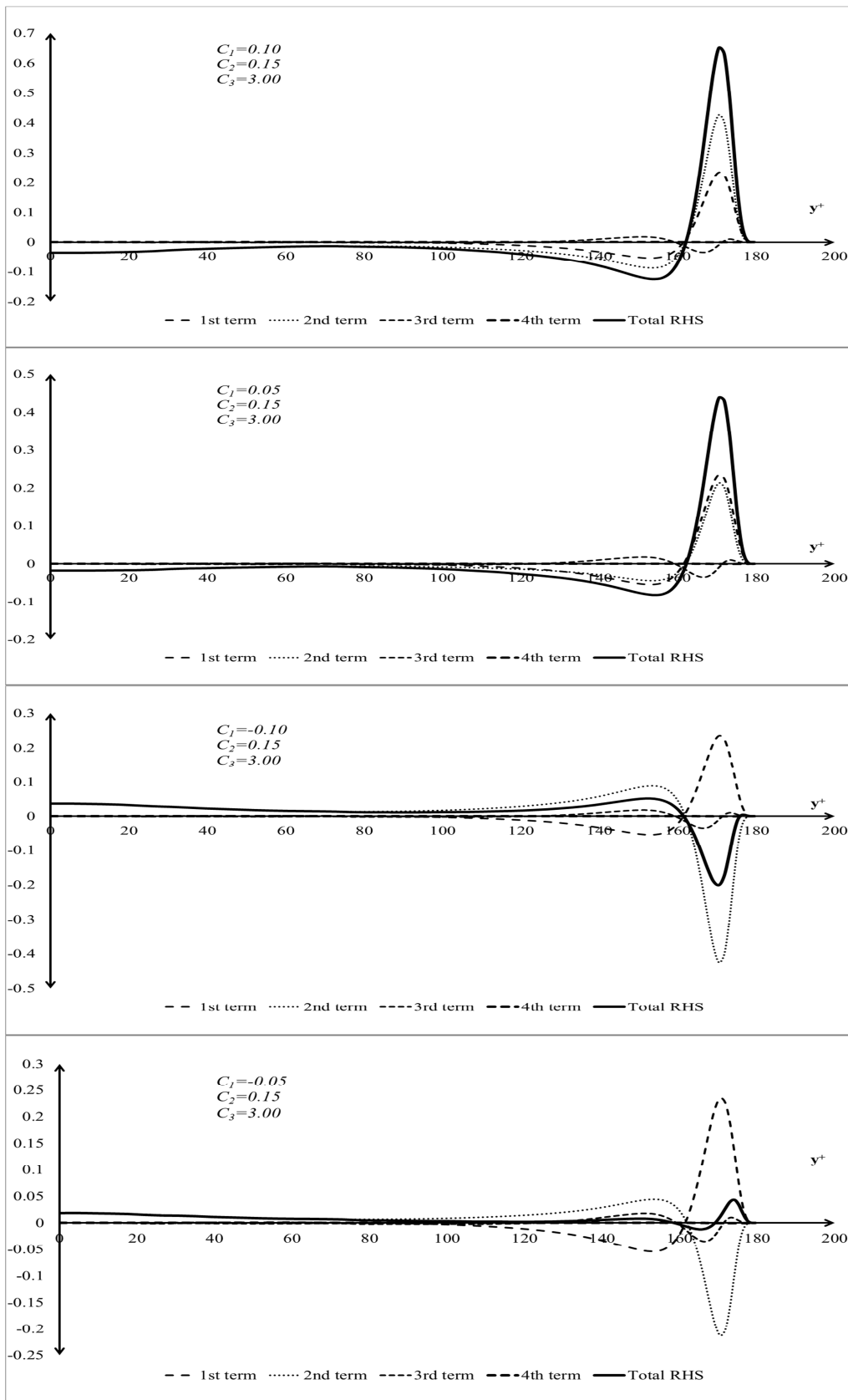


Figure 3.7 RHS of Eq (3.29) for different values of C_1 .

An analysis similar to the one conducted for Eq. (3.29) can be repeated for Eq. (3.30);

$$0 = 2C_1 \frac{k}{\varepsilon} \left(\overline{u'v'} \frac{\partial \overline{(v'T')}}{\partial y} + \overline{v'w'} \frac{\partial \overline{(w'T')}}{\partial y} \right) \frac{\partial \bar{T}}{\partial y} + C_2 \frac{k}{\varepsilon} \frac{\partial}{\partial y} \left(\overline{v'v'} \frac{\partial \overline{(v'T'^2)}}{\partial y} \right) - \frac{C_3}{\rho} \frac{\varepsilon}{k} \overline{(v'T'^2)} \quad (3.30)$$

One production term is missing in Eq. (3.30) since the mean velocity in y-direction and all of its derivatives are zero. Therefore, there are three terms at the RHS of Eq. (3.30) and the default constant values are the same as for Eq. (3.29).

In Figure 3.8, an overall view of Eq. (3.30) for the default constants can be seen.

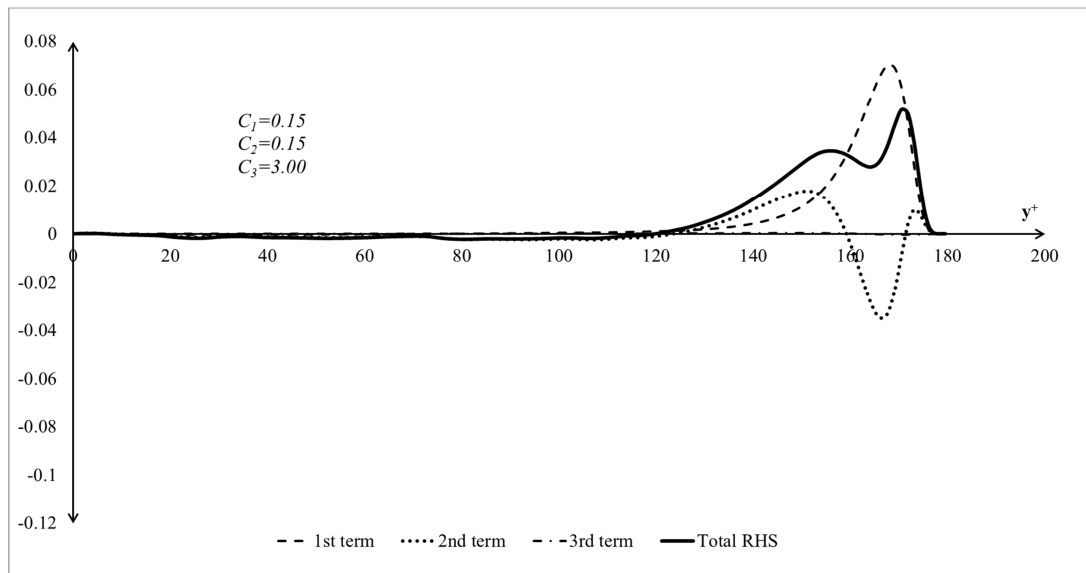


Figure 3.8 RHS of Eq (3.30) for default values of C_1 , C_2 and C_3 .

For the default values of the constants, the third term has negligible effect on the RHS terms. It can be observed that the scale of the production term is comparable to the scale of the diffusion term. However, an adjustment is necessary to have a total zero for the RHS terms. Effects of changing the default values of the constants can be seen in Figure 3.9.

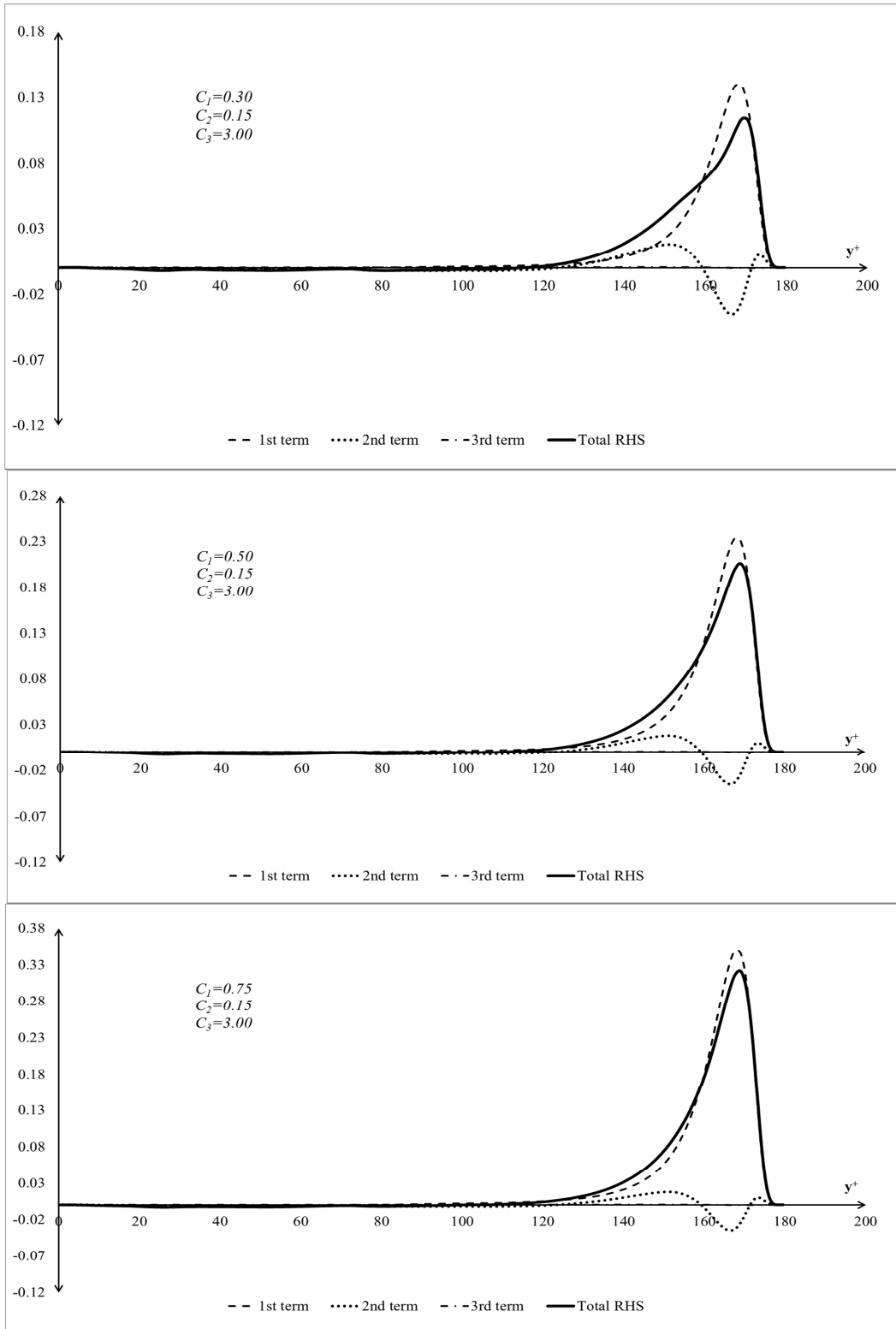


Figure 3.9 RHS of Eq (3.30) for different values of C_1 keeping C_2 and C_3 constant.

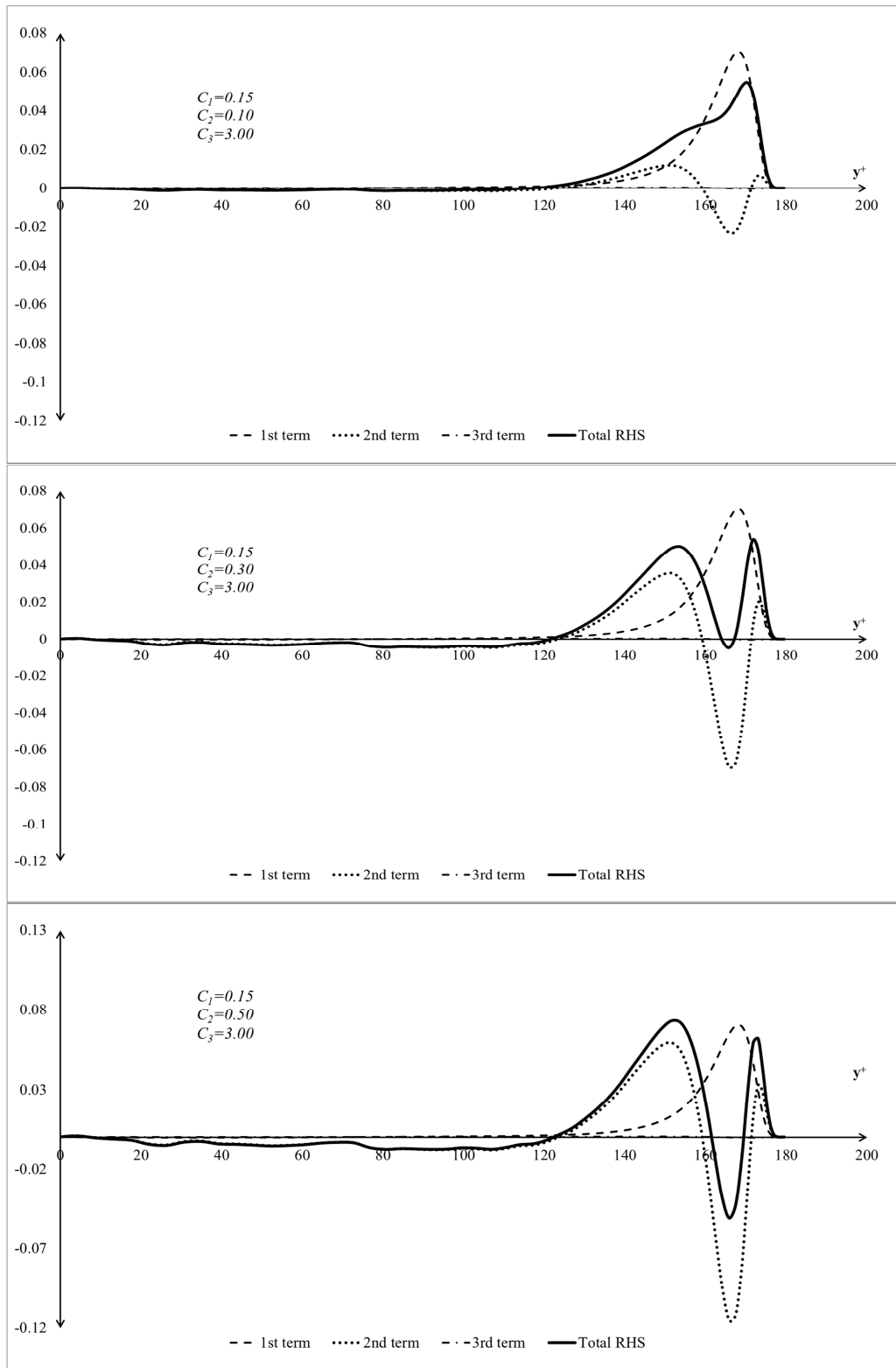


Figure 3.10 RHS of Eq (3.30) for different values of C_2 keeping C_1 and C_3 constant.

It is observed that the order of magnitude of Eq. (3.30) for the channel flow case is 10 times lower compared to Eq. (3.29). In addition, trend analysis for Eq. (3.31) for $\overline{w'T'^2}$ is not performed due to the fact that this term is relatively small compared to the other terms.

One can understand, looking at Figures 3.9 and 3.10, that adjusting the constants for Eq. (3.30) is not trivial. On the other hand, increasing C_2 has an effect of neutralizing the production very close to the wall, but it then introduces another effect around $y^+=140-160$. Therefore, it is decided to check the performance of direct modeling the $\overline{u_i'T'^2}$ term.

Direct modeling of $\overline{u_i'T'^2}$ is given by Eq. (3.17);

$$\overline{u_i'T'^2} = -C_{11} \frac{k}{\varepsilon} (\overline{u_i'u_j'} \frac{\partial(\overline{T'^2})}{\partial x_j} + 2 \overline{u_j'T'} \frac{\partial(\overline{u_i'T'})}{\partial x_j}) \quad (3.17)$$

The resulting passive scalar for $i=1$ and $j=1,2$ is;

$$\overline{u'T'^2} = -C_{11} \frac{k}{\varepsilon} (\overline{u'u'} \frac{\partial(\overline{T'^2})}{\partial x} + 2 \overline{u'T'} \frac{\partial(\overline{u'T'})}{\partial x} + \overline{u'v'} \frac{\partial(\overline{T'^2})}{\partial y} + 2 \overline{v'T'} \frac{\partial(\overline{u'T'})}{\partial y}) \quad (3.38)$$

The first two terms of Eq. (3.38) are zero due to zero derivatives in x direction. Default value of for the constant C_{11} is 0.11 as given in Schiestel [65]. Figure 3.11 presents the comparison of the LHS vs. RHS of Eq. (3.38).

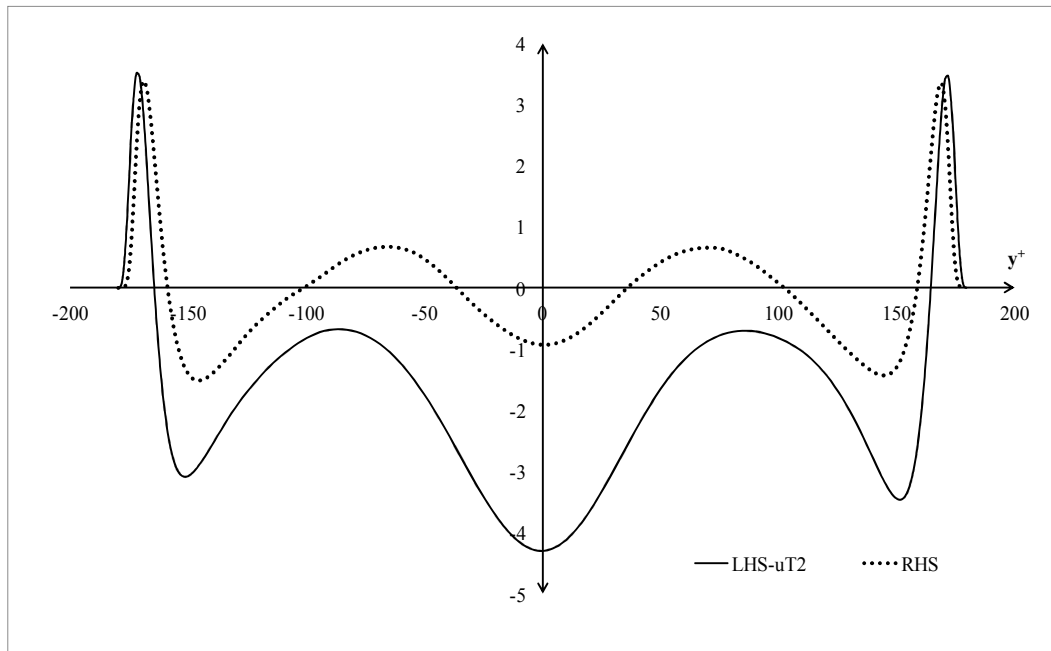


Figure 3.11 LHS vs. RHS of Eq (3.38) for default values of C_{11} .

Figure 3.11 shows that the trend fit between the both sides of the equation is very good, however an adjustment for C_{11} is necessary. Figure 3.12 presents the results for different values of C_{11} .

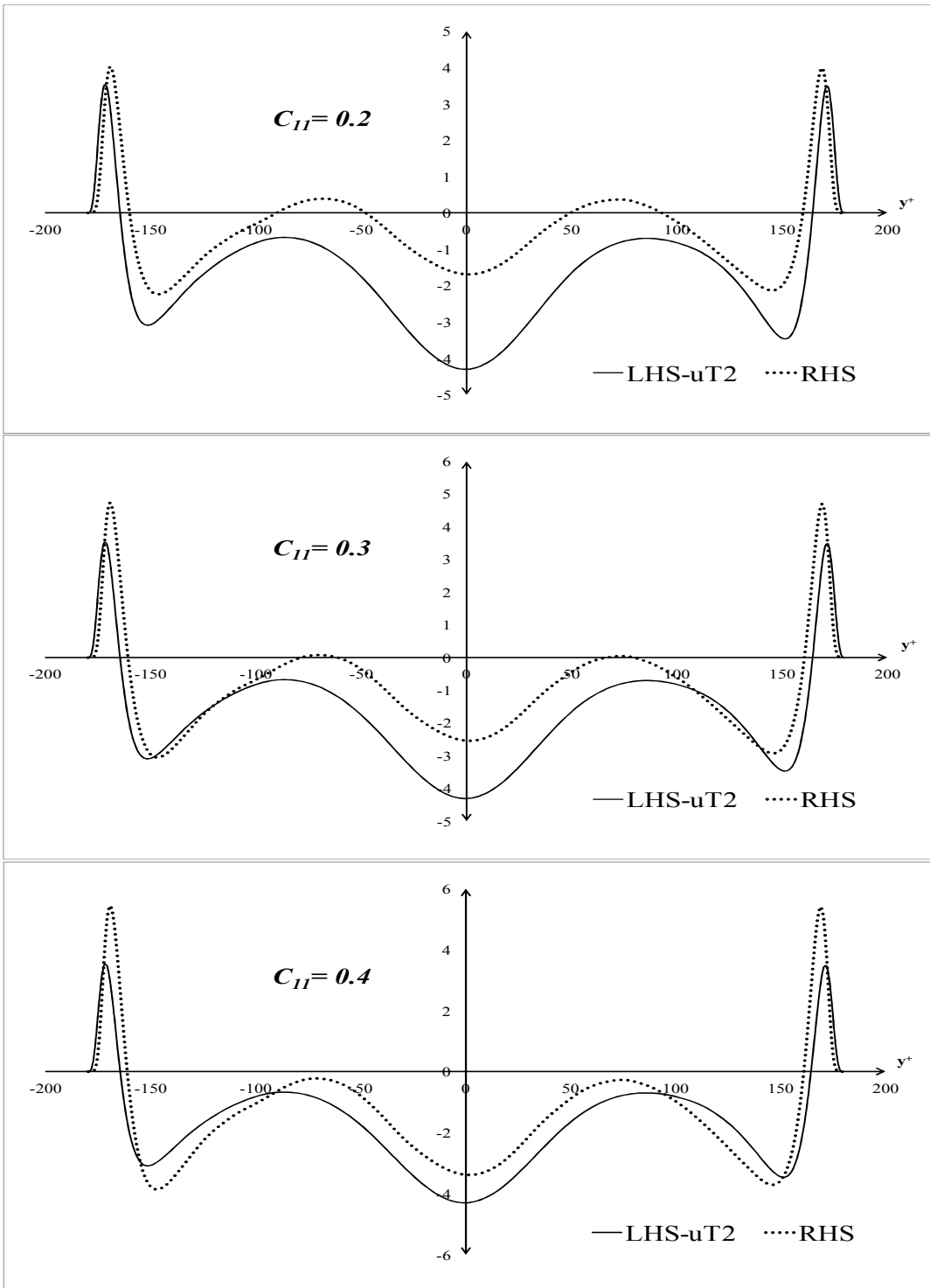


Figure 3.12 LHS vs. RHS of Eq (3.38) for different values of C_{11} .

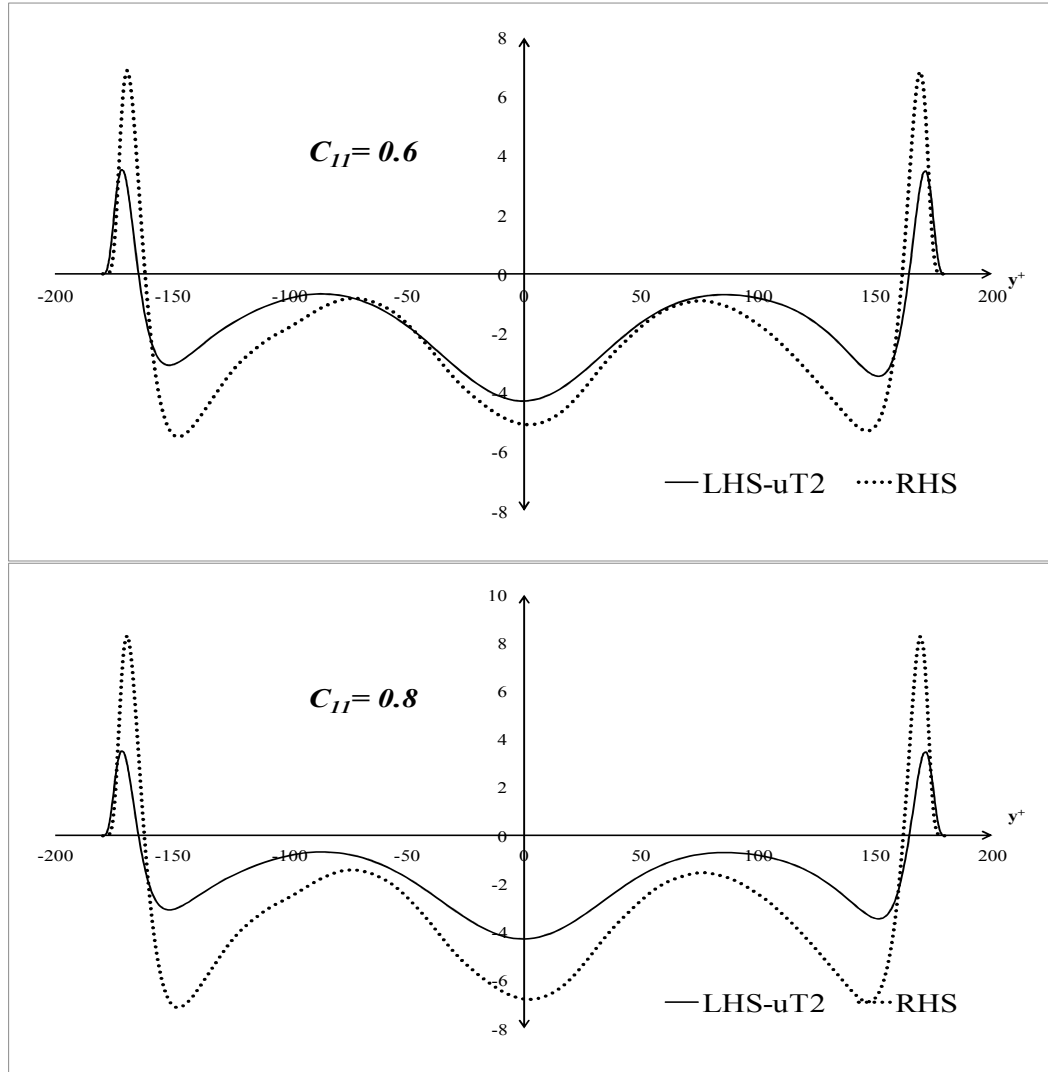


Figure 3.13 LHS vs. RHS of Eq (3.38) for different values of C_{11} .

An analysis of Figure 3.13 reveals the fact that increasing C_{11} has a negative effect on the near wall region, whereas it has a positive effect for the regions far from the boundaries. For example $C_{11}=0.4-0.6$ have very good match around the centerline but the fit is not as good as $C_{11}=0.2-0.3$ for the near wall region.

Similar trend analysis can be performed for $\overline{v'T'^2}$ as well which is given below:

$$\overline{v'T'^2} = -C_{11} \frac{k}{\varepsilon} \left(\overline{u'v'} \frac{\partial(\overline{T'^2})}{\partial x} + 2 \overline{v'T'} \frac{\partial(\overline{u'T'})}{\partial x} + \overline{v'v'} \frac{\partial(\overline{T'^2})}{\partial y} + 2 \overline{v'T'} \frac{\partial(\overline{v'T'})}{\partial y} \right) \quad (3.39)$$

For the default value of C_{11} the following plot is obtained.

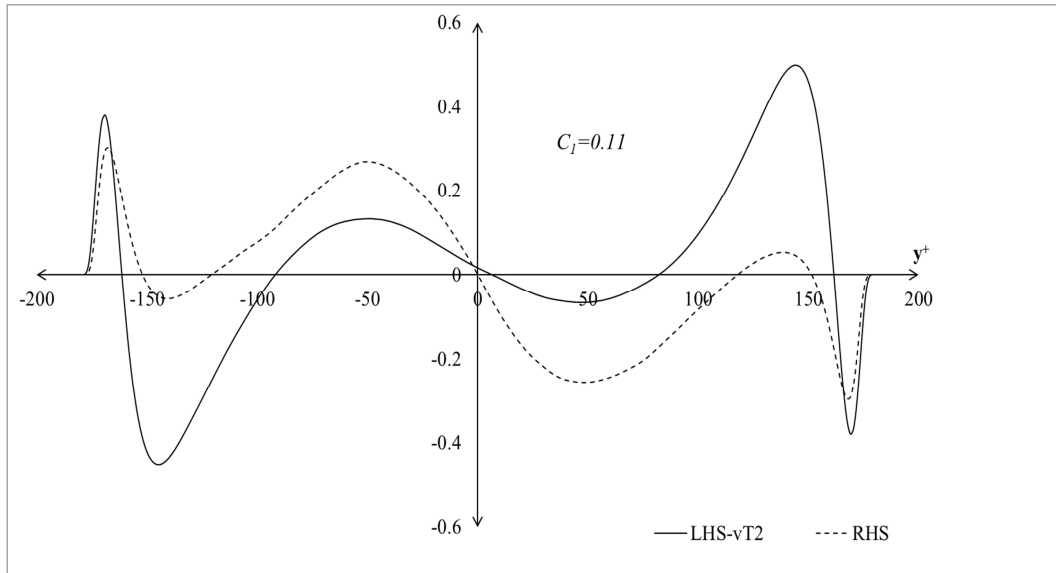


Figure 3.14 LHS vs. RHS of Eq (3.39) for default value of C_{11} .

In the flowing plots, C_{11} is adjusted to have a better fit. C_{11} is changed from 0.02 to 0.08. Decreasing C_{11} has a flattening effect on the RHS terms. This can be observed from Figure 3.15. However, a better fit is obtained increasing C_{11} especially in the near wall regions but at the same time, deviation increases approaching the centerline of the flow. It is not possible to obtain a reasonable fit either for $\overline{u'T'^2}$ or $\overline{v'T'^2}$ using algebraic models.

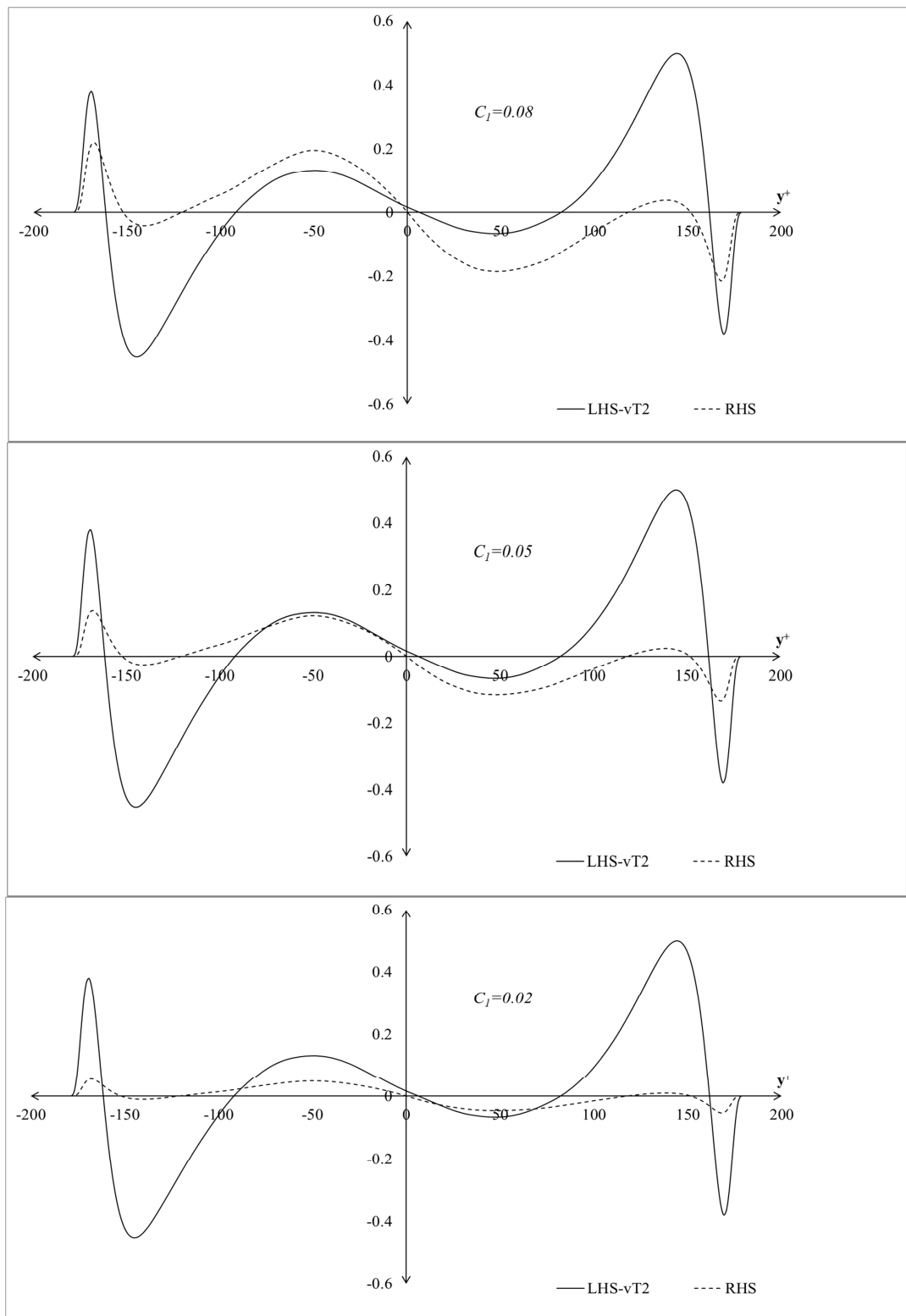


Figure 3.15 LHS vs. RHS of Eq (3.39) for different values of C_{I1} .

A comparison of the performances for the transport equation and the direct model of $\overline{u_i'T'^2}$ shows that the direct modeling is better than the transport equation. This might be due to $\overline{u_i'u_j'T'^2}$ term for which there is no model equation available. The performance of the transport equation for $\overline{u_i'T'^2}$ can later be evaluated if a reliable model for $\overline{u_i'u_j'T'^2}$ is developed. However, for the completeness of the modeling strategy, $\overline{u_i'T'^2}$ is modeled with the transport equations and the results coming from the solution of the transport equation are utilized in the following section.

3.2.3.2 Results for $\overline{u_i'T'}$

After finalizing the analysis for $\overline{u_i'T'^2}$ the same procedure will be applied for $\overline{u_i'T'}$ related terms.

The equation for $\overline{u'T'}$ is given as;

$$0 = -(1 - C_6) (\overline{u'T'}) \frac{\partial \bar{U}}{\partial y} - \overline{u'v'} \frac{\partial \bar{T}}{\partial y} + C_7 \frac{k}{\varepsilon} \frac{\partial}{\partial x_j} (\overline{v'v'} \frac{\partial (\overline{u'T'})}{\partial y}) - \frac{C_8 (\overline{u'T'})}{\rho k} \varepsilon \quad (3.32)$$

The first two terms are mechanical and thermal production terms respectively whereas the third term is coming from turbulent diffusion. The last term is coming from modeling of the fluctuating pressure-temperature correlation [25].

Default values for the constants are given as [25] [26];

$$C_6 = 0.55, C_7 = 0.15 \text{ and } C_8 = 3.50$$

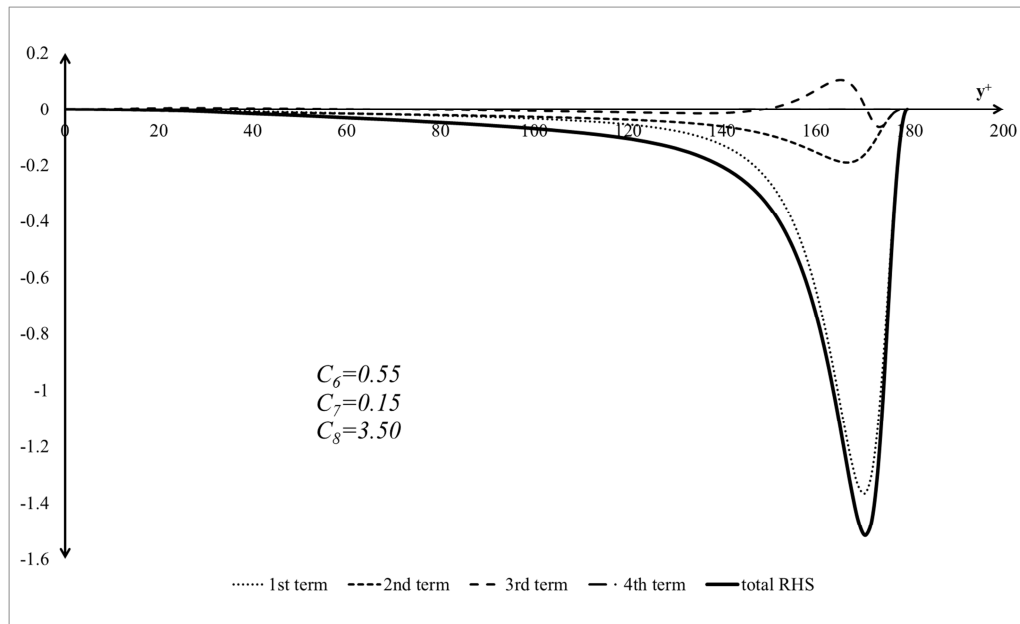


Figure 3.16 RHS of Eq (3.32) for default values of C_6 , C_7 and C_8 .

A first glance at Figure 3.16 reveals that the effect of the mechanical production term is much more dominant than the other terms. Therefore, an effort to minimize this term will lead to zero RHS of Eq. (3.32). C_6 is chosen as 0.9 in order to cancel out the effect of this term as shown in Figure 3.17.

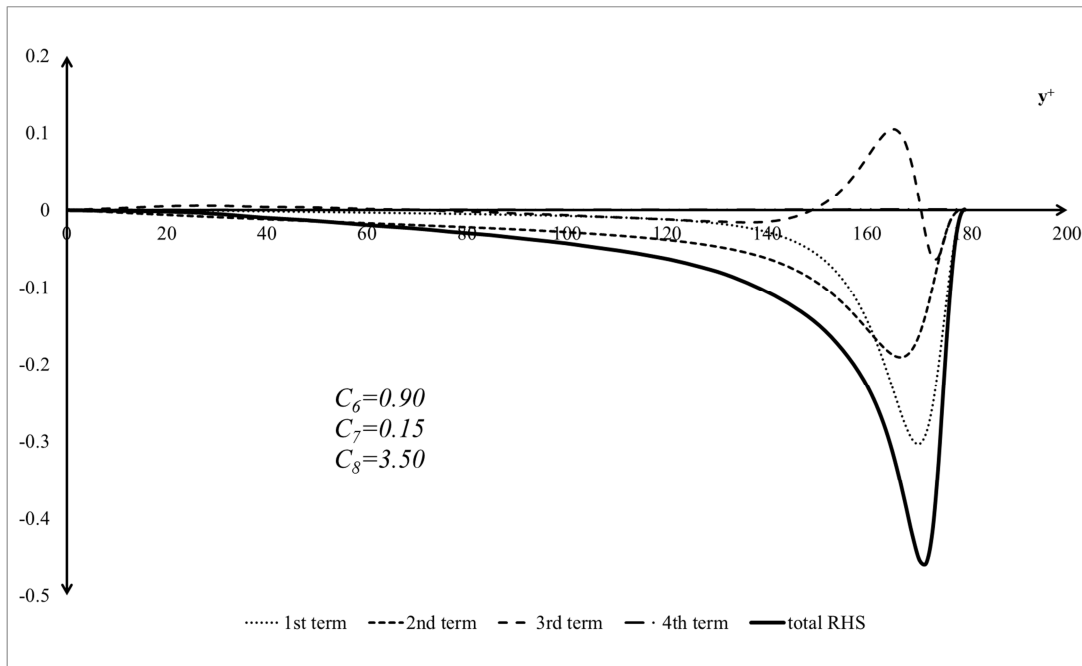


Figure 3.17 RHS of Eq (3.32) for default values of C_7 and C_8 and for $C_6=0.9$.

Although the scale of the production term is decreased, it is still very dominant over the other terms. Therefore, it would only be possible to cancel out this term choosing $C_6=1.0$. Comparison of the other terms is performed with $C_6=1.0$ in Figure 3.18.

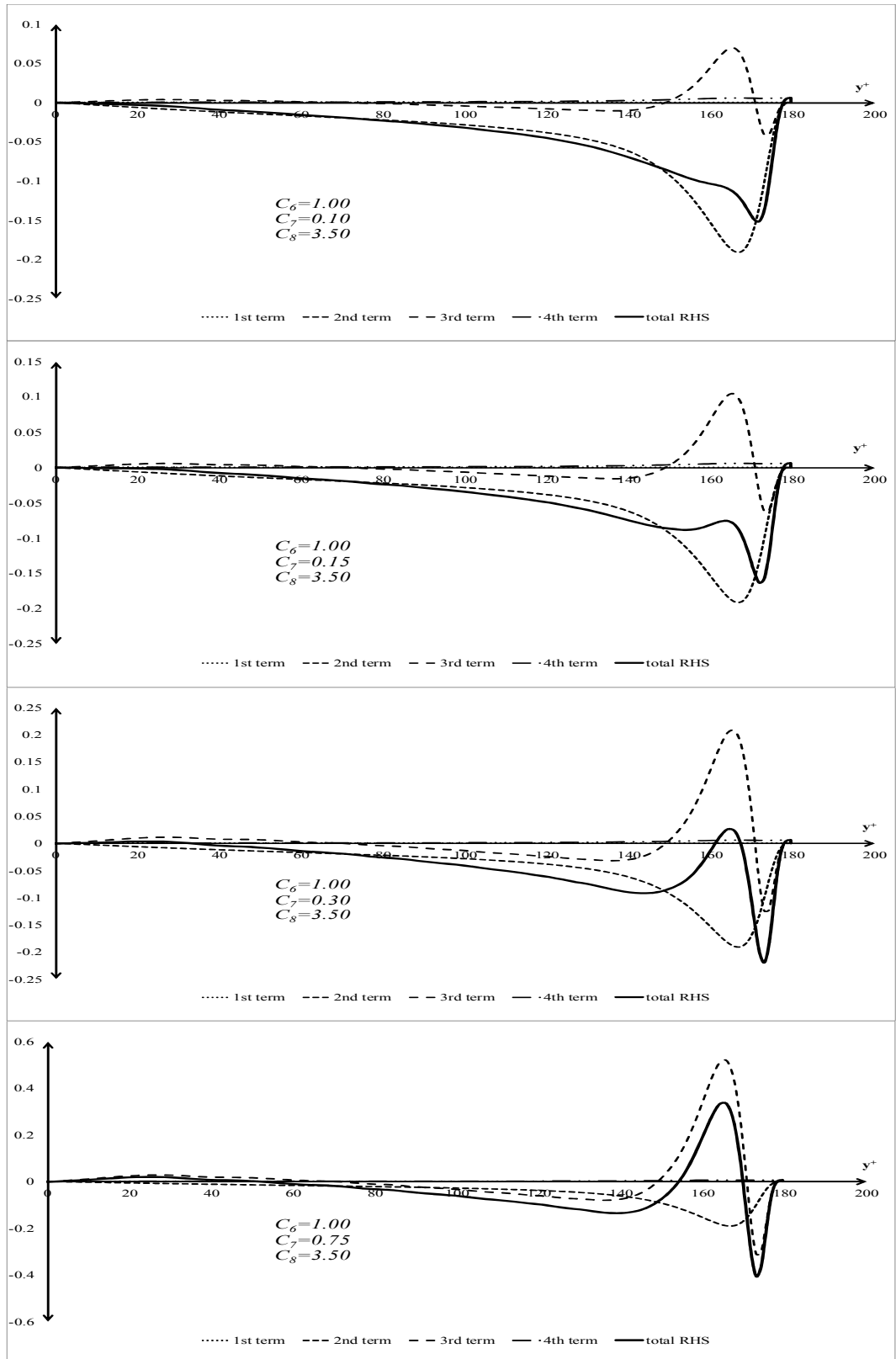


Figure 3.18 RHS of Eq (3.32) for different values of C_7 and C_8 and for $C_6 = 1.0$.

Eliminating the production term and adjusting the constant for the turbulent diffusion transport term is not satisfactory to get a zero value around the wall regions. Therefore, for this case only the following set of constants are selected;

$$C_6 = 0.90, C_7 = 0.75 \text{ and } C_8 = 3.50$$

The consequence of selecting the constants above will be evaluated later during their application in the benchmark case.

The number of RHS terms for $\overline{v'T'}$ is three as in the case of Eq. (3.30) since the mean velocity in y direction is zero for the channel flow case.

$$0 = -\overline{v'v'} \frac{\partial \bar{T}}{\partial y} + C_7 \frac{k}{\varepsilon} \frac{\partial}{\partial x_j} \left(\overline{v'v'} \frac{\partial (\overline{v'T'})}{\partial y} \right) - \frac{C_8}{\rho} \frac{(\overline{v'T'})}{k} \varepsilon \quad (3.33)$$

Default constants for Eq. (3.33) are [25] [26];

$$C_7 = 0.15 \text{ and } C_8 = 3.50$$

Figure 3.19 represents the RHS of Eq. (3.33) for default values of C_7 and C_8 . In the absence of the mechanical production term, thermal production term is the dominating one. In comparison to thermal production term, the other two terms being the turbulent diffusion transport and the term coming from the modeling of fluctuating pressure-temperature correlation are relatively smaller. However, a further analysis, as shown in Figure 3.20, is performed to see the effect of changing C_7 .

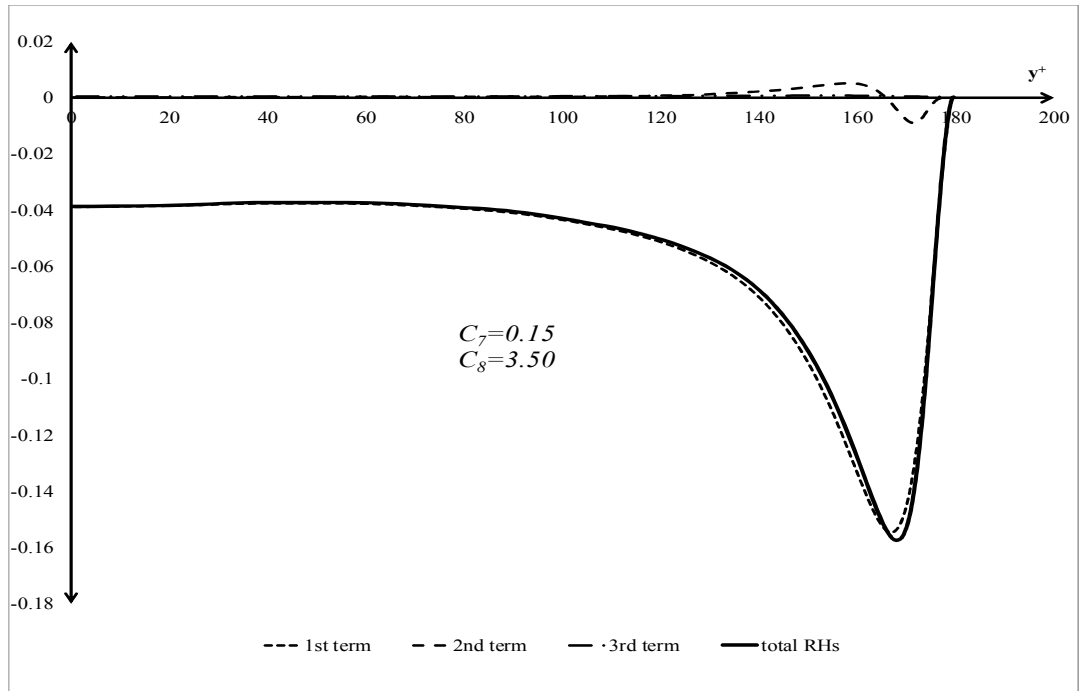


Figure 3.19 RHS of Eq (3.33) for default values of C_7 and C_8 .

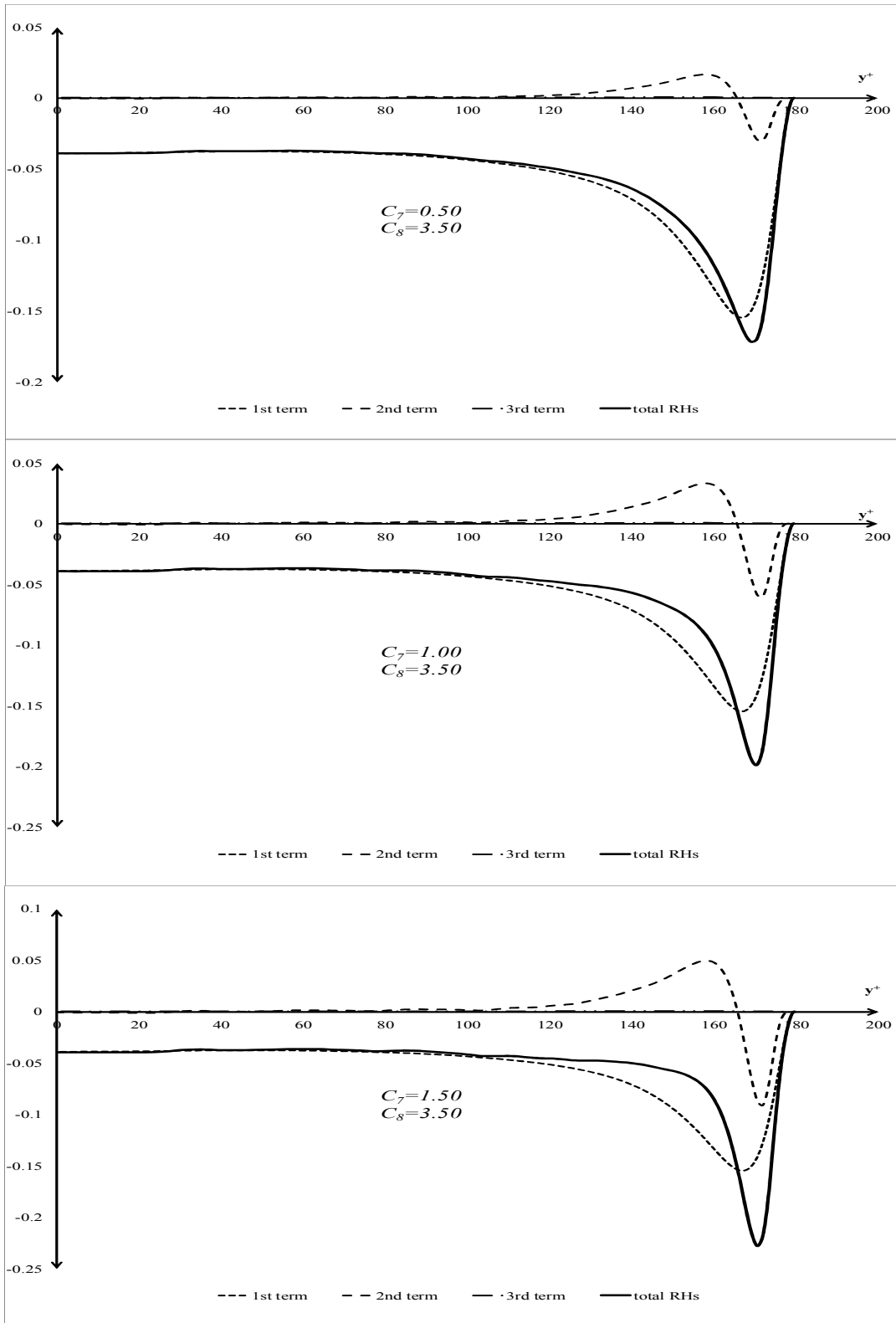


Figure 3.20 RHS of Eq (3.33) for different values of C_7 and for $C_8=3.5$.

Increasing C_7 has a neutralizing effect for $y^+ = 140-160$ but it increases the near wall effect as in Eq. (3.30). It also observed that the scale of Eq. (3.33) is around 5 times smaller than Eq. (3.32). Another observation is that, as opposed to other equations, there is a constant deviation from zero for Eq. (3.33) due to thermal production term. Although, the order of magnitude for this term is very small, it is an interesting feature that has not been observed before.

3.2.3.3 Results for $\overline{T'^2}$

After finalizing the evaluation of the correlations involving velocity, the final analysis will be performed for Eq. (3.35) for the square of the fluctuating temperature term.

$$0 = -2\overline{v'T'}\frac{\partial\bar{T}}{\partial y} - \frac{1}{2C_9}\frac{\overline{T'^2}}{2k}\varepsilon + C_{10}\frac{k}{\varepsilon}\left\{\frac{\partial}{\partial y}\left(\overline{v'v'}\frac{\partial(\overline{T'^2})}{\partial y}\right)\right\} \quad (3.35)$$

Default constants for Eq. (3.35) are given as;

$$C_9 = 0.50 \text{ and } C_{10} = 0.20$$

The results of Eq. (3.35) for the default constants are shown in Figure 3.21.

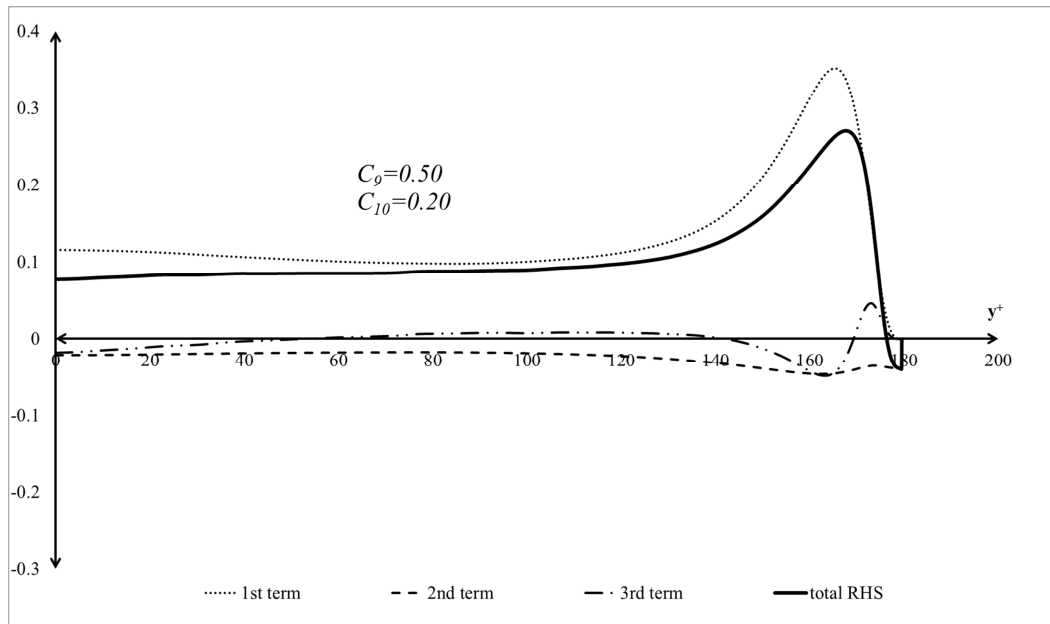


Figure 3.21 RHS of Eq (3.35) for default values of C_9 and C_{10} .

Similar trend as observed for Eq. (3.33) can be seen in Figure 3.21 for Eq. (3.35). There is a constant deviation from zero and the dominating term is the thermal production term. In order to have a better understanding of the other terms an adjustment study is performed as shown in Figures 3.22 and 3.23.

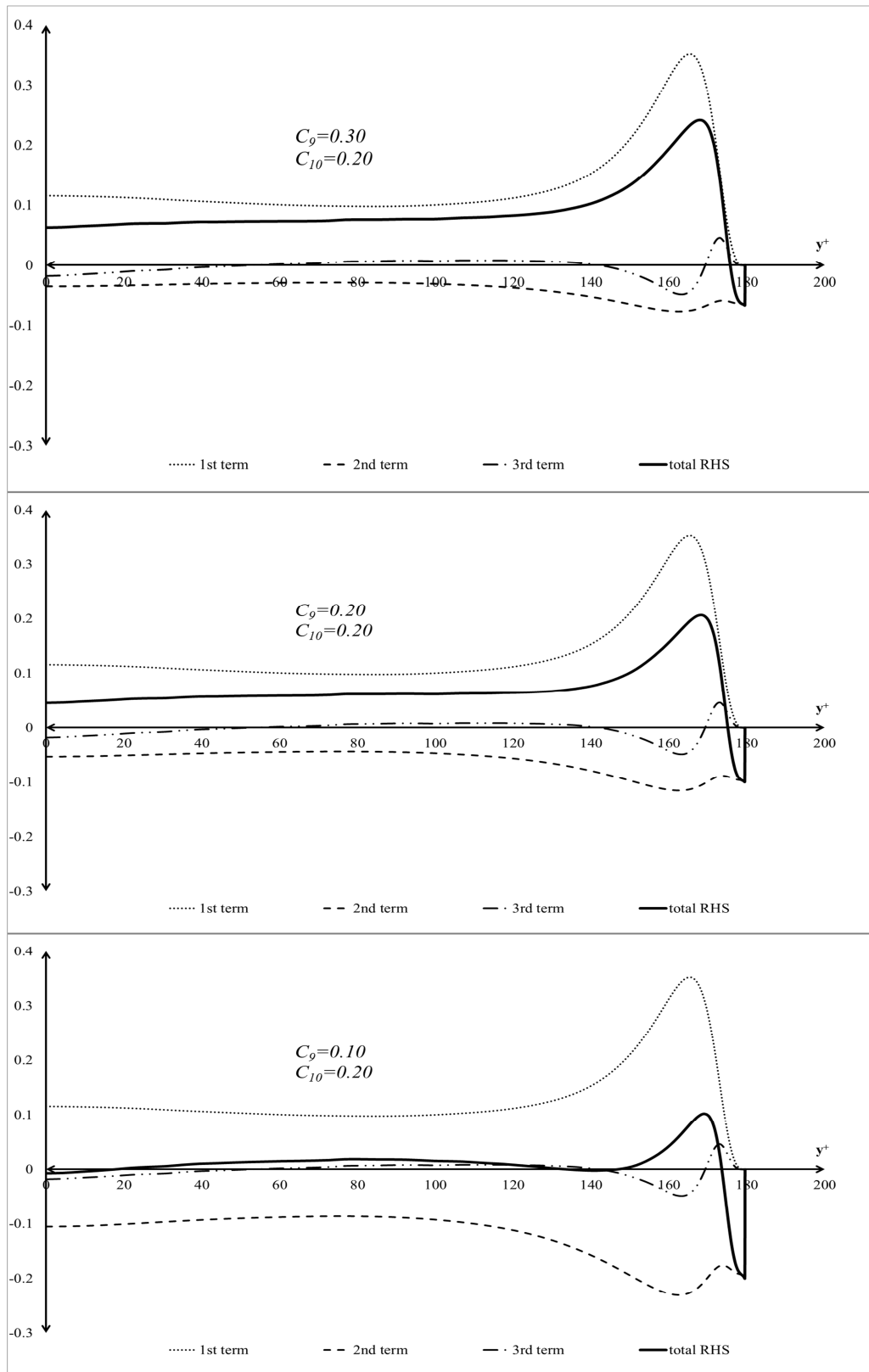


Figure 3.22 RHS of Eq (3.35) for different values of C_9 and for $C_{10}=0.20$.

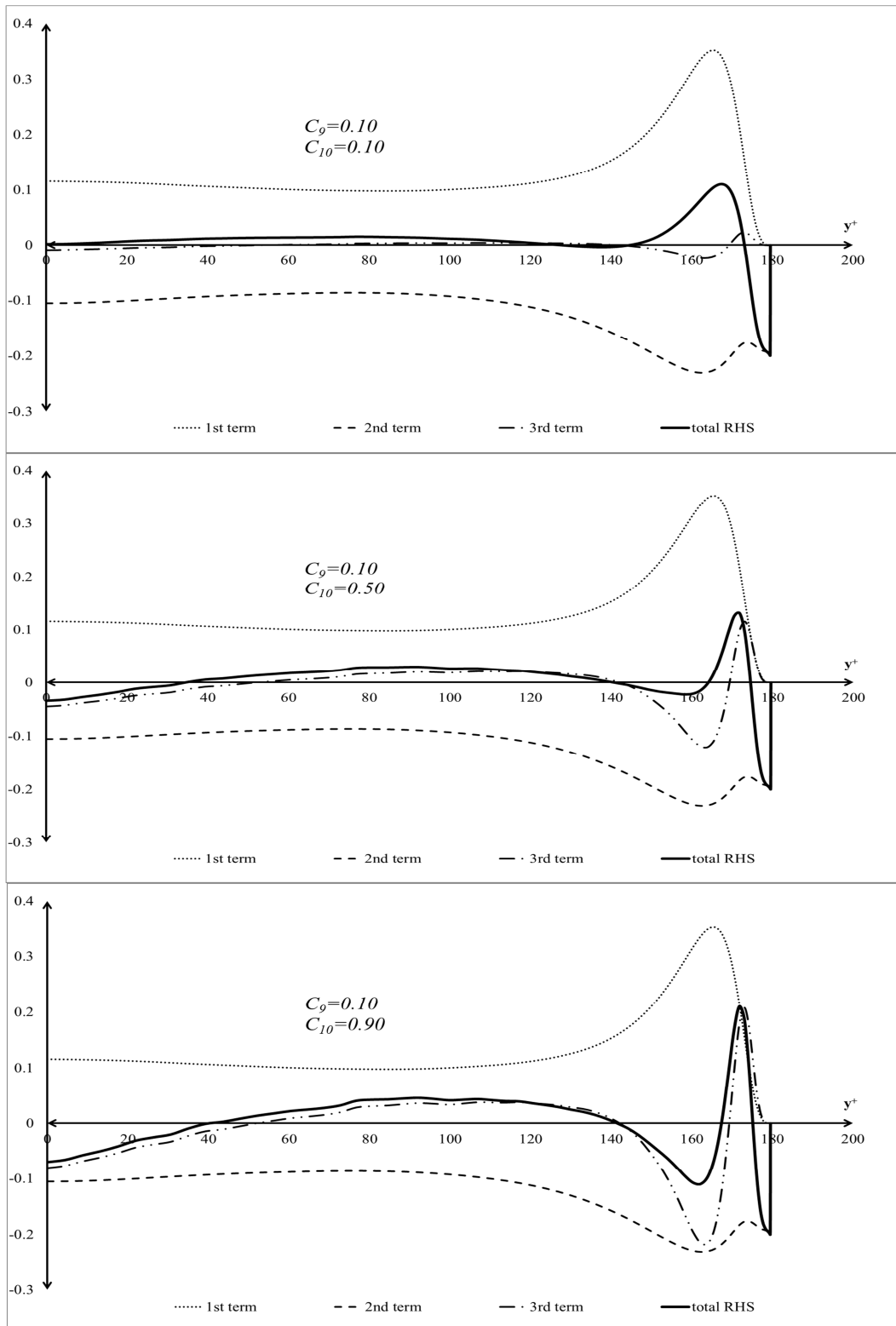


Figure 3.23 RHS of Eq (3.35) for different values of C_{10} and for $C_9=0.10$.

New constants for Eq. (3.35) are chosen as;

$$C_9 = 0.10 \text{ and } C_{10} = 0.10$$

As a result of the a-priori testing the following conclusions have been reached:

- For most of the equations default constants had to be changed with new ones to match the model results to the DNS data.
- It is clearly observed that the model equations do not perform well in the near wall regions.
- DNS data utilized here is a flow case which does not include a mean streamwise pressure gradient and no curvature effects are considered. Therefore one must be cautious when applying these models to cases like turbomachinery cascade flows. Scotti and Piomelli [67] evaluated different turbulence models using a-priori testing with DNS and LES data. *Marquillie et al.* performed a DNS study of a channel with curved surface for a moderate Reynolds number [68]. The results of the models could be modified in case a DNS database with curvature effects is obtained. However, only modifying the existing constants or models from the results of DNS studies with curvature effects might be misleading. This has to be investigated thoroughly.
- For the adjustment of the constants, only general trend analysis is applied. For the channel flow case, the equations of interest are overdetermined. In the literature there are methods to calculate the constants for an overdetermined case. One possibility is to calculate the coefficients using matrix representation as shown below in Eq. (3.38):

$$\begin{pmatrix} a_1 & b_1 & c_1 \\ a_2 & b_2 & c_2 \\ \vdots & \ddots & \vdots \\ a_n & b_n & c_n \end{pmatrix} \begin{pmatrix} C_{2T} \\ C_{1T} \\ C_T \end{pmatrix} = \begin{pmatrix} 1^{st} \text{ term}_1 \\ 1^{st} \text{ term}_2 \\ \vdots \\ 1^{st} \text{ term}_n \end{pmatrix} \quad (3.38)$$

This representation is of the form $Ax = B$ but matrix A is not in diagonal form. Therefore first it has to be transformed into a diagonal matrix using its transpose and then the solution can be obtained with the inverse of the diagonal matrix.

$$(A^T A)^{-1} (A^T A)x = A^{-1} A^T B \xrightarrow{\text{yields}} x = A^{-1} A^T B \quad (3.39)$$

Solution of Eq. (3.39) will give the coefficient matrix x which is composed of the constants for the model equations.

- Although, the near wall region performance is poor, general trend fit between the model and DNS results is observed. The way to improve the near wall performance shall be checked during future studies.
- For the channel flow case, production terms are more dominant than the diffusion terms. The effect of production terms are clearly seen in the near wall region.
- Scales of turbulent effects are dominant in the streamwise direction for the channel flow case. The scales are 5-10 times smaller in the spanwise direction. However, this might not be the case for other flow cases. Therefore, flow characteristics of each flow shall be evaluated separately.
- Turbulent terms can also be modeled using algebraic models. An example of this is performed in Section 3.2.4.3 for $\overline{u_i' T'^2}$. There are several algebraic models for $\overline{u_i' T'}$ as well. One of the famous ones can be obtained through Reynolds' analogy:

$$\overline{u_i' T'} = -\frac{k_t}{\rho C_p} \frac{\partial \bar{T}}{\partial x_i} \quad (3.40)$$

Modeling of the turbulent terms using algebraic equations are easier and require less computational power. However, transport equations contain more terms compared to algebraic models which enable them to capture more turbulence related physics.

CHAPTER 4

DIRECT AND APPROXIMATE LOCAL ENTROPY CALCULATION FOR A NON-ISOTHERMAL AXIAL TURBINE CASCADE

This chapter presents a sample application of the direct and approximate local entropy calculation on a non-isothermal axial turbine cascade. The local entropy generation calculations are obtained by solving the direct and approximate forms of the RAET equation. Keep in mind that the approximate equation does not include any turbulence related terms. The direct solution involves the solution of additional model transport equations related to the velocity-temperature fluctuations as presented in the previous chapters.

4.1 Cascade Geometry

The two dimensional cascade geometry is given in Natalini and Sciubba [6]. This is an air-cooled turbine stator cascade. For the purpose of this study, the air cooling holes inside blade have not been modeled, but the blade surface is kept at constant temperature. A generic representation of the geometry can be seen in Figure 4.1.

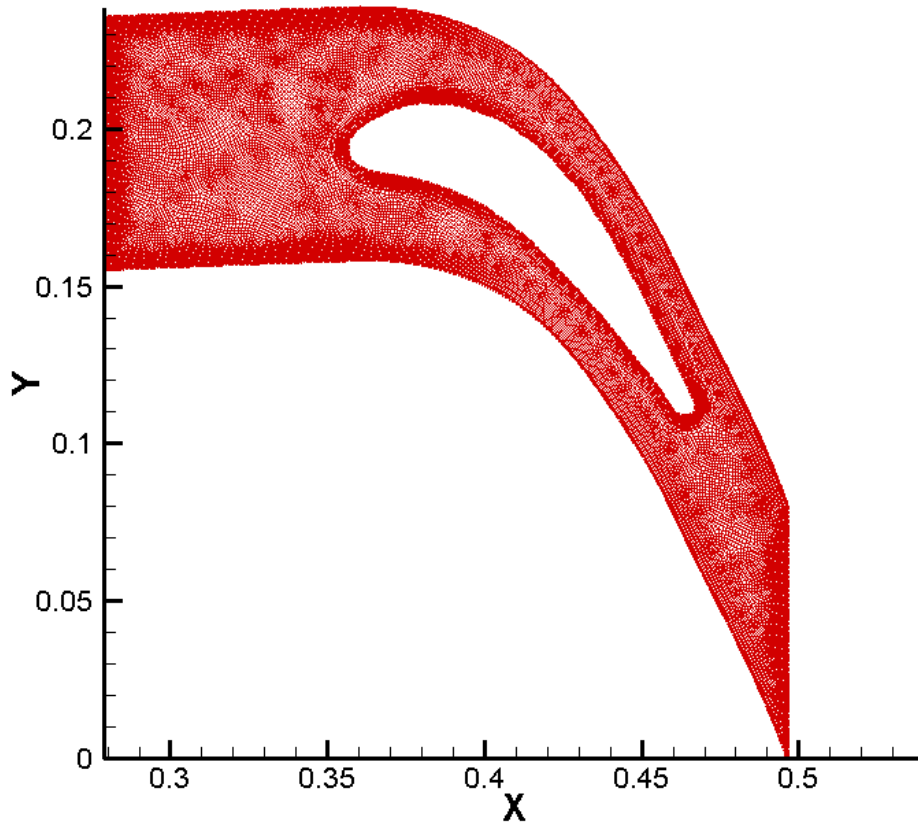


Figure 4.1 Two dimensional cascade geometry in meters.

The governing equations are solved using commercial CFD software Ansys FLUENT version 14.5.

4.2 Boundary Conditions

Velocity inlet is applied as inlet boundary condition and pressure outlet as outlet boundary condition. Upper and lower surfaces are selected as periodic. They are half pitch distance away from the chord representing surfaces exposed to the flow conditions. The details of the applied boundary conditions are given in Figure 4.2.

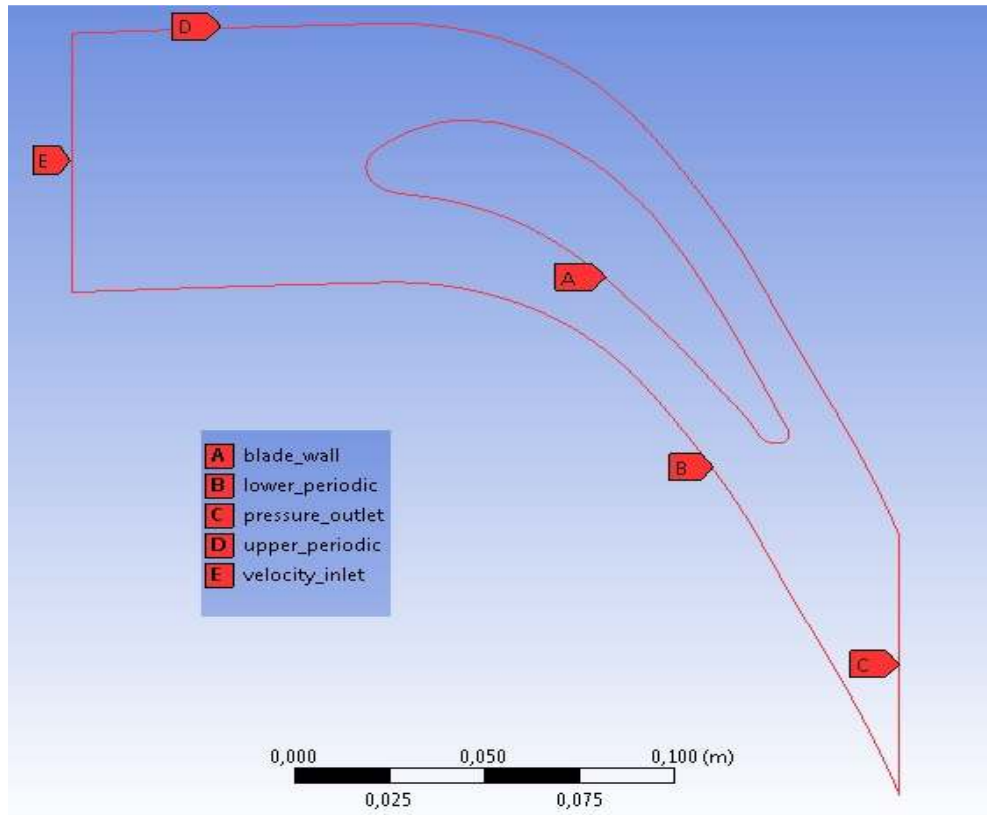


Figure 4.2 Boundary conditions applied to the stator blade.

The boundary conditions are applied as given in [6] such as the blade surface and the air temperatures are 1118 K and 1300 K, respectively. The inlet velocity is $V_g=103$ m/s. The inlet conditions for turbulence are $k_g=0.01 V_g^2$ and $\epsilon_g=0.006 V_g^2$ for the turbulent kinetic energy and dissipation rate of turbulent kinetic energy, respectively.

After identifying the geometry together with the boundary conditions, a mesh is generated which is capable of capturing the flow features around the stator blade.

Since the entropy generation involves both the viscous and thermal components, the mesh shall be sufficient enough to capture the viscous effects especially around the blade as seen in Figure 4.3. Therefore, a comparison of the mesh with or without boundary layers is performed. In Figure 4.4, it is possible to visualize both meshes without boundary layers and with boundary layers.

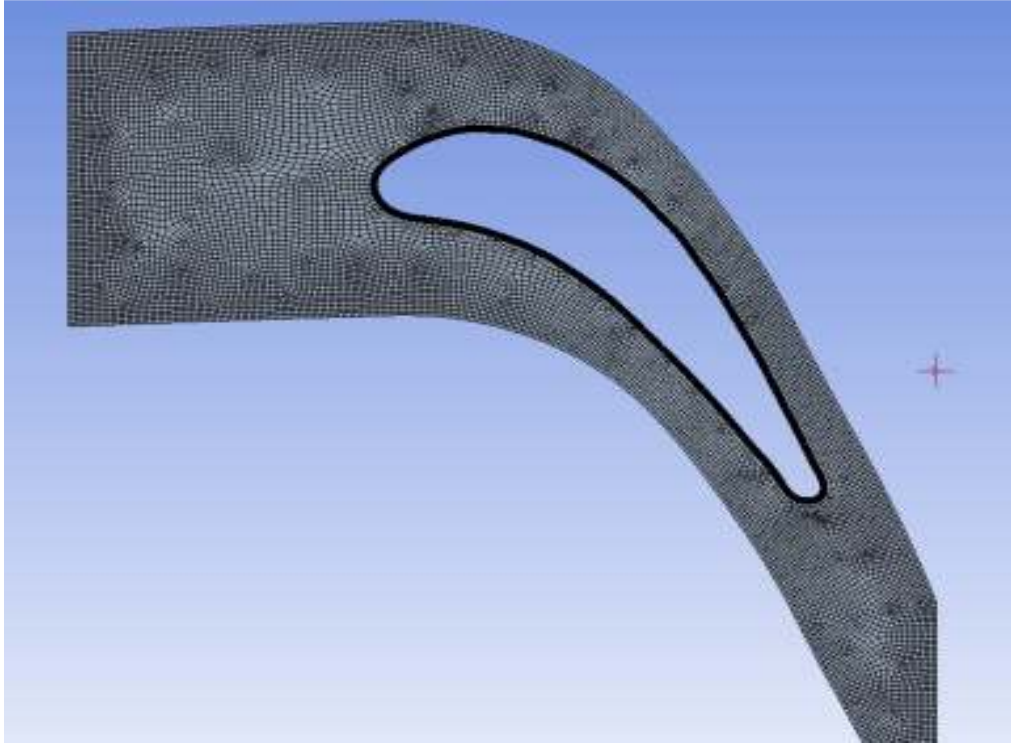


Figure 4.3 Overall view of the mesh generated.

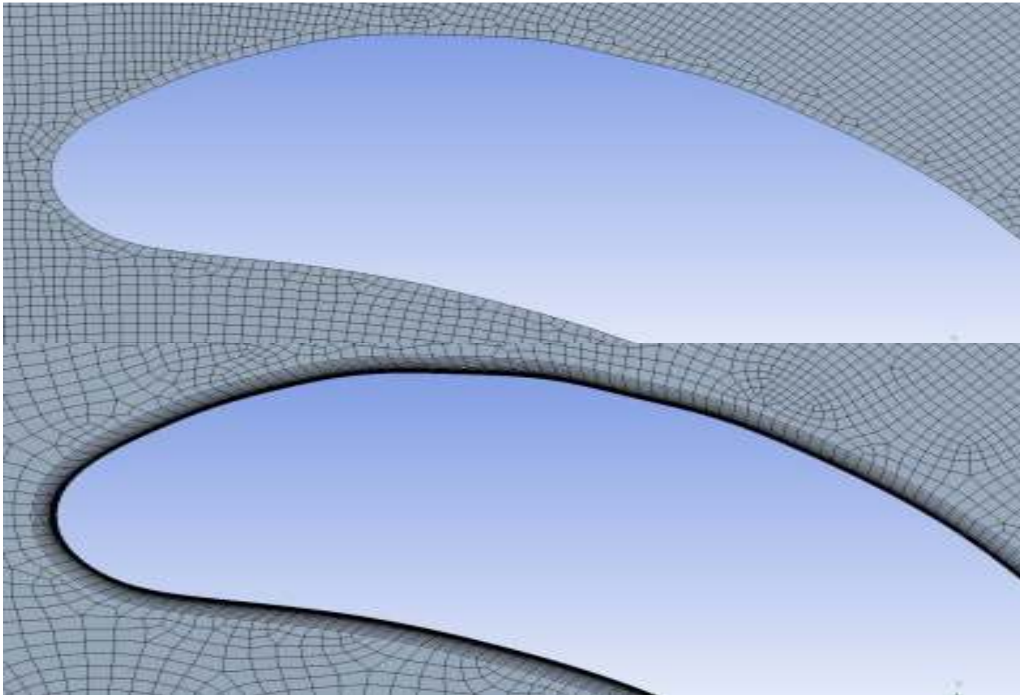


Figure 4.4 Mesh around the blade. upper: no BL, lower: with 20 levels of BL.

In order to obtain a wall y^+ value around 1, a boundary of 20 layers is attached for the accurate calculation of especially the viscous phenomena. Approximately 35000 elements are used. The number of grid points is decided after a grid convergence study up to about 50000 elements, which showed that the calculated total entropy generation rate values do not change much after about 35000 elements.

Grid convergence is decided after checking different models with different number of cells. Figure 4.5 presents the velocity magnitude on a line passing through the wake region of the flow. It is clearly evident from Figure 4.5 that, there is a sharp change between the model with 20899 elements and the model with 35117 elements. However, that deviation cannot be observed clearly between the models with 35117 and 51195 elements. Therefore, it is decided to continue with the model containing 35117 elements for further studies.

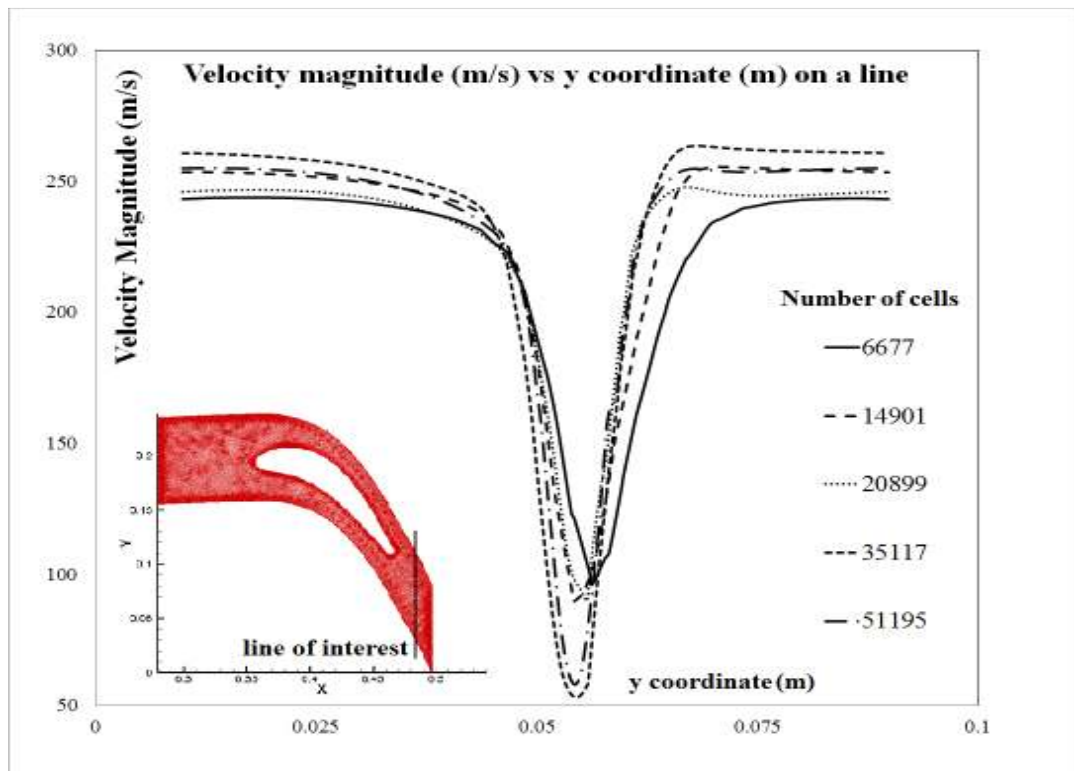


Figure 4.5 Velocity profiles on a line at the wake region with respect to number of cells.

4.3 Results

After it is decided that a satisfactory mesh is obtained with sufficient number of elements, the flow field around the stator blade cascade is solved using a pressure based solver. As turbulence model, Reynolds Stress Model (RSM) is chosen. Reynolds stress model solves the transport equations for the Reynolds stresses, therefore is considered to be more accurate than two or one equation models in most of the flow cases. This is also in line with the aim of this thesis which is to obtain the entropy generation via solving the entropy transport equation. Before solving the transport equations for the passive scalars, a stable solution is obtained solving the continuity, momentum and energy equations. Later, the transport equations are solved and more than 100000 iterations have been performed in order to reach a converged solution.

The effect of additional transport equations on the equations governing the fluid flow is evaluated on the basis of computational time. It has been observed that solution of the entropy transport equation using the direct approach increases the computational time by 15%. This includes solution of the transport equations for turbulent terms $\overline{u_i' T'^2}$, $\overline{u_i' T'}$ and $\overline{T'^2}$.

4.3.1 Calculated Velocity and Pressure Field

Before going into the details of entropy generation calculations, general characteristics of the flow are evaluated. Figure 4.6 and Figure 4.7 show the axial and vertical velocity as well as the velocity magnitude distributions within the cascade. The stagnation regions, high velocity peaks on the blade suction side, the acceleration of the flow through the cascade and the low momentum wake zones are clearly observed from the distributions.

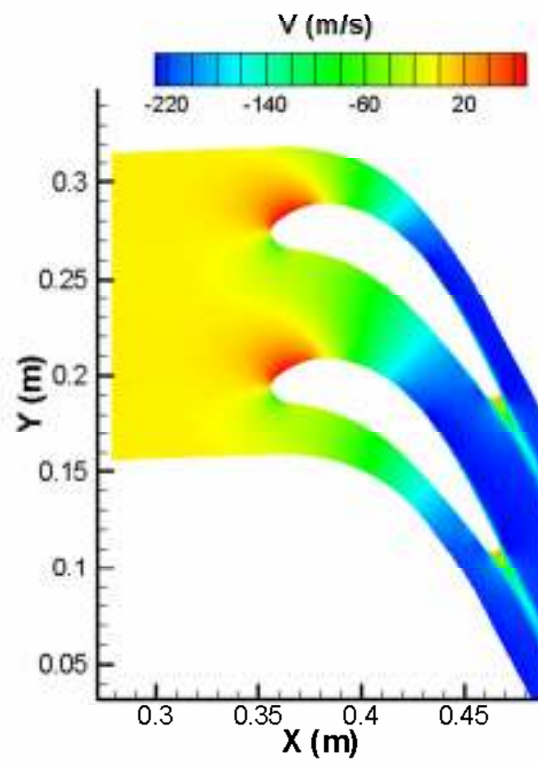
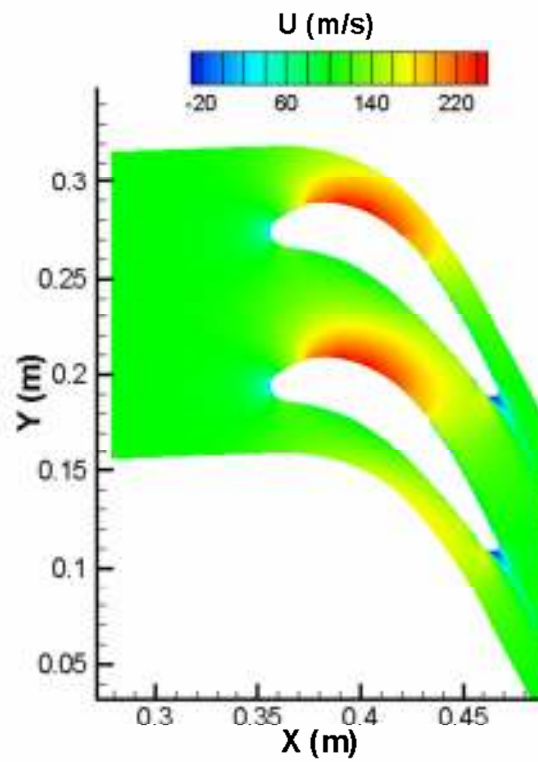


Figure 4.6 Axial and vertical velocity contours around the stator blades.

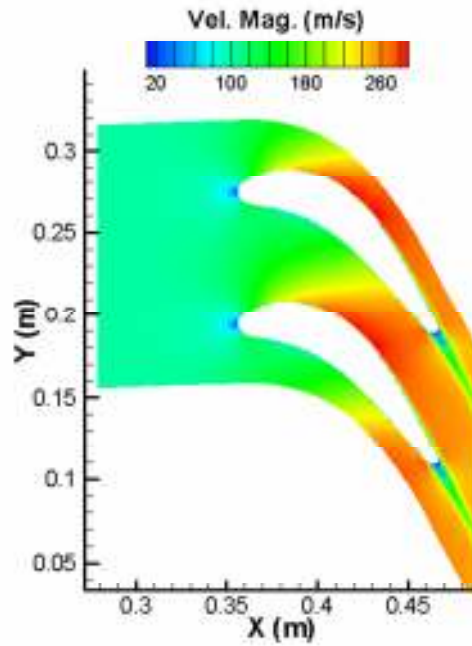


Figure 4.7 Velocity magnitude contours around the stator blades.

On the blade suction surface the boundary layer gets thicker after mid-chord location due to the adverse pressure gradient near the blade surface, which can be seen in the static pressure distribution given in Figure 4.8.

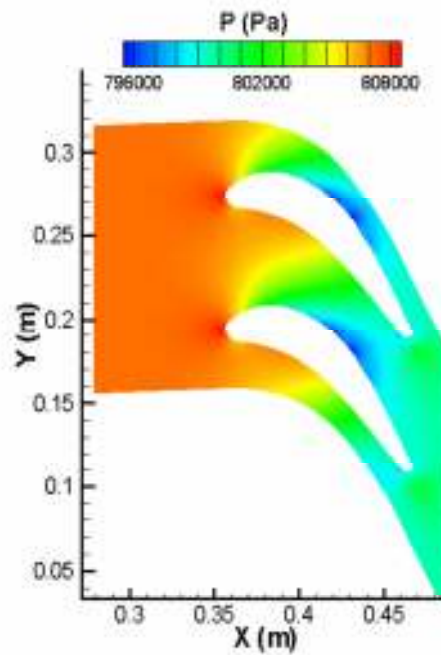


Figure 4.8 Static pressure contours around the stator blades.

The total pressure and total temperature contours are given in Figure 4.9. The loss in total pressure due to blade boundary layers and wakes is clearly visible. General drop in total temperature is observed, which is accentuated within the blade wakes.

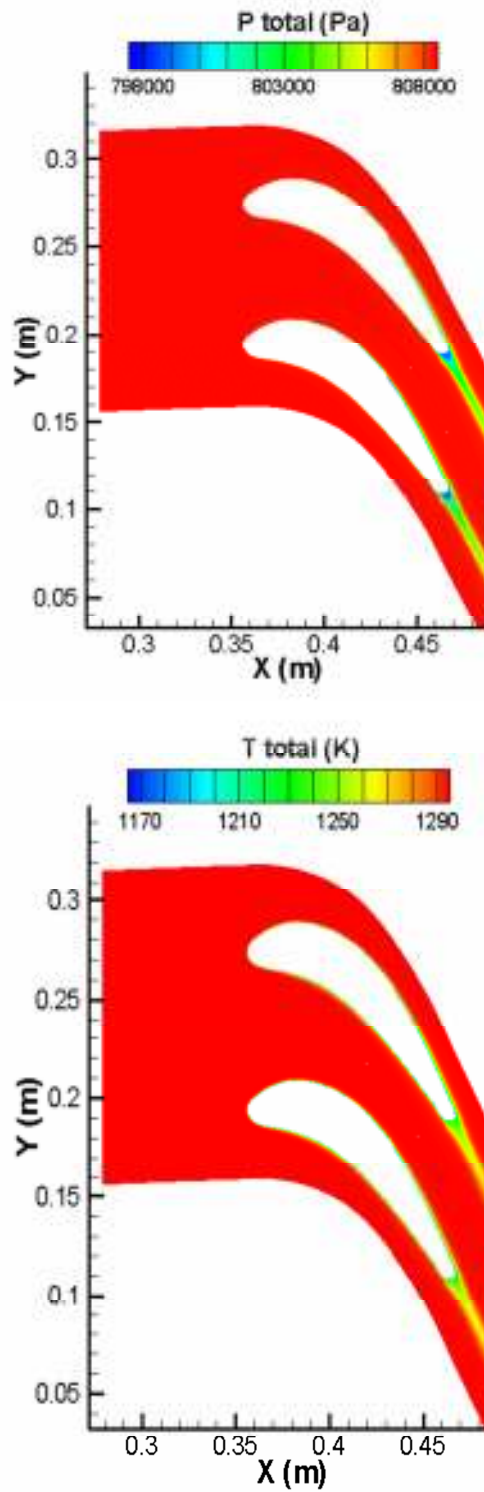


Figure 4.9 Total pressure and temperature contours around the stator blades.

Comparison of the calculated flow field with the study performed by Natalini and Sciubba [6], will be based on contours of Bejan numbers. Bejan number is a useful parameter in understanding the relation between the viscous and thermal entropy generation rates and is defined by formulation given below:

$$s_V = \frac{2}{T} \mu \left\{ \left(\frac{\partial u}{\partial x} \right)^2 + \left(\frac{\partial v}{\partial y} \right)^2 + \frac{1}{2} \left(\frac{\partial u}{\partial y} + \frac{\partial v}{\partial x} \right)^2 \right\} \quad (4.1)$$

$$s_T = \frac{k_{air}}{T^2} \left\{ \left(\frac{\partial T}{\partial x} \right)^2 + \left(\frac{\partial T}{\partial y} \right)^2 \right\} \quad (4.2)$$

$$Be = \frac{s_V}{s_T + s_V} \quad (4.3)$$

where s_V and s_T are viscous and thermal entropy generation respectively.

As defined by Eq. (4.3), Bejan number gives the ratio of the viscous entropy generation rate to total entropy generation rate. Figure 4.10 presents the Bejan number contours around the stator blade. As expected, the viscous entropy generation is seen around the blade since this is the region where high viscous effects are dominant.

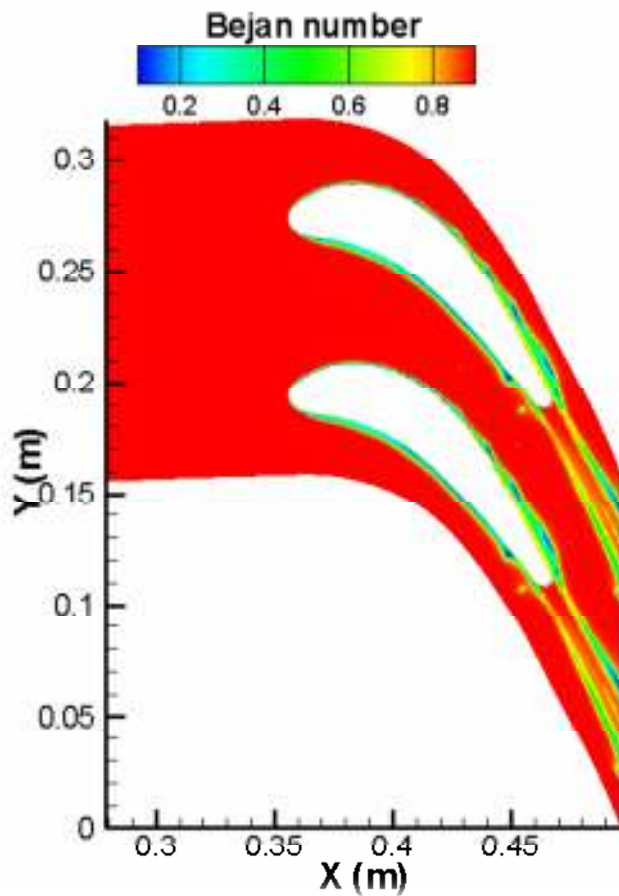


Figure 4.10 Bejan number contours around the stator blade.

A closer view of the Bejan numbers around the blade is given in Figure 4.11. Bejan number has a value of 0.4-0.6 in the vicinity of the wall. This is in accordance with the study performed by Natalini and Sciubba [6]. There are some regions where the Bejan number decreases to 0-0.2. The effect of thermal boundary layer in this region is diminishing whereas viscous effects start dominating. Figure 4.11 indicates that the thermal entropy generation effects are limited to a very thin boundary layer region around the blade. Over this thin boundary layer, viscous effects become dominant in specific regions, especially in some regions around the wake. This is believed to be due to high levels of turbulence being more dominant on the thermal effects.

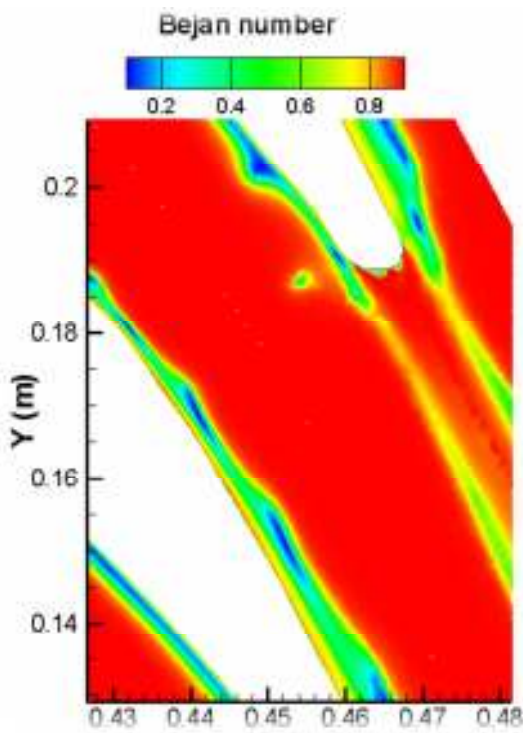
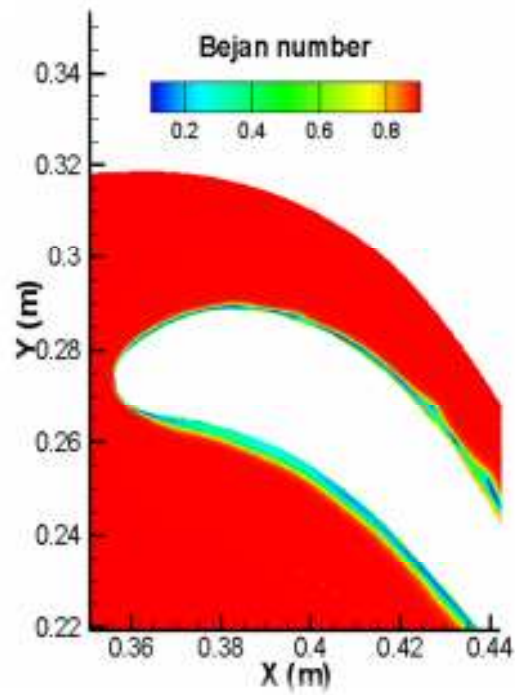


Figure 4.11 Detailed view of Bejan number contours around the stator blade.

4.3.2 Results About Entropy Generation

Entropy transport equation is solved using the UDF (User Defined Function) capability of Ansys Fluent. A total of 6 different transport equations have been solved. These transport equations can be listed as:

$$\begin{aligned}
& \frac{\partial(\rho\bar{s})}{\partial t} + \frac{\partial}{\partial x_i} \left[\rho\bar{u}_i\bar{s} - \frac{k}{C_v} \frac{\partial\bar{s}}{\partial x_i} \right] = \\
& - \frac{\partial}{\partial x_i} (\rho\overline{u_i' s'}) + \frac{k}{\bar{T}^2} \left(\frac{\partial\bar{T}}{\partial x_i} \right)^2 + \frac{k}{\bar{T}^2} \left(\frac{\partial T'}{\partial x_i} \right)^2 + \frac{k}{2} \frac{\partial}{\partial x_i} \left(\frac{1}{\bar{T}} \right) \frac{\partial(T'^2)}{\partial x_i} + \frac{\bar{\tau}_{ij}}{\bar{T}} \frac{\partial\bar{u}_i}{\partial x_j} + \frac{\epsilon}{\bar{T}} - \\
& \left(\frac{\rho}{\bar{T}} \overline{T' u_i'} \frac{\partial\bar{s}}{\partial x_i} \right) - \frac{\rho C_v}{\bar{T}} \bar{u}_i \overline{(T')^2} \frac{\partial}{\partial x_i} \left(\frac{1}{\bar{T}} \right) - \frac{\rho C_v}{2\bar{T}^2} \left(\frac{\partial(T'^2)}{\partial x_i} \right) - \frac{\rho C_v}{\bar{T}} \overline{u_i' (T')^2} \frac{\partial}{\partial x_i} \left(\frac{1}{\bar{T}} \right) - \\
& \frac{\rho C_v}{2\bar{T}^2} \frac{\partial(\overline{u_i' T'^2})}{\partial x_i}
\end{aligned} \tag{2.52}$$

$$\begin{aligned}
\frac{D(\overline{u_i' T'^2})}{Dt} &= -\overline{u_j' T'^2} \frac{\partial\bar{U}_i}{\partial x_j} + 2C_1 \frac{k}{\epsilon} (\overline{u_j' u_k'}) \frac{\partial(\overline{u_i' T'})}{\partial x_k} + \overline{u_i' u_k'} \frac{\partial(\overline{u_j' T'})}{\partial x_k} \frac{\partial\bar{T}}{\partial x_j} + \\
C_2 \frac{k}{\epsilon} \frac{\partial}{\partial x_j} \left[\overline{u_j' u_k'} \frac{\partial(\overline{u_i' T'^2})}{\partial x_k} \right] &- \frac{1}{\rho} (C_3 \frac{\epsilon}{k} \overline{u_i' T'^2})
\end{aligned} \tag{3.16}$$

$$\frac{D(\overline{u_i' T'})}{Dt} = -(1 - C_6) (\overline{u_j' T'}) \frac{\partial\bar{U}_i}{\partial x_j} - \overline{u_i' u_j'} \frac{\partial\bar{T}}{\partial x_j} + C_7 \frac{k}{\epsilon} \frac{\partial}{\partial x_j} (\overline{u_j' u_k'} \frac{\partial(\overline{u_i' T'})}{\partial x_k}) - C_8 \frac{1}{\rho} \frac{(\overline{u_i' T'})}{k} \epsilon \tag{3.24}$$

$$\frac{D\bar{T}'^2}{Dt} = -2(\overline{u_i' T'}) \frac{\partial\bar{T}}{\partial x_i} - \frac{1}{2C_9} \frac{\bar{T}'^2}{2k} \epsilon + C_{10} \frac{k}{\epsilon} \frac{\partial}{\partial x_j} (\overline{u_i' u_j'} \frac{\partial\bar{T}'^2}{\partial x_i}) \tag{3.28}$$

All of the above equations can be converted into a form;

$$\frac{\partial(\rho\phi_k)}{\partial t} + \frac{\partial}{\partial x_i} \left(\rho u_i \phi_k - \Gamma_k \frac{\partial\phi_k}{\partial x_i} \right) = S_{\phi_k} \tag{2.51}$$

This is the form of a general transport equation with Γ_k and S_{ϕ_k} being the diffusivity

and source terms. It is possible to define such equations using the UDS (User Defined Scalar) feature of Fluent. Details of the scalar, such as the diffusivity and source are defined via UDF and then implemented in the software interface. Details of the UDF and UDS can be found in Appendix A.

Entropy generation calculations can be considered to be approximate and direct. The details of the direct calculation are explained above. In approximate calculations, first the flow field is obtained with quantitative descriptions of velocity and temperature fields. Then, the viscous and thermal components of the entropy are calculated using the available definitions as given in [6]:

$$s_V = \frac{2}{T} \mu \left\{ \left(\frac{\partial u}{\partial x} \right)^2 + \left(\frac{\partial v}{\partial y} \right)^2 + \frac{1}{2} \left(\frac{\partial u}{\partial y} + \frac{\partial v}{\partial x} \right)^2 \right\} \quad (4.1)$$

$$s_T = \frac{k_{air}}{T^2} \left\{ \left(\frac{\partial T}{\partial x} \right)^2 + \left(\frac{\partial T}{\partial y} \right)^2 \right\} \quad (4.2)$$

Eq.s (2.52), (3.16), (3.24) and (3.28) involve terms like Reynolds stresses and passive scalars which are created by the turbulent nature of the flow. Below details of these parameters are discussed before going into the details of entropy generation itself. In Figures 4.12 and 4.13, flow characteristics of the Reynolds stresses are given.

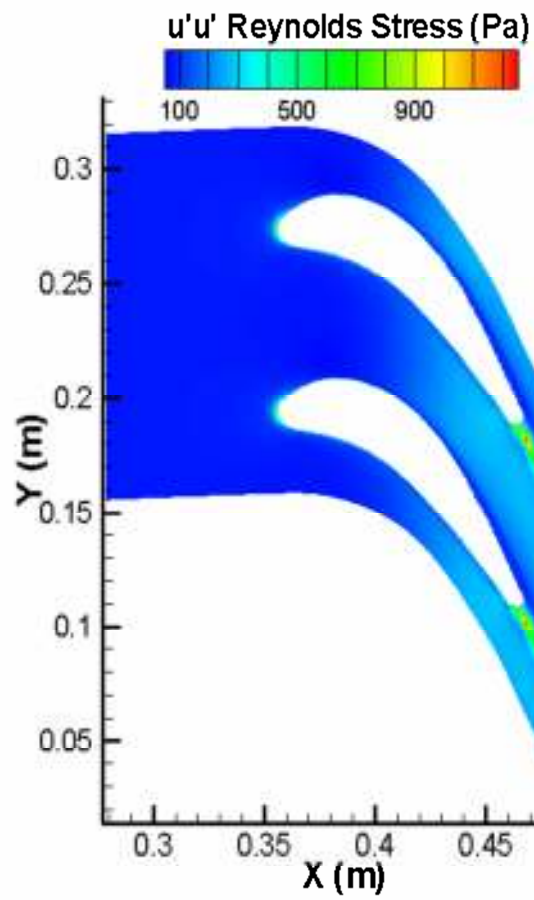


Figure 4.12 Reynolds stress contours around the stator blades, $\overline{u'u'}$.

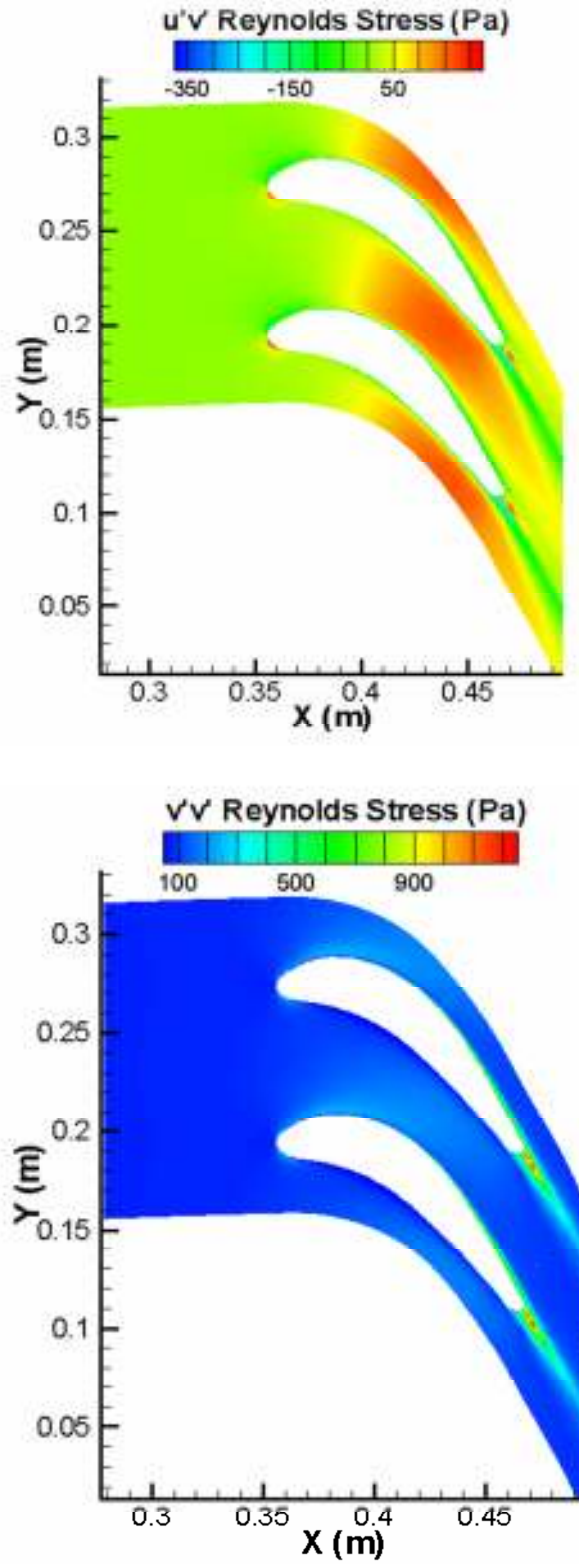


Figure 4.13 Reynolds stress contours around the stator blades; $\overline{u'v'}$ and $\overline{v'v'}$ respectively.

Looking at Figures 4.12 and 4.13, it can be seen that the Reynolds stresses are dominant in the wake related regions, especially for $\overline{u'u'}$ and $\overline{v'v'}$. On the other hand, $\overline{u'v'}$ is more concentrated in a region between the blades starting with one-third of the chord.

Figure 4.14 and 4.15 show the contours for heat fluxes $\overline{u'T'}$, $\overline{v'T'}$ and $\overline{T'^2}$ respectively. The concentration in the regions where there is high turbulence intensity is apparent. $\overline{u'T'}$ is much more effective in the wake region like $\overline{u'u'}$ and $\overline{v'v'}$. However, $\overline{v'T'}$ is concentrated in a very confined region in the wake but is widely spread in the lower boundary layer of each blade. It can also be observed that the concentration of both terms is around the boundary layers. This is an expected feature since the transport equations for both are dominated by the production terms which are mainly happening in and around the boundary layers.

In Figure 4.15, $\overline{T'^2}$ gets the peak values around the blade walls where the thermal gradients are highest. The level of generation decreases as one gets away from the blade walls. In addition, considerable values are observed in the wake region and this effect is carried with the wake.

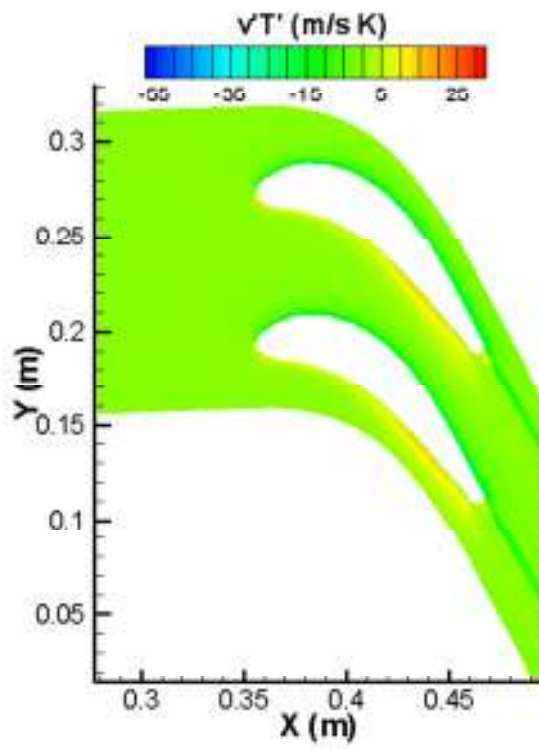
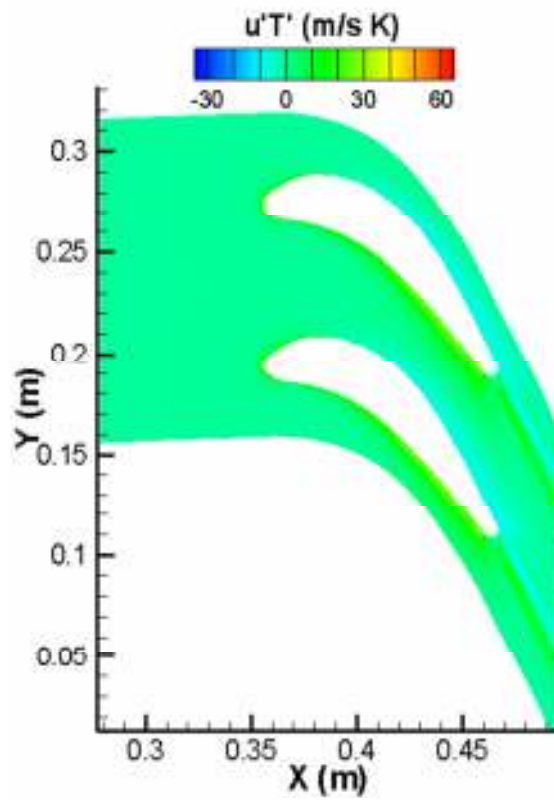


Figure 4.14 $\overline{u'T'}$ and $\overline{v'T'}$ contours around the stator blades.

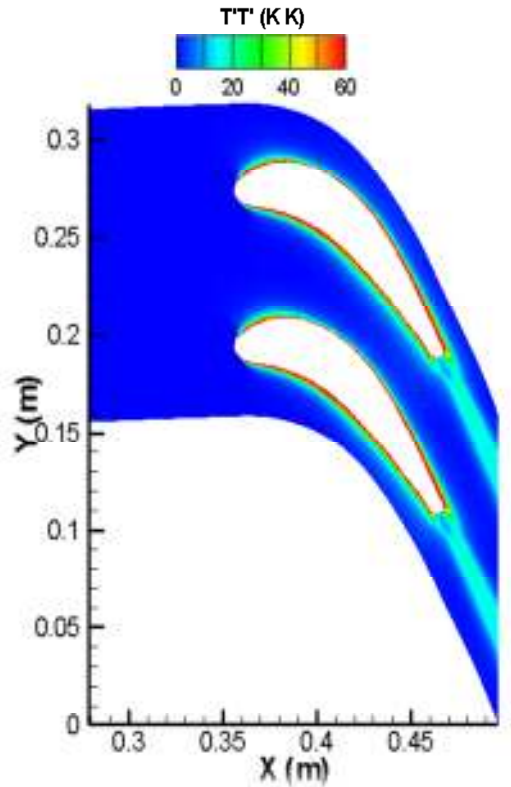


Figure 4.15 $\overline{T'^2}$ contours around the stator blades.

Figure 4.16 shows the contours for heat fluxes $\overline{u'T'^2}$ and $\overline{v'T'^2}$ respectively. As opposed to what is observed in Figures 4.12, 4.13 and 4.14, this time the wake region concentration of the scalars is not clearly visible. However, the concentration around the blade surface is more. This is where the thermal boundary layer develops between the flow and the blade surface due to the highest temperature gradient. Another concentration region is around the stagnation region, especially for $\overline{u'T'^2}$. This is found to be reasonable due to the fact that the flow is mainly in the streamwise direction. A similar region is also visible for $\overline{v'T'^2}$ but it is not as clear and dominant as $\overline{u'T'^2}$.

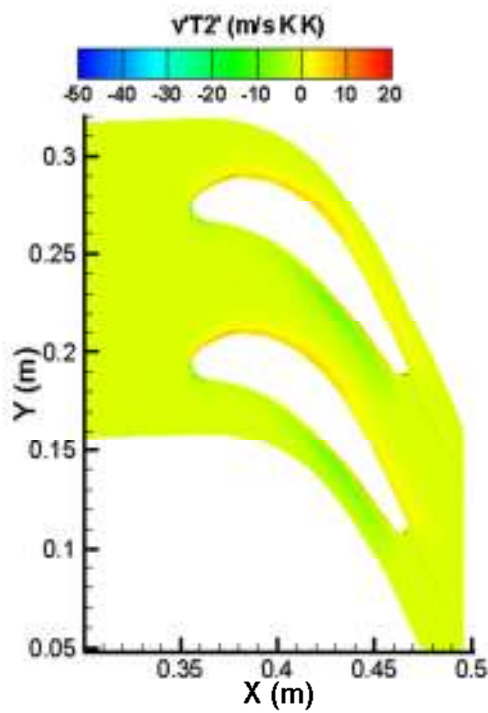
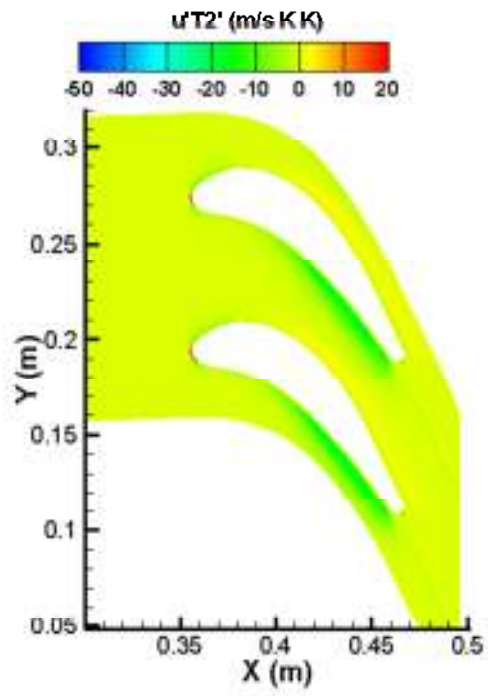


Figure 4.16 $\overline{u'T'^2}$ and $\overline{v'T'^2}$ contours around the stator blades.

After analyzing the parameters which are important in the calculation of entropy and entropy generation, details of specific entropy and entropy generation are discussed. Figures 4.17 and 4.18 present all the turbulent related parameters that are needed for the direct calculation of the specific entropy. From the figures, it can be concluded that the correlations involving only one parameter like $\overline{u'u'}$, $\overline{v'v'}$ and $\overline{T'^2}$ have a similar trend. It can be seen in Figure 4.17 that the effective region for all the parameters is the wake region and the region around the boundary layers. This is also valid for $\overline{T'^2}$ but this parameter is more dominant than the Reynolds stresses in the boundary layer. However, the diffusive character of the Reynolds stresses is more apparent than $\overline{T'^2}$.

When it comes to correlations involving two parameters like $\overline{u'v'}$, $\overline{u'T'}$ and $\overline{v'T'}$, a kind of similarity can be seen as well. Localization of the gradients for the stagnation region and the inter-blade spacing is evident. For $\overline{u'v'}$, high levels of Reynolds stresses start to form after almost one third of the chord and continues to the end of wake region. However, $\overline{u'T'}$ and $\overline{v'T'}$ are more localized near the boundary layer.

Finally, a comparison of the two parameter correlations with the three parameter correlations show that, the effect of fluctuating temperature is more for the three parameter correlations. This is because $\overline{u'T'^2}$ and $\overline{v'T'^2}$ are not intensively carried to the wake region. However, this feature can be seen for $\overline{u'T'}$ and $\overline{v'T'}$. For all the parameters, it is also possible to see a concentrated region in the inter-blade spacing. The size of this effected region is larger for $\overline{u'T'^2}$ and $\overline{v'T'^2}$ than $\overline{u'T'}$ and $\overline{v'T'}$.

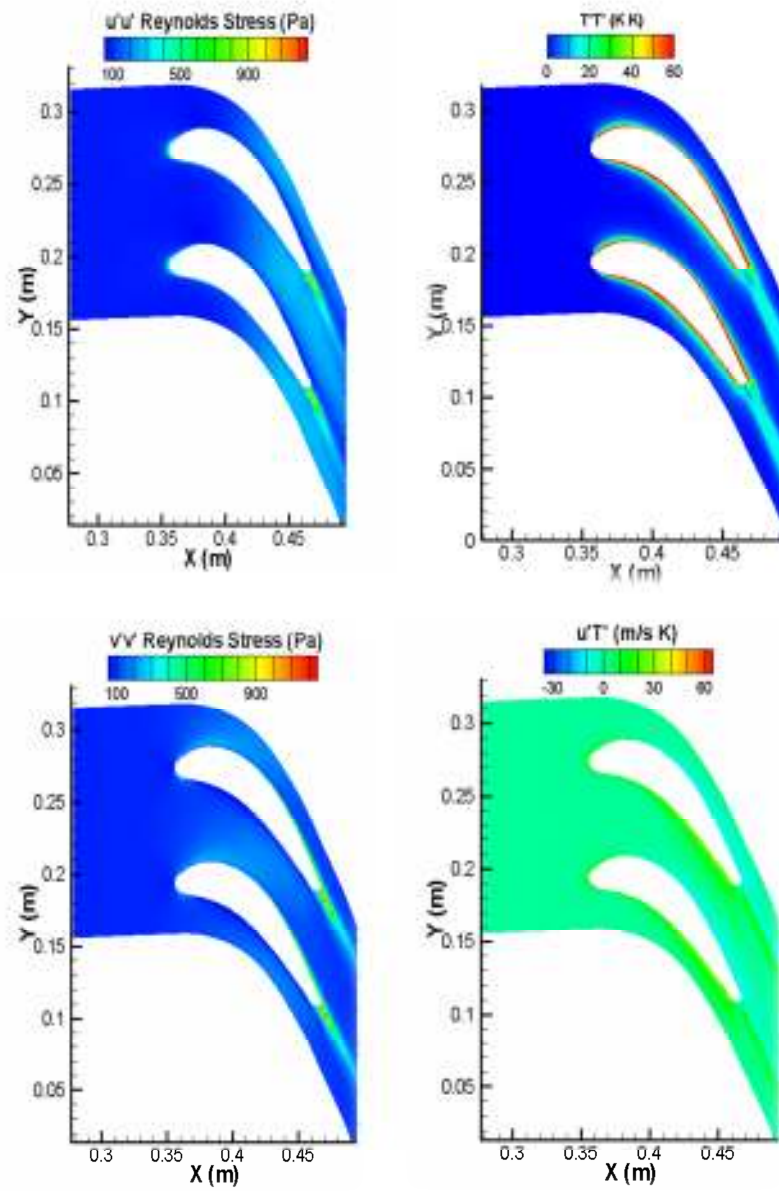


Figure 4.17 Contours of $\overline{u'u'}$, $\overline{v'v'}$, $\overline{u'T'}$ and $\overline{T'^2}$.

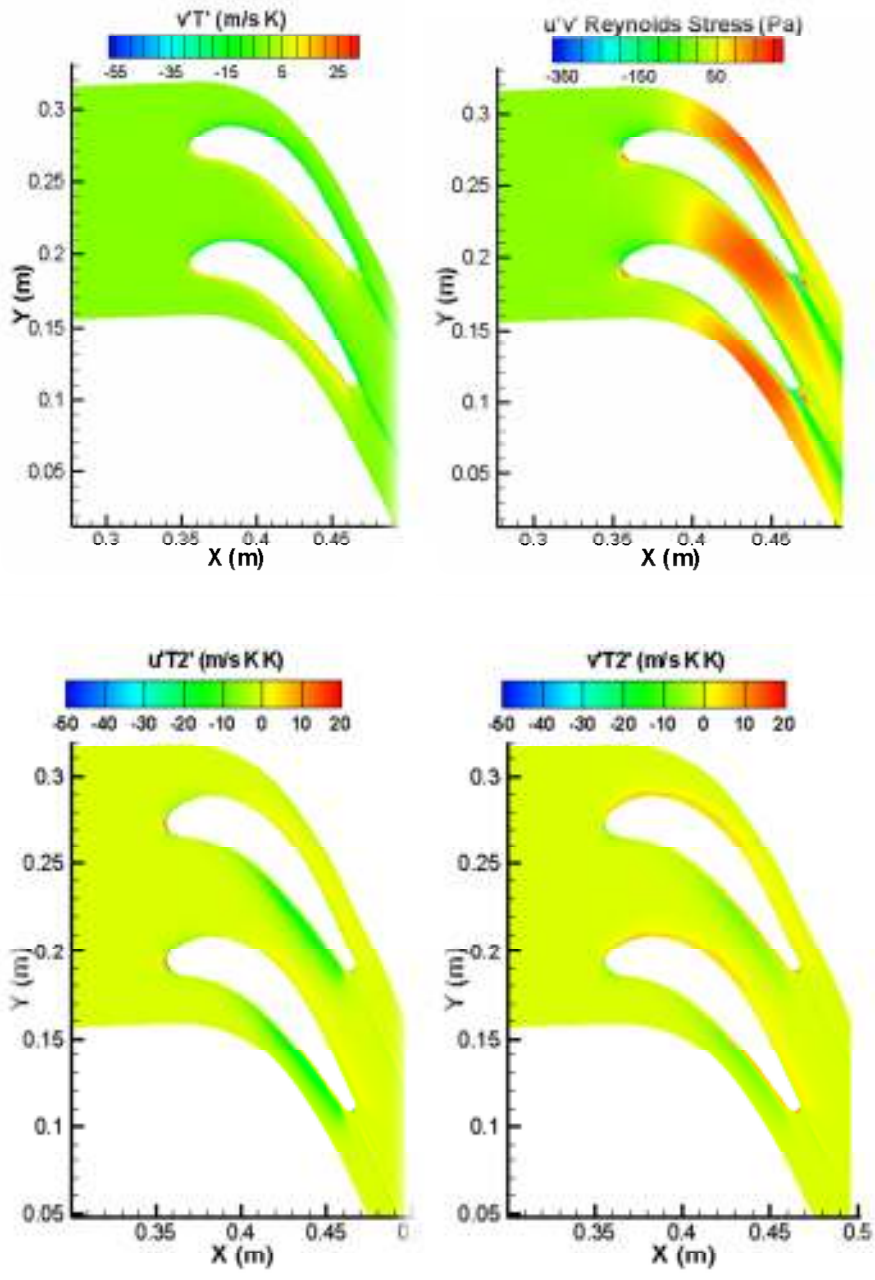


Figure 4.18 Contours of $\overline{u'v'}$, $\overline{v'T'}$, $\overline{u'T'^2}$ and $\overline{v'T'^2}$.

Results up to now have been presented based on the default coefficients of the model transport equations. However, as a result of a-priori testing, different model coefficients have been obtained. Figures below represent the comparisons of turbulent parameters obtained using default model coefficients and coefficients after a-priori testing.

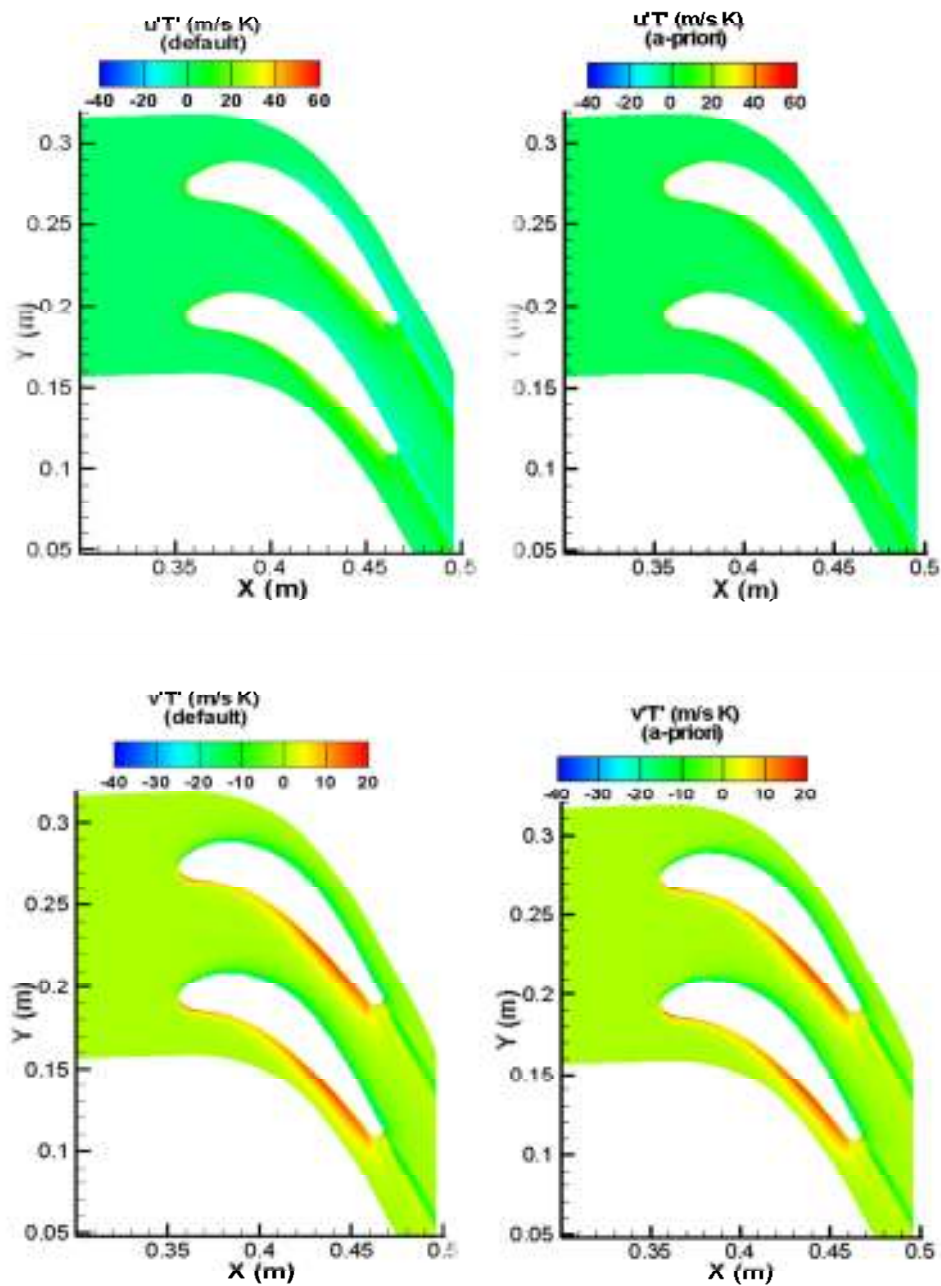


Figure 4.19 Contours of $\overline{u'T'}$ and $\overline{v'T'}$ for default and a-priori coefficients.

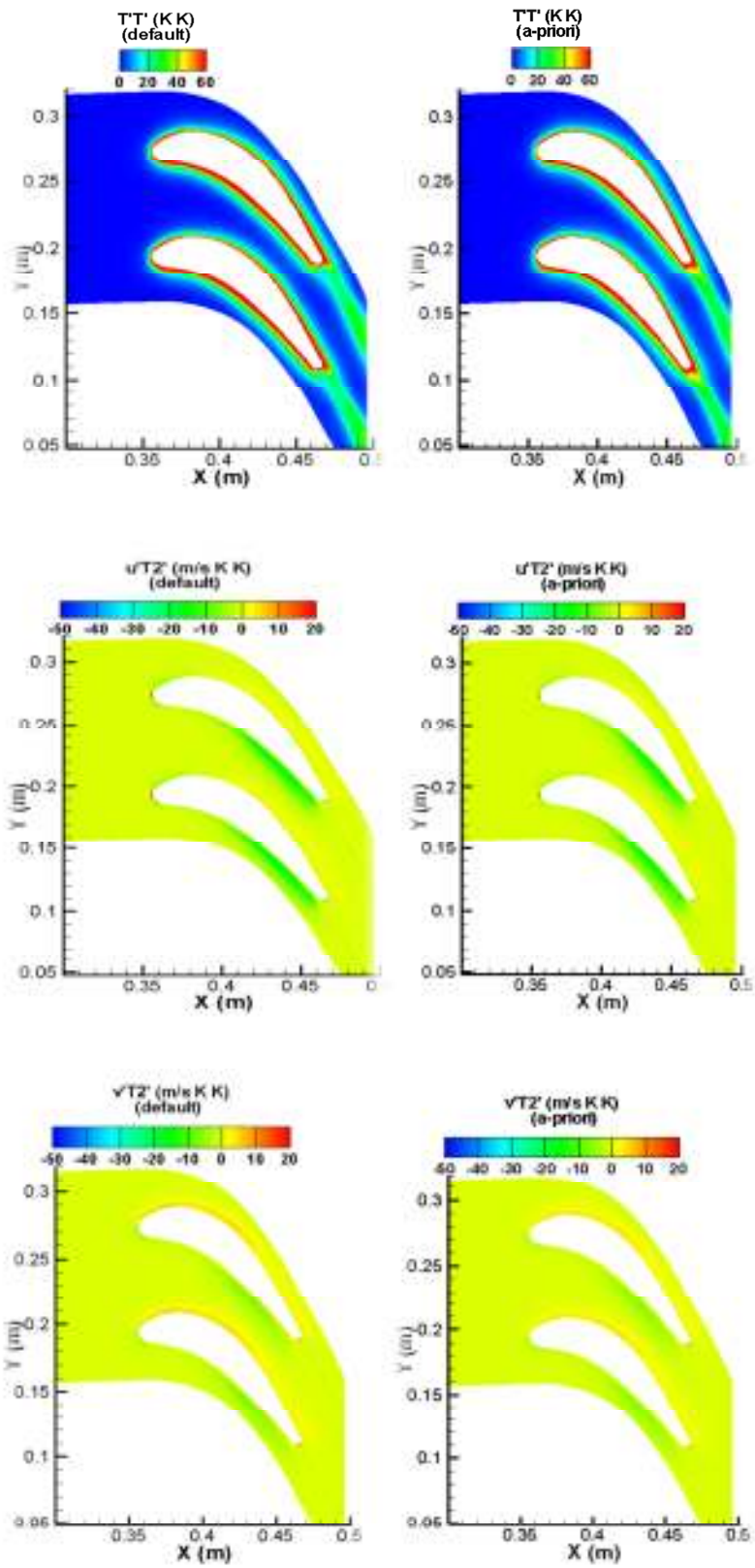


Figure 4.20 Contours of $\overline{T'^2}$, $\overline{u'T'^2}$ and $\overline{v'T'^2}$ for default and a-priori coefficients.

Left hand sides of Figures 4.19 and 4.20 are the results from default coefficients whereas the right hand sides are coming from the results after a-priori testing. In Figure 4.19, contours for $\overline{u'T'}$ and $\overline{v'T'}$ are plotted. Having a close look at both figures, one cannot observe a significant difference in results. The same can be observed for Figure 4.20 for which the contours of $\overline{T'^2}$, $\overline{u'T'^2}$ and $\overline{v'T'^2}$ are plotted. As a result of this conclusion, for the upcoming sections, results of the a-priori tested case will be presented for the sake of completeness.

As discussed in the previous sections, specific entropy can be calculated in two main ways; directly and approximately. Direct calculation can be performed using Eq. (2.53) which includes many terms related with turbulence.

$$\begin{aligned} \frac{\partial(\rho\bar{s})}{\partial t} + \frac{\partial}{\partial x_i} \left[\rho\overline{u_i\bar{s}} - \left(\frac{k+k_t}{C_v} \right) \frac{\partial\bar{s}}{\partial x_i} \right] &= \frac{k}{\bar{T}^2} \left(\frac{\partial\bar{T}}{\partial x_i} \right)^2 + \frac{k}{\bar{T}^2} \overline{\left(\frac{\partial T'}{\partial x_i} \right)^2} + \frac{k}{2} \frac{\partial}{\partial x_i} \left(\frac{1}{\bar{T}} \right) \frac{\partial(\overline{T'^2})}{\partial x_i} + \frac{\overline{\tau_{ij}}}{\bar{T}} \frac{\partial\overline{u_i}}{\partial x_j} + \\ \frac{\bar{\epsilon}}{\bar{T}} - \left(\frac{\rho}{\bar{T}} \overline{u_i'T'} \frac{\partial\bar{s}}{\partial x_i} \right) - \frac{\rho C_v}{\bar{T}} \overline{u_i} \overline{(T')^2} \frac{\partial}{\partial x_i} \left(\frac{1}{\bar{T}} \right) - \frac{\rho C_v}{2\bar{T}^2} \overline{\left(\frac{\partial(T'^2)}{\partial x_i} \right)} - \frac{\rho C_v}{\bar{T}} \overline{u_i'(T')^2} \frac{\partial}{\partial x_i} \left(\frac{1}{\bar{T}} \right) - \\ \frac{\rho C_v}{2\bar{T}^2} \overline{\left(\frac{\partial(u_i'T'^2)}{\partial x_i} \right)} \end{aligned} \quad (2.53)$$

Another method is to calculate the entropy approximately combining Eqs (4.1) and (4.2) to get the total of viscous and thermal entropy generation. Eqs (4.1) and (4.2) can be combined to give:

$$S_{gen} = \frac{2}{T} \mu \left\{ \left(\frac{\partial u}{\partial x} \right)^2 + \left(\frac{\partial v}{\partial y} \right)^2 + \frac{1}{2} \left(\frac{\partial u}{\partial y} + \frac{\partial v}{\partial x} \right)^2 \right\} + \frac{k}{T^2} \left\{ \left(\frac{\partial T}{\partial x} \right)^2 + \left(\frac{\partial T}{\partial y} \right)^2 \right\} \quad (4.3)$$

which forms the RHS of the approximate entropy generation equation:

$$\frac{\partial(\rho\bar{s})}{\partial t} + \frac{\partial}{\partial x_i} \left[\rho\overline{u_i\bar{s}} - \left(\frac{k}{C_v} \right) \frac{\partial\bar{s}}{\partial x_i} \right] = \frac{k}{\bar{T}^2} \left(\frac{\partial\bar{T}}{\partial x_i} \right)^2 + \frac{\overline{\tau_{ij}}}{\bar{T}} \frac{\partial\overline{u_i}}{\partial x_j} \quad (4.4)$$

Eq. (4.4) can be considered to be Reynolds averaged form of Eq. (2.16).

Direct specific entropy is calculated using Eq. (2.53) whereas approximate specific

entropy is obtained through Eq. (4.4).

Figure 4.21 presents the results for direct and approximate specific entropies calculated from Eqs (2.53) and (4.4). In addition, RHS terms for Eqs (2.53) and (4.4) are plotted in Figure 4.22.

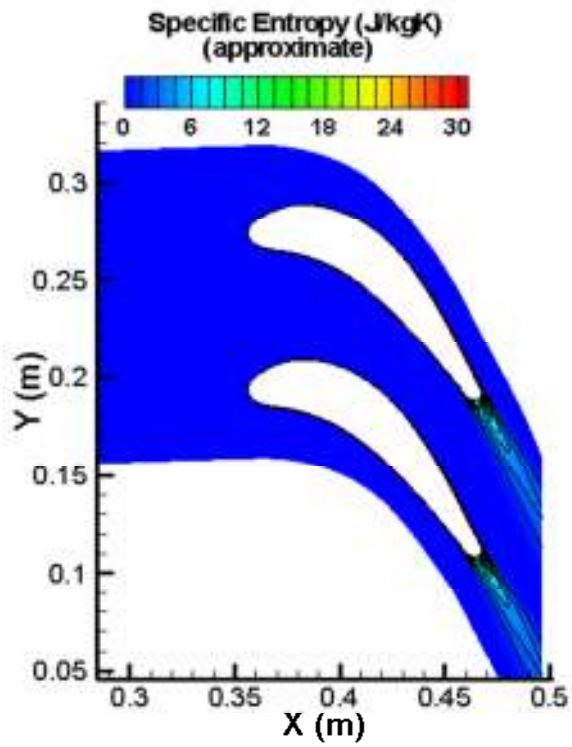
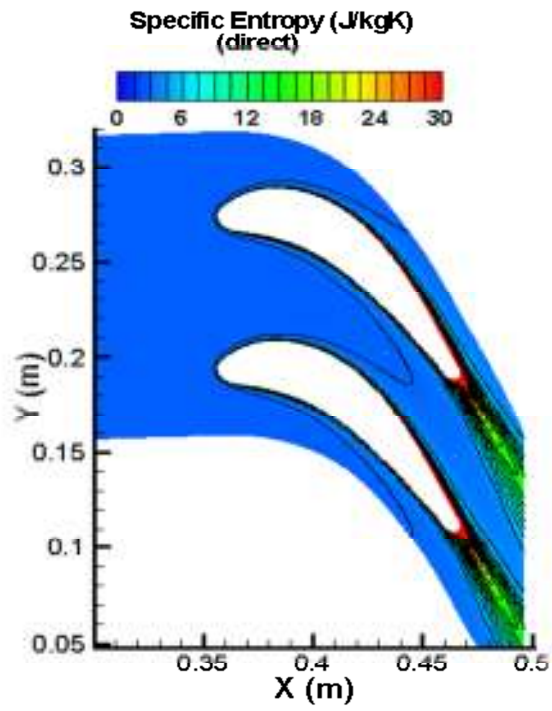


Figure 4.21 Direct and approximate specific entropy contours.

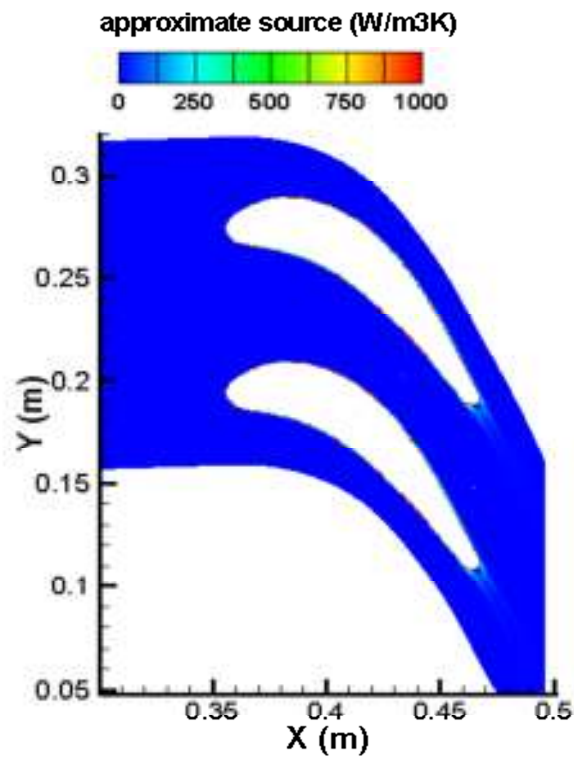
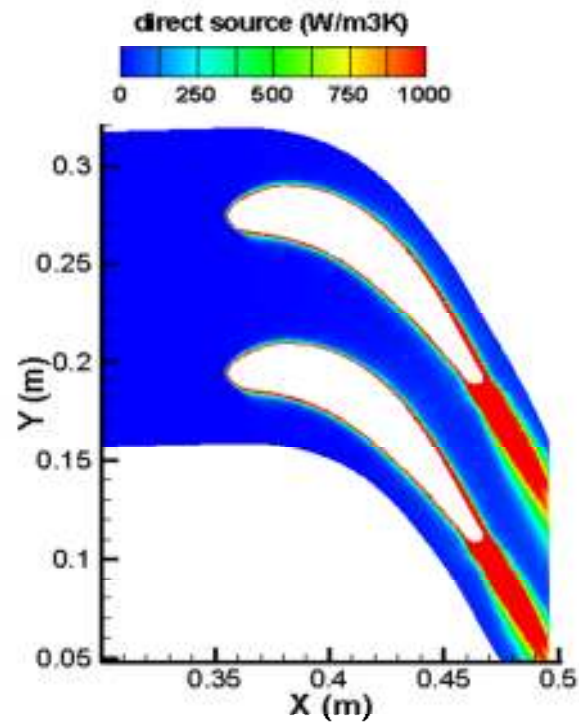


Figure 4.22 Direct and approximate source terms.

Figure 4.21 clearly shows that the entropy is much more widely spread in the direct calculation case. However, it is more confined to just after the blade region for the approximate calculations and the thickness of the wake is approximately constant after the blade. In the direct case, the spreading of the wake is visible and shall be expected due to high turbulence at the wake region.

Diffusivity of entropy is a lot higher for the direct case whereas almost no diffusivity is observed for the approximate one. In both cases, the decay of entropy can be seen going away from the blade. The same is observed for RHS terms for which are responsible for the generation of specific entropies.

The level of specific entropies is different for both cases. From the contour plots, it seems that the levels are higher for the direct case especially at the tip of the blade. In order to see this phenomenon in a more quantitative manner, a line is drawn perpendicular to the wake core. The location of the line with respect to the blade can be seen in Figure 4.23.

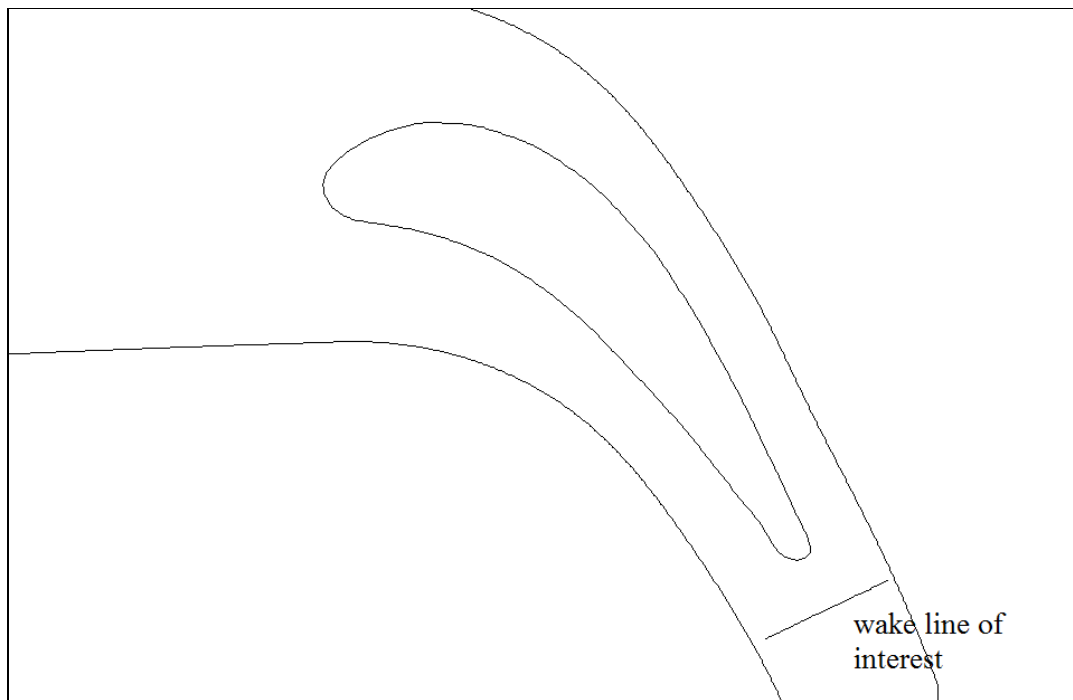


Figure 4.23 Location of the wake line considered for comparison.

Wake line extends from the almost freestream flow region on both sides and crosses through the wake effective region.

Before going into the details of entropies along the wake line, static pressure and velocity profiles are drawn in Figure 4.24.

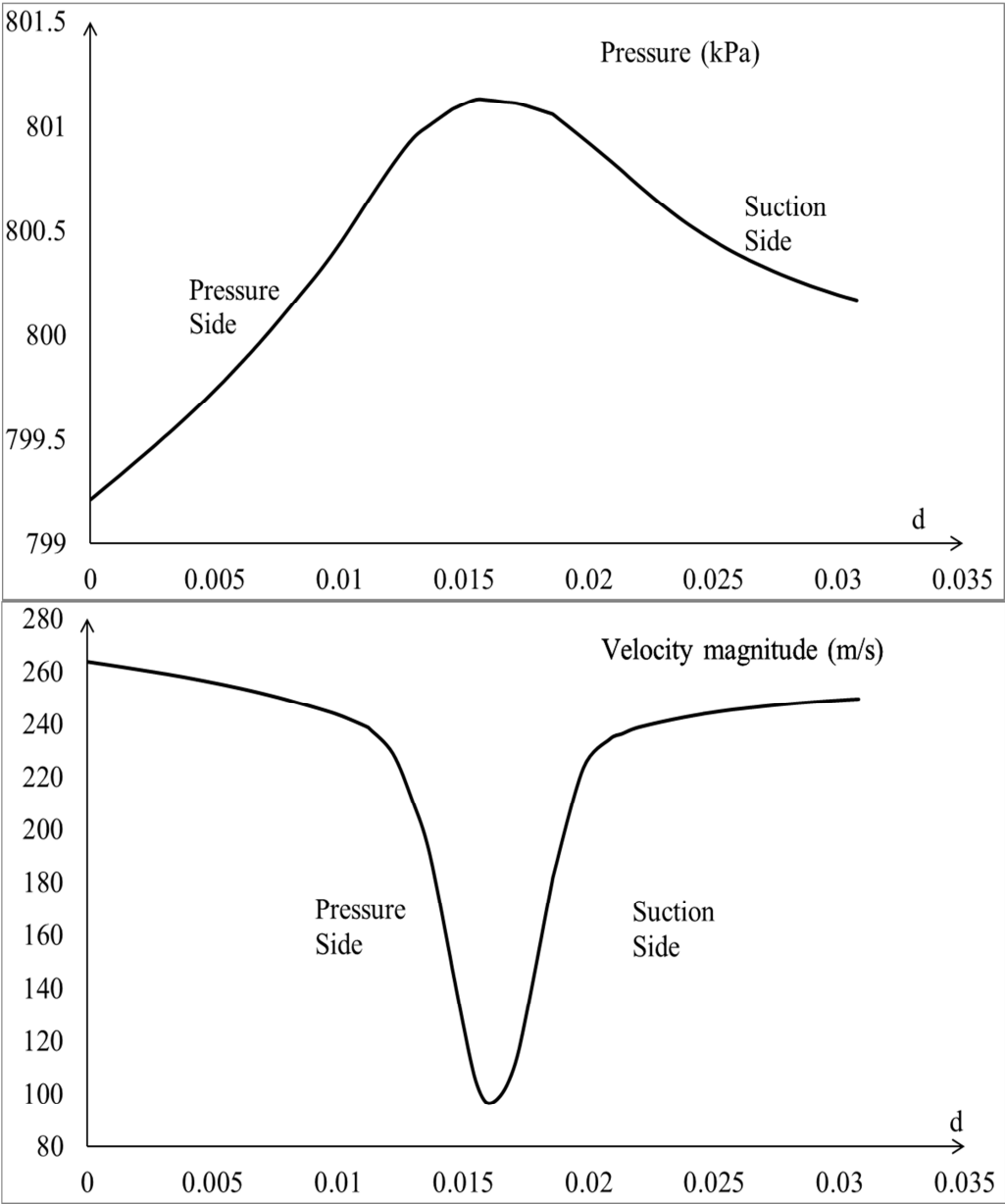


Figure 4.24 Static pressure and velocity magnitude profiles along the wake line respectively.

In Figures 4.25 and 4.26, profiles for $\overline{T'^2}$, $\overline{u'T'}$, $\overline{v'T'}$, $\overline{u'T'^2}$ and $\overline{v'T'^2}$ are plotted respectively.

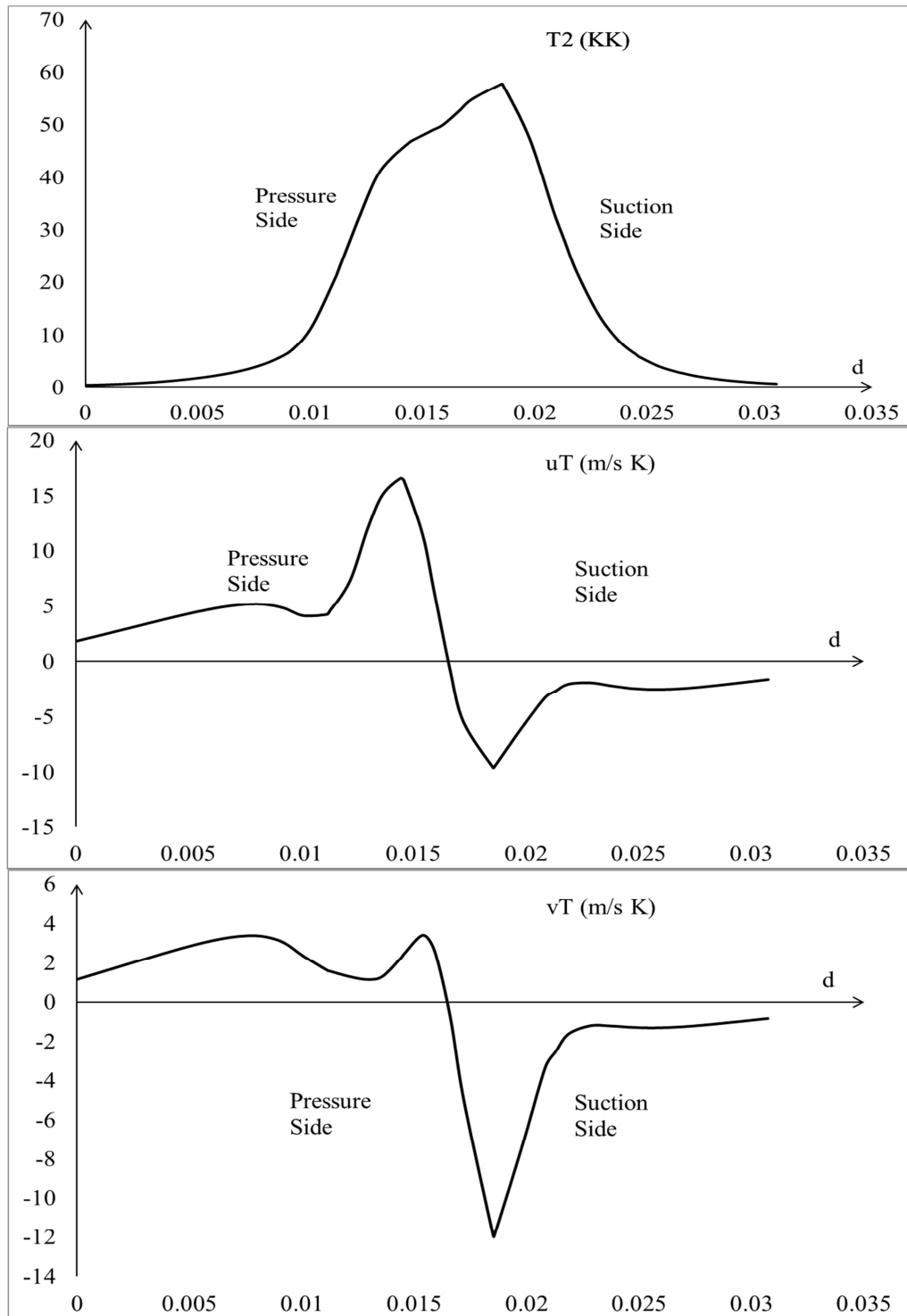


Figure 4.25 $\overline{T'^2}$, $\overline{u'T'}$ and $\overline{v'T'}$ profiles along the wake line respectively.

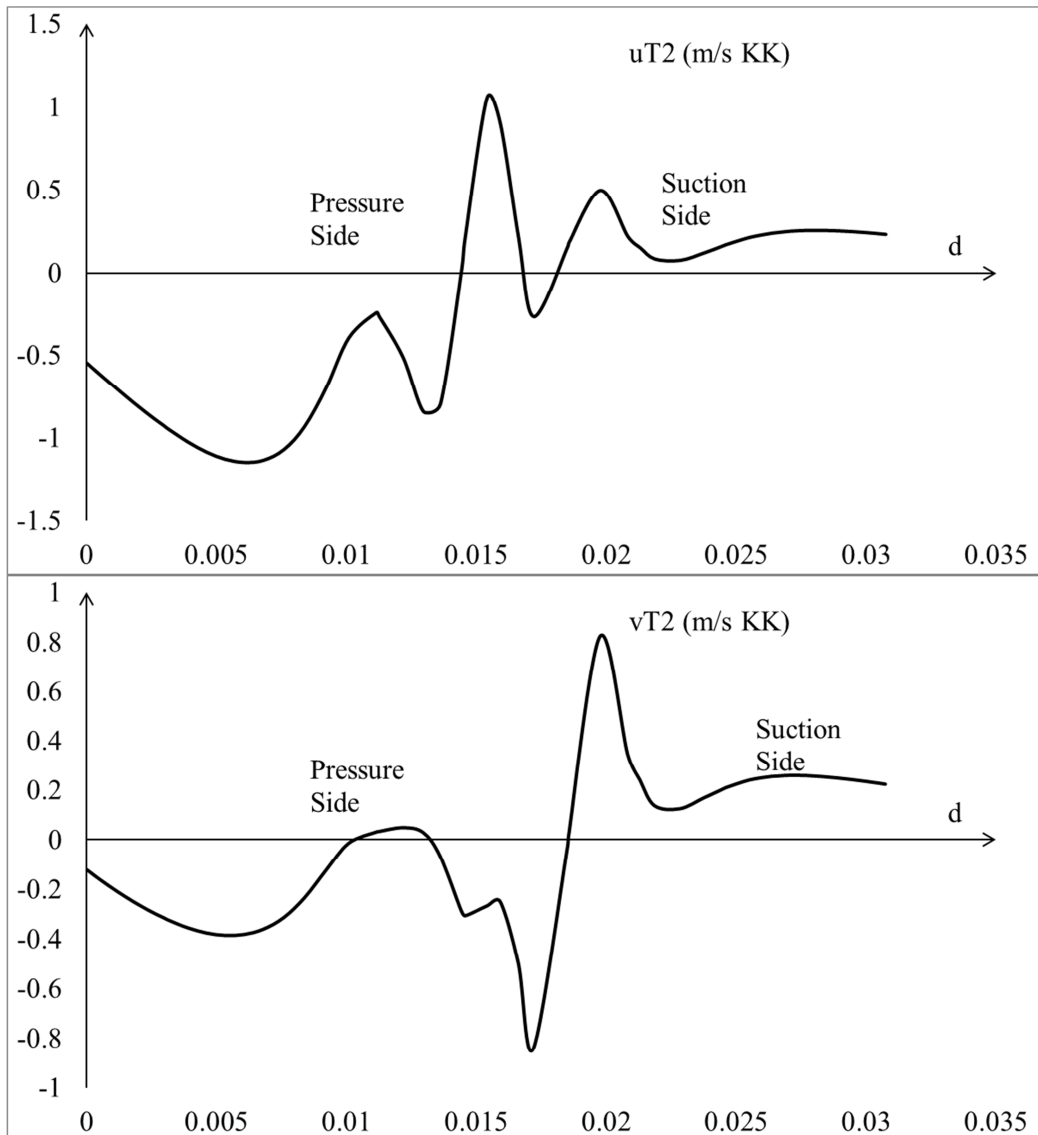


Figure 4.26 $\overline{u'T'^2}$ and $\overline{v'T'^2}$ profiles along the wake line respectively.

Following figure quantitatively compare both the direct and the approximate specific entropies.

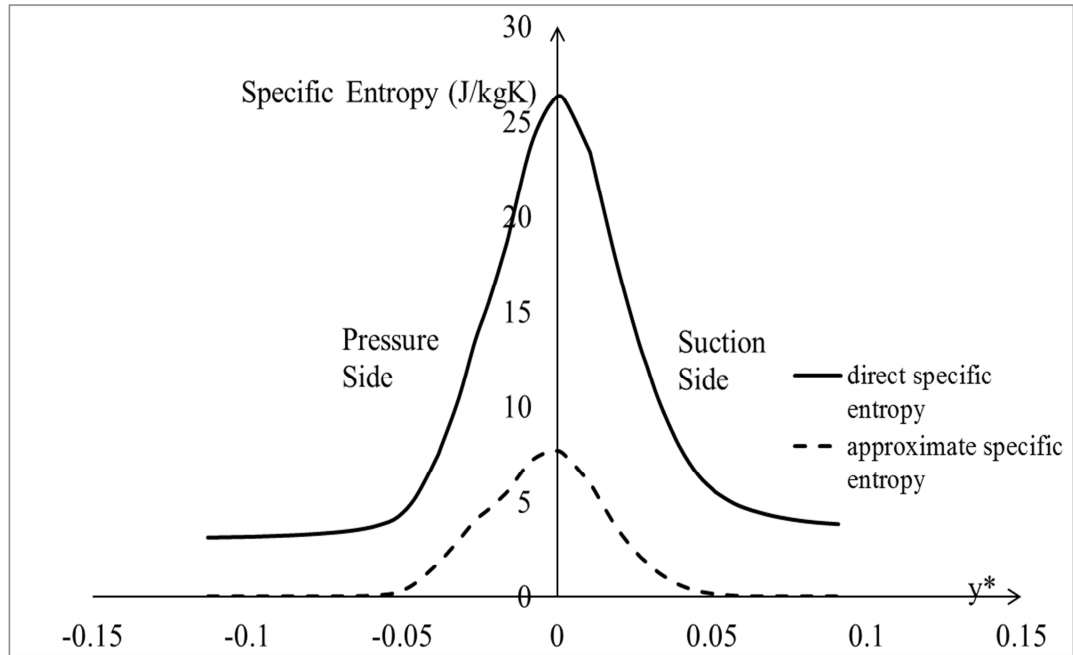


Figure 4.27 Specific entropies for direct and approximate solutions on the wake line.

In Figure 4.27, y axis is the specific entropy values and x axis is the nondimensional curve length which is

$$y^* = \frac{d-d_{max}}{l_{ref}} \quad (4.5)$$

where d is the coordinate along the wake line, d_{max} is the coordinate where the maximum entropy occurs and l_{ref} is a reference length.

Looking at Figure 4.27, direct specific entropy is almost four times higher than approximate entropy generation values at the point where the maximum entropy occurs. This difference diminishes along the freestream flow. However, there is an almost constant offset between the freestream entropy values of 3 J/kgK. This offset is believed to be coming from turbulence effects included in the direct calculation. Boundary layer induced turbulence penetrates into the freestream causing a difference between the freestream entropy values.

For the approximate entropy values, only the mean quantities are considered and the gradients of the mean quantities are effective in the core region of the wake.

Since the scales are different for direct and approximate specific entropies, a non-dimensional parameter, s^* for entropy is formed in order to have a better insight.

Nondimensional entropy is formulated as:

$$s^* = \frac{s}{s_{max}} \quad (4.6)$$

where s_{max} is the maximum specific entropy.

For the direct specific entropy, offset value is subtracted from all values to have the same basis of comparison.

In Figure 4.28, nondimensional specific entropy is plotted as a function of nondimensional curve length. Along the pressure side of the blade, two lines are almost identical but approximate entropy has a slight wider distribution. However, along the suction side, the wake region is wider starting from the center and the gap increases while approaching the freestream. This is due to the additional source terms coming mainly from turbulence.

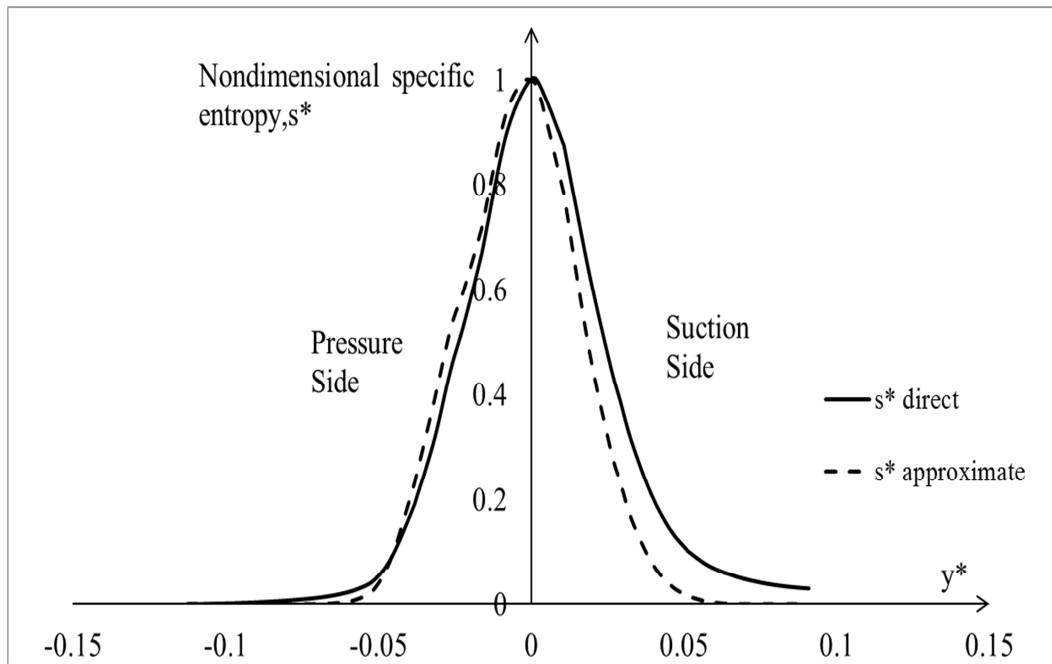


Figure 4.28 Nondimensional specific entropies for direct and approximate solutions on the wake line.

Comparison of the source terms appearing in both methods can illustrate the reason for this difference. Figure 4.29 presents the source terms for direct and approximate methods.

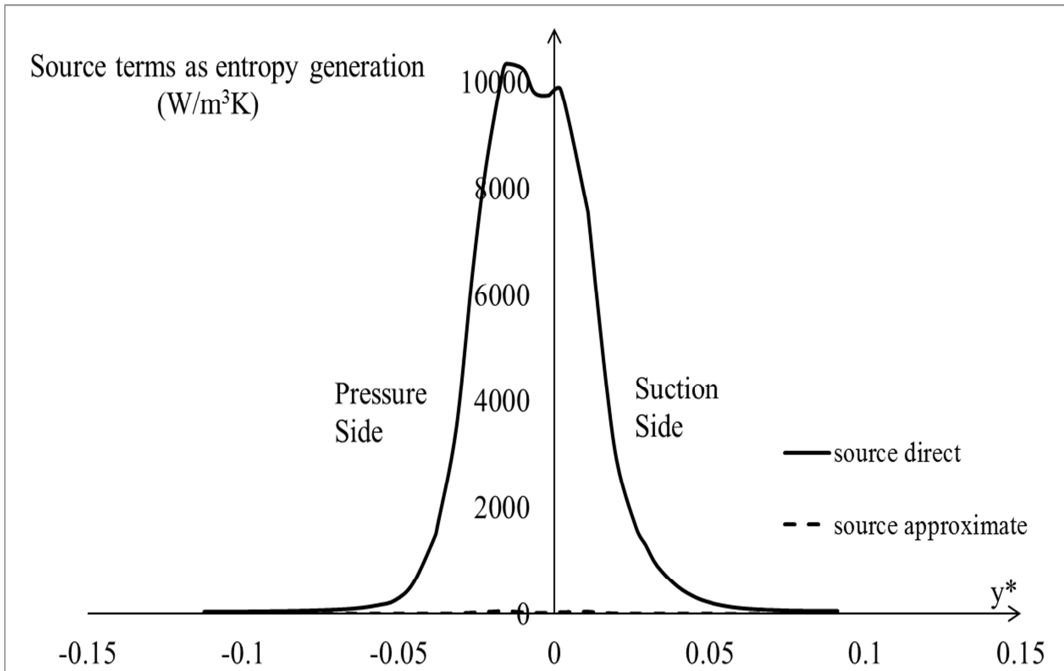


Figure 4.29 Source terms for direct and approximate solutions on the wake line.

The level of source terms is in the order of thousands whereas it is around fifty for the approximate case. This difference is responsible for the additional entropy generation that can be captured by the direct method.

Source terms can also be nondimensionalized to have a better overview about the evolution of the parameters. If each of the source terms is nondimensionalized by its maximum value over the wake line, the pattern in Figure 4.30 is obtained.

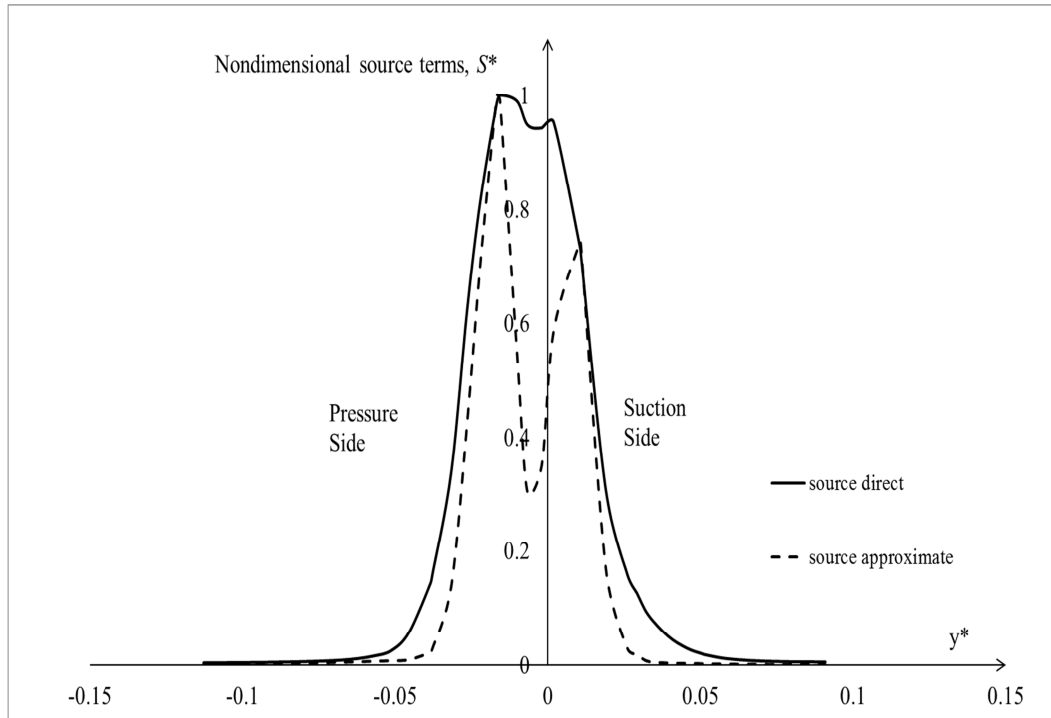


Figure 4.30 Nondimensional source terms for direct and approximate solutions on the wake line.

A direct observation from Figure 4.30 is the perfect fit of the extremes for the approximate terms with the values on the direct terms. It is clear from this figure that the additional source terms are responsible for higher entropy values. This can also be observed through the area between both curves.

A final check of what is discussed above could be done through visualization of the contour plots for both the direct and approximate specific entropies around the wake line in a detailed manner. Figure 4.31 presents the contours for direct and approximate specific entropies respectively.

From the detailed views around the wake line, it is easier to capture the effect of the suction side. In both figures, specific entropy is higher towards the suction side and this also explains the difference being more on the suction side for Figures 4.28 and 4.30.

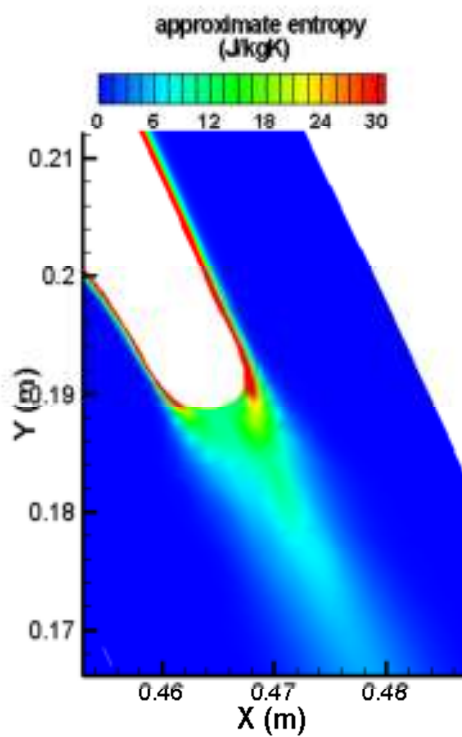
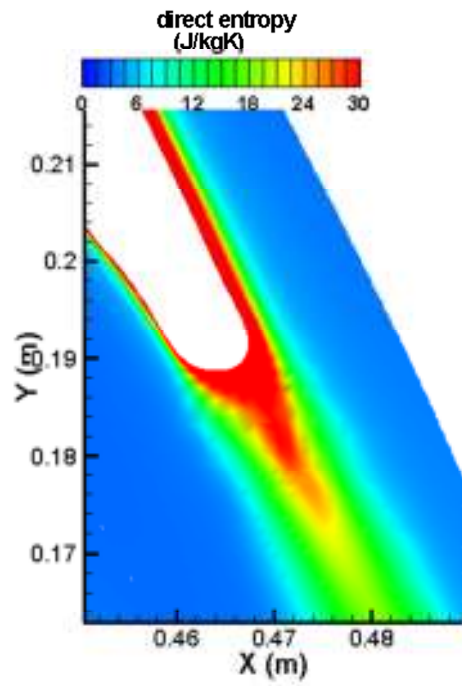


Figure 4.31 Detailed contours of specific entropies for direct and approximate solutions around the wake line.

Finally, starting with Figure 4.21 and then proceeding figures till Figures 4.31 clearly demonstrates the difference between the direct and approximate entropy calculations. It is believed that the approximate entropy can serve the designers and pioneers up to a certain level. For someone who is interested in detailed design and understanding of a system involving high turbulence certainly needs a thorough understanding of loss mechanisms. Since loss mechanisms are strongly related with entropy, a full understanding of entropy is needed as discussed before. Although, it is computationally more intense and requires longer simulation times, direct entropy calculations are needed for complex systems like turbines, compressors and engines.

CHAPTER 5

CONCLUSION AND FUTURE WORK

The effect of calculating the entropy generation rate directly using the Reynolds-Averaged Entropy Transport equation is demonstrated by comparing the direct results with the ones that are calculated by post-processing the velocity and temperature fields for a two-dimensional turbine cascade configuration. Results show that there could be significant differences especially in the spatial distributions of entropy fields. This type of approach could offer significant improvements in entropy and loss prediction in turbomachinery flows. However, this approach needs more studies especially for accurate modeling of temperature fluctuations and temperature-velocity correlations in the entropy transport equation.

The main difficulty in modeling the direct calculation of entropy through solving the entropy transport equation lies in the turbulence modeling part. Entropy transport equation involving turbulent effects requires a lot of modeling efforts. Especially the scalar parameters that are results of fluctuating velocity and temperature correlations have to be investigated in detail.

Within this study, only limited modeling approaches have been tested, but turbulence modeling world is like a bottomless well as explained by Phil Thompson, senior scientist of NCAR [27]:

“Lots of people have tried to develop a fundamental theory of turbulence. Some very well known people have given up on it. But I just can’t give up on it – it’s like a beautiful mistress. You know that she treats you badly, she’s being ornery, but you just can’t stay away from her. So periodically, this question comes up again in my mind, and I keep casting about for some different and simple and natural way of representing the motion of a fluid, and some way of treating the analytical

difficulties. And I seem to get a little bit closer sometimes....”

It has not been possible to cover all complex phenomena related with entropy within the contents of this thesis and it is believed that the following list of subjects could be further investigated to have a better feeling about what has been done within this study:

- A different model for the turbulent entropy generation could be developed other than proposed in this thesis
- DNS data used here is a channel flow without pressure gradient and curvature effects. The results of a-priori testing could be modified if a better DNS data is found.
- Model equations for the turbulent terms are complex in their nature that there is a lot of modeling effort in them. Turbulence modeling is a very active research subject and the model equations for the turbulent related terms could be improved to have better result for the turbulent related terms.
- The benchmark case studied here is a 2D model with a fixed turbine stator blade. However, there are more complex flow cases in real engineering applications. This 2D model shall be extended to 3D models involving rotational fluid motion.
- Other systems shall also be used as benchmark like compressors and engines where entropy also plays a big role in loss mechanisms. If the methodology discussed here can be utilized globally for most of the complex systems involving entropy, then it is possible to conclude that the method has achieved a great success.

In conclusion, entropy generation calculation is one of the most attractive topics in engineering fields. Entropy generation coupled with turbulence has gained some

attention in the past but there are still some mysterious points waiting to be resolved. Therefore, it is expected by the author that more interesting studies will come in the future and use of entropy generation as a tool will be much broader.

REFERENCES

- [1] <http://en.wikipedia.org/wiki/Entropy> (last accessed on 31.07.2013)
- [2] Clausius, R., “Mechanical Theory of Heat with Its Applications to the Steam Engine and to the Physical Properties of Bodies”, Taylor and Francis, 1870.
- [3] Sonntag, E.R., Borgnakke C., Van Wylen, G.J., “Fundamentals of Thermodynamics”, John Wiley and Sons, 1998.
- [4] http://nuclearpowertraining.tpub.com/h1012v1/css/h1012v1_82.htm (last accessed on 18.07.2013)
- [5] A. Bejan, “Entropy Generation Through Heat and Fluid Flow”, John Wiley and Sons, 1982.
- [6] G. Natalini, E.Sciubba, “Minimization of the Local Rates of Entropy Production in the Design of Air Cooled Gas Turbine Blades”, Journal of Engineering for Gas Turbines and Power, pp. 466-475, vol. 121, November 1999.
- [7] E. Sciubba, “Numerical Calculation of Local Irreversibilities in Compact Heat Exchangers”, Proceedings NATO-TIBTD Workshop on 2nd Law, Erciyes University, Kayseri, Turkey, 1990.
- [8] M.K. Drost, M.D. White, “Numerical Predictions of Local Entropy Generation in an Impinging Jet”, Journal of Heat Transfer, pp. 823-829, vol. 113, November 1991.
- [9] F. Kock,H. Herwig, “Entropy Production Calculation for Turbulent Shear

Flows and Their Implementation in CFD codes”, International Journal of Heat and Fluid Flow, pp. 672-680, vol. 26, June 2005.

[10] D. M. McEligot, E.J. Walsh, E. Laurien “Entropy Generation in the Viscous Layer of a Turbulent Channel Flow”, 5th International Symposium on Turbulence, Heat and Mass Transfer, September 2006.

[11] H. Abe, H. Kawamura, Y. Matsuo, “Direct Numerical Simulation of a Fully Developed Turbulent Channel Flow With Respect to the Reynolds Number Dependence”, Journal of Fluids Engineering, pp. 382-393, February 2001.

[12] O.B. Adeyinka, G.F. Naterer, “Modeling of Entropy Production in Turbulent Flows”, Journal of Fluids Engineering, pp. 893-899, vol. 126, November 2004.

[13] R. D. Moser, J. Kim, N.N. Mansour “Direct Numerical Simulation of Turbulent Channel Flow up to $Re_\tau = 590$ ”, Physics of Fluids, pp. 943-945, December 1998.

[14] Chevalier, M. and Schlatter, P. and Lundbladh, A. and Henningson D. S., A Pseudo-Spectral Solver for Incompressible Boundary Layer Flows, KTH Mechanics, Stockholm, Sweden, 2007

[15] C.L. Iandoli, E.Sciubba, N. Zeoli, “The Computation of the Entropy Generation rate for Turbomachinery Design Applications: Some Theoretical Remarks and Practical Examples”, Int. Journal Energy Technology and Policy, pp. 64-95, vol. 6, 2008.

[16] K. Alabi, F. Ladeinde, M. v. Spakovsky, D. Moorehouse, J. Camberos “Assessing CFD Modeling of Entropy Generation for the Air Frame Subsystem in an Integrated Aircraft Design/Synthesis Procedure”, 44th AIAA Aerospace Sciences Meeting and Exhibit, Reno-Nevada, 9-12 January 2006.

- [17] A. Bejan, “Entropy Generation Minimization: The Method of Thermodynamic Optimization of Finite-Size Systems and Finite-Time Processes”, CRC Press, 1996.
- [18] M. Gouy, “Sur l’energie utilisable”, Journal of Physics, Vol:8, 501, 1889
- [19] A. Stodola, “Steam and Gas Turbines”, McGraw Hill, New York, 1910
- [20] O. B. Adeyinka, “Numerical and Experimental Studies of Available Energy Losses in Laminar and Turbulent Flows”, PhD Thesis, University of Manitoba, 2005
- [21] M.J. Morgan, H.N. Shapiro “Fundamentals of Engineering Thermodynamics”, John Wiley and Sons Inc., 1988
- [22] H. Tennekes, J. L. Lumley “A First Course in Turbulence”, The MIT Press, 1972
- [23] K. E. Jansen, “The Role of Entropy in Turbulence and Stabilized Finite Element Methods”, PhD Thesis, Stanford University, 1993
- [24] J. S Kramer-Bevan, A Tool for Analysing Fluid Flow Losses, M.sc., University of Waterloo, 1992.
- [25] K. Hanjalic, S. Jakirlic, “Chapter 2: Second-Moment Turbulence Closure Modelling”, Closure Strategies for Turbulent and Transitional Flows, pp. 47-101, 2002.
- [26] Durbin and Pettersson Reif, “Statistical Theory and Modeling for Turbulent Flow”, John Wiley and Sons Ltd.,2010.
- [27] Wyngaard, John C., “Turbulence in the Atmosphere”, Cambridge University Press, 2010.

[28] http://www.emeraldinsight.com/content_images/fig/1340160206018.png (last accessed on 18.07.2013).

[29] Ansys Fluent, User Guide.

[30] E. Sciubba, "Computing the Entropy Generation Rate for Turbomachinery Design Applications: Can a Diagnostic Tool Become a Predictive One?", ASME International Mechanical Engineering Congress and Exposition, 5-11 November 2005, Orlando, Florida, USA.

[31] E. Sciubba, "Entropy Generation Minimization as a Design Tool. Part 1: Analysis of Different Configurations of Branched and Non-branched Laminar Isothermal Flow Through a Circular Pipe", International Journal of Thermodynamics, Vol. 14 (No.1), pp. 11-20, 2011.

[32] A. Bejan, S. Lorente, "The Constructal Law and the Design of the Biosphere: Nature and Globalization", Journal of Heat Transfer, Vol. 133, January 2011.

[33] L.B. Erbay, M. Ş. Ercan, B. Sülüş, M. M. Yalçın, "Entropy Generation During Fluid Flow Between Two Parallel Plates With Moving Bottom Plate", Entropy, Vol. 5, pp. 506-518, 2003.

[34] H. Yapıcı, N. Kayataş, N. Kahraman, G. Baştürk, "Numerical Study On Local Entropy Generation In Compressible Flow Through A Suddenly Expanding Pipe", Entropy, Vol. 7, pp. 38-67, 2005.

[35] G. Giangaspero, E. Sciubba "Application of the EGM Method to a LED-Based Spotlight: A Constrained Pseudo-Optimization Design Process Based on the Analysis of the Local Entropy Generation Maps", Entropy, Vol. 13, pp. 1212-1228, 2011.

[36] I. S. Ertesvåg, J. Kolbu, "Entropy Production Modeling in CFD of Turbulent

Combustion Flow”, 18th International Conference on Efficiency, Cost, Optimization, Simulation and Environmental Impact of Energy Systems, 2005, Trondheim, Norway.

[37] G. F. Naterer, J. A. Camberos, “Entropy and the Second Law Fluid Flow and Heat Transfer Simulation, Journal of Thermophysics and Heat Transfer, Vol. 17, No.3, pp.360-371, July-September 2003.

[38] S.H. Lui, G. F. Naterer, “Upper Entropy Bounds for Transient Forced Convection”, Heat Mass Transfer, Vol. 43, pp. 295-308, 2007.

[39] O.B. Adeyinka, G.F. Naterer, “Measured Turbulent Entropy Production with Large Eddy Particle Image Velocimetry”, Experimental Fluids, Vol.42, pp. 881-891, 2007.

[40] G. Hauke, “A Unified Approach to Compressible and Incompressible Flows and a New Entropy Consistent Formulation of the k-epsilon Model”, PhD Thesis, Stanford University, February 1995.

[41] J. K. Edward, “The Role of Entropy in Turbulence and Stabilized Finite Element Methods”, PhD Thesis, Stanford University, 1993.

[42] M. B. Schmitz, O. Schafer, J. Szwedowicz, T. Secall-Wimmel, T.P. Sommer, “Axial Turbine Blade Vibrations Induced by the Stator Flow: Comparison of Calculations and Experiment”, Unsteady Aerodynamics, Aeroacoustics and Aeroelasticity of Turbomachines, pp. 107-118, 2006.

[43] B. Song, “Experimental and Numerical Investigations of Optimized High-Turning Supercritical Compressor Blades”, PhD Thesis, Virginia Polytechnic Institute and State University, November 2003.

[44] R. M. Culver, “Modeling Multi-stage Flows and Aeroelasticity in Transonic

Gas Turbine Compressors”, PhD Thesis, University of California, 2009.

[45] A. Shavalikul, “A Time Accurate Prediction of the Viscous Flow in a Turbine Stage Including a Rotor in Motion”, PhD Thesis, The Pennsylvania State University, August 2009.

[46] K. V. Bulusu, “On Dissipative Flow Structures in Supersonic Pressure Exchange - An Experimental Investigation”, PhD Thesis, Osmania University, India, 1998.

[47] M. Kozuka, Y. Seki, H. Kawamura, “DNS of Turbulent Heat Transfer in a Channel Flow With a High Spatial Resolution”, International Journal of Heat and Fluid Flow, Vol. 30, pp. 514-524, 2009.

[48] H. Kawamura, K. Ohsaka, H. Abe, K. Yamamoto, “DNS of Turbulent Heat Transfer in a Channel Flow With Low to Medium-High Prandtl Number Fluid”, International Journal of Heat and Fluid Flow, Vol. 19, pp. 482-491, 1998.

[49] H. Kawamura, H. Abe, Y. Matsuo, “DNS of Turbulent Heat Transfer in a Channel Flow With Respect to Reynolds and Prandtl Number Effects”, International Journal of Heat and Fluid Flow, Vol. 20, pp. 196-207, 1999.

[50] H. Abe, H. Kawamura, Y. Matsuo, “Surface Heat Flux Fluctuations in a Turbulent Channel Flow up to $Re_{\tau} = 1020$ and $Pr = 0.025$ and 0.71 ”, International Journal of Heat and Fluid Flow, Vol. 25, pp. 404-419, 2004.

[51] S. Makino, K. Iwamoto, H. Kawamura, “Turbulent Structures and Statistics in Turbulent Channel Flow With Two-Dimensional Slits”, International Journal of Heat and Fluid Flow, Vol. 29, pp. 602-611, 2008.

[52] J. Kim, P. Moin, R. Moser, “Turbulence Statistics in Fully Developed Channel Flow at Low Reynolds Number, Journal of Fluid Mechanics, Vol. 177, pp.

133-166, 1987.

[53] P. Moin, K. Mahesh, “Direct Numerical Simulation: A Tool in Turbulence Research”, *Annual Review Fluid Mechanics*, Vol. 30, pp. 539-578, 1998.

[54] X. Wu, P. Moin, “Direct Numerical Simulation of Turbulence in a Nominally Zero-Pressure-Gradient Flat-Plate Boundary Layer”, *Journal of Fluid Mechanics*, Vol. 630, pp. 5-41, 2009.

[55] X. Wu, P. Moin, “Transitional and Turbulent Boundary Layer with Heat Transfer”, *Physics of Fluids*, Vol. 22, 2010.

[56] K. Iwamoto, N. Kasagi, Y. Suzuki, “Direct Numerical Simulation of Turbulent Channel Flow at $Re_\tau = 2320$ ”, *Proceedings of 6th Symposium of Smart Control of Turbulence*, Tokyo, March 6-9 2005.

[57] T. Brandt, “Direct Numerical Simulation of Turbulent Channel Flow Using Finite Difference Scheme”, *Laboratory of Aerodynamics, HUT*.

[58] J. M. Österlund, “Experimental Studies of Zero Pressure-Gradient Turbulent Boundary-Layer Flow”, *Technical Reports from Royal Institute of Technology, Sweden*, December 1999.

[59] Y. Na, D.V. Papavassiliou, T. J. Hanratty, “Use of Direct Numerical Simulation to Study the Effect of Prandtl Number on Temperature Fields”, *International Journal of Heat and Fluid Flow*, Vol. 20, pp. 187-195, 1999.

[60] H. D. Pasinato, “Velocity and Temperature Dissimilarity in Fully Developed Turbulent Channel and Plane Couette Flows”, *International Journal of Heat and Fluid Flow*, Vol. 32, pp. 11-25, 2011.

- [61] D. A Donzis, K R. Sreenivasan, P. K. Yeung, “Scalar Dissipation Rate and Dissipative Anomaly in Isotropic Turbulence”, *Journal of Fluid Mechanics*, Vol. 532, pp. 199-216, 2005.
- [62] D. A Donzis, P. K. Yeung and K R. Sreenivasan, “Dissipation and Enstrophy in Isotropic Turbulence: Resolution Effects and Scaling in Direct Numerical Simulations”, *Physics of Fluids*, Vol. 20, 2008.
- [63] Z. Warhaft, “Passive Scalars in Turbulent Flows”, *Annual Review Fluid Mechanics*, Vol. 32, pp. 203-240, 2000.
- [64] J. C. Wyngaard, O. R. Cote, “The Evolution of a Convective Planetary Boundary Layer – A Higher Order Closure Model Study”, *Boundary Layer Meteorology*, Vol.7, pp. 289-308, 1974.
- [65] R. Schiestel, “Modeling and Simulation of Turbulent Flows”, John Wiley and Sons Inc., 2008.
- [66] Q.Li, P.Schlatter, L. Brandt, and D. S.Henningson , “DNS of a spatially developing turbulent boundary layer with passive scalar transport”, *Int. J. Heat Fluid Flow*, 30, 916-929, 2009.
- [67] P. Scotti, U. Piomelli, “Turbulence Models in Pulsating Flows”, *AIAA Journal*, Vol. 40, No:3, March 2002.
- [68] M. Marquillie, J. P. Laval, R. Dolganov, “Direct Numerical Simulation of a Separated Channel Flow with a Smooth Profile”, *Journal of Turbulence*, February 5, 2008.

APPENDIX A

USER DEFINED FUNCTION (UDF) USED IN ANSYS FLUENT

/* This UDF is about the calculation of transport equations for the passive scalars t2, ut , vt, ut2, vt2 and specific entropy,s*/

```
#include "udf.h"
#include "mem.h"
#include "math.h"
/* C_UDSI(c,t,0) = t2 */
/* C_UDSI(c,t,1) = ut */
/* C_UDSI(c,t,2) = vt */
/* C_UDSI(c,t,3) = ut2 */
/* C_UDSI(c,t,4) = vt2 */
/* C_UDSI(c,t,5) = s */
DEFINE_ON_DEMAND(entropy)
{
Domain *d;
Thread *t;
cell_t c;
d=Get_Domain(1);
thread_loop_c(t,d)
{
begin_c_loop(c,t)
{
C_UDSI(c,t,6)=C_RUU(c,t);
C_UDSI(c,t,7)=C_RUV(c,t);
C_UDSI(c,t,8)=C_RVV(c,t);
```


$C_UDSI(c,t,9)=C_UDSI(c,t,1)/C_T(c,t); /* ut/T */$
 $C_UDSI(c,t,10)=C_UDSI(c,t,2)/C_T(c,t); /* vt/T */$
 $C_UDSI(c,t,11)=(1/C_T(c,t)); /* 1/T */$
 $C_UDSI(c,t,12)=C_UDSI(c,t,3)/C_T(c,t); /* ut^2/T */$
 $C_UDSI(c,t,13)=C_UDSI(c,t,4)/C_T(c,t); /* vt^2/T */$
 $C_UDSI(c,t,14)=C_UDSI(c,t,0)/C_T(c,t); /* t^2/T */$
 $C_UDSI(c,t,15)=C_UDSI_G(c,t,0)[0];$
 $C_UDSI(c,t,16)=C_UDSI_G(c,t,0)[1];$
 $C_UDSI(c,t,17)=C_UDSI_G(c,t,1)[0];$
 $C_UDSI(c,t,18)=C_UDSI_G(c,t,1)[1];$
 $C_UDSI(c,t,19)=C_UDSI_G(c,t,2)[0];$
 $C_UDSI(c,t,20)=C_UDSI_G(c,t,2)[1];$
 $C_UDSI(c,t,21)=C_UDSI_G(c,t,3)[0];$
 $C_UDSI(c,t,22)=C_UDSI_G(c,t,3)[1];$
 $C_UDSI(c,t,23)=C_UDSI_G(c,t,4)[0];$
 $C_UDSI(c,t,24)=C_UDSI_G(c,t,4)[1];$
 $C_UDSI(c,t,25)=\log(C_T(c,t));$
 $C_UDSI(c,t,26)=C_UDSI_G(c,t,25)[0];$
 $C_UDSI(c,t,27)=C_UDSI_G(c,t,25)[1];$
 $C_UDSI(c,t,28)=C_T_G(c,t)[0];$
 $C_UDSI(c,t,29)=C_T_G(c,t)[1];$
 $C_UDSI(c,t,30)=((C_R(c,t)*C_CP(c,t)/C_K_L(c,t))*C_UDSI(c,t,3))-$
 $C_UDSI_G(c,t,0)[0];$
 $C_UDSI(c,t,31)=((C_R(c,t)*C_CP(c,t)/C_K_L(c,t))*C_UDSI(c,t,4))-$
 $C_UDSI_G(c,t,0)[1];$
 $C_UDSI(c,t,0)=0;$
 $C_UDSI(c,t,1)=0;$
 $C_UDSI(c,t,2)=0;$
 $C_UDSI(c,t,3)=0;$
 $C_UDSI(c,t,4)=0;$
 $C_UDSI(c,t,5)=0;$
 $C_UDSI(c,t,9)=0;$

```

C_UDSI(c,t,10)=0;
C_UDSI(c,t,12)=0;
C_UDSI(c,t,13)=0;
C_UDSI(c,t,14)=0;
C_UDSI(c,t,15)=0;
C_UDSI(c,t,16)=0;
C_UDSI(c,t,17)=0;
C_UDSI(c,t,18)=0;
C_UDSI(c,t,19)=0;
C_UDSI(c,t,20)=0;
C_UDSI(c,t,21)=0;
C_UDSI(c,t,22)=0;
C_UDSI(c,t,23)=0;
C_UDSI(c,t,24)=0;
C_UDSI(c,t,25)=0;
C_UDSI(c,t,26)=0;
C_UDSI(c,t,27)=0;
C_UDSI(c,t,28)=0;
C_UDSI(c,t,29)=0;
C_UDSI(c,t,30)=0;
C_UDSI(c,t,31)=0;
C_UDSI(c,t,32)=0;
}
end_c_loop(c,t)
}
}
/*t2 source*/
DEFINE_SOURCE(t2_src,c,t,dS,eqn)
{
real source;
C_UDSI(c,t,6)=C_RUU(c,t);
C_UDSI(c,t,7)=C_RUV(c,t);

```

```

C_UDSI(c,t,8)=C_RVV(c,t);
C_UDSI(c,t,15)=C_UDSI_G(c,t,0)[0];
C_UDSI(c,t,16)=C_UDSI_G(c,t,0)[1];
/*1st source */
C_UDMI(c,t,0)=-
4*C_R(c,t)*((C_UDSI(c,t,1)*C_T_G(c,t)[0])+(C_UDSI(c,t,2)*C_T_G(c,t)[1]));
/*2nd source */
#define c9 0.5
C_UDMI(c,t,1)=C_R(c,t)*((-
(1/c9)*(C_D(c,t)/C_K(c,t))*C_UDSI(c,t,0))+(2*C_UDSI(c,t,0)*
C_DUDX(c,t)+C_DVDY(c,t)));
/*3rd source */
#define c10 0.2
C_UDMI(c,t,2)=c10*C_R(c,t)*(C_K(c,t)/C_D(c,t))*((C_UDSI_G(c,t,7)[1]*C_UDSI
_G(c,t,0)[0])+(
C_RUV(c,t)*C_UDSI_G(c,t,15)[1])+(C_UDSI_G(c,t,7)[0]*C_UDSI_G(c,t,0)[1])+(
C_RUV(c,t)*
C_UDSI_G(c,t,16)[1]));
C_UDMI(c,t,37)=C_UDMI(c,t,0)+C_UDMI(c,t,1)+C_UDMI(c,t,2);
source=C_UDMI(c,t,37);
dS[eqn]=0.0;
return source;
}
/*t2 diffisuvity*/
DEFINE_ANISOTROPIC_DIFFUSIVITY(t2_aniso_diff,c,t,i,t2_aniso)
{
#define c10 0.2
t2_aniso[0][0]=c10*(C_K(c,t)/C_D(c,t))*C_RUU(c,t);
t2_aniso[1][1]=c10*(C_K(c,t)/C_D(c,t))*C_RVV(c,t);
t2_aniso[0][1]=t2_aniso[1][0]=0.0;
}
/*ut source*/

```

```

DEFINE_SOURCE(ut_src,c,t,dS,eqn)
{
real source;
C_UDSI(c,t,6)=C_RUU(c,t);
C_UDSI(c,t,7)=C_RUV(c,t);
C_UDSI(c,t,8)=C_RVV(c,t);
C_UDSI(c,t,17)=C_UDSI_G(c,t,1)[0];
C_UDSI(c,t,18)=C_UDSI_G(c,t,1)[1];
/*1st source */
#define c6 0.55
C_UDMI(c,t,4)=2*c6*C_R(c,t)*((C_UDSI(c,t,1)*C_DUDX(c,t))+(C_UDSI(c,t,2)*C
_DUDY(c,t)));
/*2nd source */
C_UDMI(c,t,5)=-
2*C_R(c,t)*((C_RUU(c,t)*C_T_G(c,t)[0])+(C_RUV(c,t)*C_T_G(c,t)[1]));
/*3rd source */
#define c7 0.15
C_UDMI(c,t,6)=c7*C_R(c,t)*(C_K(c,t)/C_D(c,t))*((C_UDSI_G(c,t,7)[1]*C_UDSI_
G(c,t,1)[0])+(
C_RUV(c,t)*C_UDSI_G(c,t,17)[1])+(C_UDSI_G(c,t,7)[0]*C_UDSI_G(c,t,1)[1])+(
C_RUV(c,t)*
C_UDSI_G(c,t,18)[1]));
/*4th source */
#define c8 3.5
C_UDMI(c,t,7)=-4*c8*(C_D(c,t)/C_K(c,t))*C_UDSI(c,t,1);
C_UDMI(c,t,38)=C_UDMI(c,t,4)+C_UDMI(c,t,5)+C_UDMI(c,t,6)+C_UDMI(c,t,7);
source=C_UDMI(c,t,38);
dS[eqn]=-((1-c6)*C_DUDX(c,t))-(4*c8*(C_D(c,t)/C_K(c,t)));
return source;
}
/*ut diffisuvity*/
DEFINE_ANISOTROPIC_DIFFUSIVITY(ut_aniso_diff,c,t,i,ut_aniso)

```

```

{
#define c7 0.15
ut_aniso[0][0]=c7*(C_K(c,t)/C_D(c,t))*C_RUU(c,t);
ut_aniso[1][1]=c7*(C_K(c,t)/C_D(c,t))*C_RVV(c,t);
ut_aniso[0][1]=ut_aniso[1][0]=0.0;
}
/*vt source*/
DEFINE_SOURCE(vt_src,c,t,dS,eqn)
{
real source;
C_UDSI(c,t,6)=C_RUU(c,t);
C_UDSI(c,t,7)=C_RUV(c,t);
C_UDSI(c,t,8)=C_RVV(c,t);
C_UDSI(c,t,19)=C_UDSI_G(c,t,2)[0];
C_UDSI(c,t,20)=C_UDSI_G(c,t,2)[1];
/*1st source */
#define c6 0.55
C_UDMI(c,t,8)=2*c6*C_R(c,t)*((C_UDSI(c,t,1)*C_DVDX(c,t))+(C_UDSI(c,t,2)*C
_DVDY(c,t)));
/*2nd source */
C_UDMI(c,t,9)=-
2*C_R(c,t)*((C_RUV(c,t)*C_T_G(c,t)[0])+(C_RVV(c,t)*C_T_G(c,t)[1]));
/*3rd source */
#define c7 0.15
C_UDMI(c,t,10)=c7*C_R(c,t)*(C_K(c,t)/C_D(c,t))*((C_UDSI_G(c,t,7)[1]*C_UDSI
_G(c,t,2)[0])+(
C_RUV(c,t)*C_UDSI_G(c,t,19)[1])+(C_UDSI_G(c,t,7)[0]*C_UDSI_G(c,t,2)[1])+(
C_RUV(c,t)*
C_UDSI_G(c,t,20)[1]));
/*4th source */
#define c8 3.5
C_UDMI(c,t,11)=-4*c8*(C_D(c,t)/C_K(c,t))*C_UDSI(c,t,2);

```

```

C_UDMI(c,t,39)=C_UDMI(c,t,8)+C_UDMI(c,t,9)+C_UDMI(c,t,10)+C_UDMI(c,t,1
1);
source=C_UDMI(c,t,39);
dS[eqn]=0.0;
return source;
}
/*vt diffusivity*/
DEFINE_ANISOTROPIC_DIFFUSIVITY(vt_aniso_diff,c,t,i,vt_aniso)
{
#define c7 0.15
vt_aniso[0][0]=c7*(C_K(c,t)/C_D(c,t))*C_RUU(c,t);
vt_aniso[1][1]=c7*(C_K(c,t)/C_D(c,t))*C_RVV(c,t);
vt_aniso[0][1]=vt_aniso[1][0]=0.0;
}
/*ut2 source*/
DEFINE_SOURCE(ut2_src,c,t,dS,eqn)
{
real source;
C_UDSI(c,t,6)=C_RUU(c,t);
C_UDSI(c,t,7)=C_RUV(c,t);
C_UDSI(c,t,8)=C_RVV(c,t);
C_UDSI(c,t,21)=C_UDSI_G(c,t,3)[0];
C_UDSI(c,t,22)=C_UDSI_G(c,t,3)[1];
/*1st source */
C_UDMI(c,t,12)=2*C_R(c,t)*(C_UDSI(c,t,3)*C_DVDY(c,t)-
C_UDSI(c,t,4)*C_DUDY(c,t));
/*C_UDMI(c,t,12)=0; */
/*2nd source */
#define c3 3.0
C_UDMI(c,t,13)=-4*c3*(C_D(c,t)/C_K(c,t))*C_UDSI(c,t,3);
/*3rd source */
#define c1 0.15

```

```

C_UDMI(c,t,14)=2*c1*C_R(c,t)*(C_K(c,t)/C_D(c,t))*((C_RUU(c,t)*C_UDSI_G(c,
t,1)[0]*C_T_G(c,t)[0])+(C_RUV(c,t)*C_UDSI_G(c,t,1)[1]*C_T_G(c,t)[0])+(C_RU
V(c,t)*C_UDSI_G(c,t,1)[0]*C_T_G
(c,t)[1])+(C_RVV(c,t)*C_UDSI_G(c,t,1)[1]*C_T_G(c,t)[1]));
/*4th source */
#define c2 0.15
C_UDMI(c,t,15)=c2*C_R(c,t)*(C_K(c,t)/C_D(c,t))*((C_UDSI_G(c,t,7)[0]*C_UDSI
_G(c,t,3)[1])+(
C_RUV(c,t)*C_UDSI_G(c,t,22)[0])+(C_UDSI_G(c,t,7)[1]*C_UDSI_G(c,t,3)[0])+(
C_RUV(c,t)*
C_UDSI_G(c,t,21)[1]));
/*C_UDMI(c,t,15)=0;*/
C_UDMI(c,t,40)=C_UDMI(c,t,12)+C_UDMI(c,t,13)+C_UDMI(c,t,14)+C_UDMI(c,
t,15);
source=C_UDMI(c,t,40);
dS[eqn]=0.0;
return source;
}
/*ut2 diffisuvity*/
DEFINE_ANISOTROPIC_DIFFUSIVITY(ut2_aniso_diff,c,t,i,ut2_aniso)
{
#define c2 0.15
ut2_aniso[0][0]=c2*(C_K(c,t)/C_D(c,t))*C_RUU(c,t);
ut2_aniso[1][1]=c2*(C_K(c,t)/C_D(c,t))*C_RVV(c,t);
ut2_aniso[0][1]=ut2_aniso[1][0]=0.0;
}
/*vt2 source*/
DEFINE_SOURCE(vt2_src,c,t,dS,eqn)
{
real source;
C_UDSI(c,t,6)=C_RUU(c,t);
C_UDSI(c,t,7)=C_RUV(c,t);

```

```

C_UDSI(c,t,8)=C_RVV(c,t);
C_UDSI(c,t,23)=C_UDSI_G(c,t,4)[0];
C_UDSI(c,t,24)=C_UDSI_G(c,t,4)[1];
/* 1st source */
C_UDMI(c,t,16)=2*C_R(c,t)*(C_UDSI(c,t,4)*C_DUDX(c,t)-
C_UDSI(c,t,3)*C_DVDX(c,t));
/*C_UDMI(c,t,16)=0; */
/* 2nd source */
#define c3 3.0
C_UDMI(c,t,17)=-4*c3*(C_D(c,t)/C_K(c,t))*C_UDSI(c,t,4);
/* 3rd source */
#define c1 0.15
C_UDMI(c,t,18)=2*c1*C_R(c,t)*(C_K(c,t)/C_D(c,t))*((C_RUU(c,t)*C_UDSI_G(c,
t,2)[0]*C_T_G(c,
t)[0])+(C_RUV(c,t)*C_UDSI_G(c,t,2)[1]*C_T_G(c,t)[0])+(C_RUV(c,t)*C_UDSI_
G(c,t,2)[0]*C_T_G
(c,t)[1])+(C_RVV(c,t)*C_UDSI_G(c,t,2)[1]*C_T_G(c,t)[1]));
/* 4th source */
#define c2 0.3
C_UDMI(c,t,19)=c2*C_R(c,t)*(C_K(c,t)/C_D(c,t))*((C_UDSI_G(c,t,7)[0]*C_UDSI
_G(c,t,4)[1])+(
C_RUV(c,t)*C_UDSI_G(c,t,24)[0])+(C_UDSI_G(c,t,7)[1]*C_UDSI_G(c,t,4)[0])+(
C_RUV(c,t)*
C_UDSI_G(c,t,23)[1]));
/*C_UDMI(c,t,19)=0; */
C_UDMI(c,t,41)=C_UDMI(c,t,16)+C_UDMI(c,t,17)+C_UDMI(c,t,18)+C_UDMI(c,
t,19);
source=C_UDMI(c,t,41);
dS[eqn]=0.0;
return source;
}
/*vt2 diffisuvity*/

```



```

DEFINE_ANISOTROPIC_DIFFUSIVITY(vt2_aniso_diff,c,t,i,vt2_aniso)
{
#define c2 0.15
vt2_aniso[0][0]=c2*(C_K(c,t)/C_D(c,t))*C_RUU(c,t);
vt2_aniso[1][1]=c2*(C_K(c,t)/C_D(c,t))*C_RVV(c,t);
vt2_aniso[0][1]=vt2_aniso[1][0]=0.0;
}
/*direct entropy source*/
DEFINE_SOURCE(entropy_src,c,t,dS,eqn)
{
real source;
real prt=0.7;
C_UDSI(c,t,11)=(1/C_T(c,t));
C_UDSI(c,t,26)=C_UDSI_G(c,t,25)[0];
C_UDSI(c,t,27)=C_UDSI_G(c,t,25)[1];
C_UDSI(c,t,9)=C_UDSI(c,t,1)/C_T(c,t); /* ut/T */
C_UDSI(c,t,10)=C_UDSI(c,t,2)/C_T(c,t); /* vt/T */
C_UDSI(c,t,28)=C_T_G(c,t)[0];
C_UDSI(c,t,29)=C_T_G(c,t)[1];
C_UDSI(c,t,30)=((C_R(c,t)*C_CP(c,t)/C_K_L(c,t))*C_UDSI(c,t,3))-
C_UDSI_G(c,t,0)[0];
C_UDSI(c,t,31)=((C_R(c,t)*C_CP(c,t)/C_K_L(c,t))*C_UDSI(c,t,4))-
C_UDSI_G(c,t,0)[1];
/*1st RHS term*/
/*C_UDMI(c,t,20)=(-
2*C_R(c,t)/C_T(c,t))*(C_UDSI(c,t,1)*C_UDSI_G(c,t,5)[0]+C_UDSI(c,t,2
)*C_UDSI_G(c,t,5)[1]);
*/
C_UDMI(c,t,20)=2*C_K_T(c,t,prt)*((pow(C_T_G(c,t)[0],2))+((pow(C_T_G(c,t)[1],2
)));
/*2nd RHS term*/
/*C_UDMI(c,t,21)=2*C_K_L(c,t)*(((C_UDSI_G(c,t,11)[0]*C_T_G(c,t)[0])+((1/C_

```

```

T(c,t))*C_UD
SI_G(c,t,28)[0]))+((C_UDSI_G(c,t,11)[1]*C_T_G(c,t)[1])+((1/C_T(c,t))*C_UDSI_
G(c,t,29)[
1]]));
*/
C_UDMI(c,t,21)=0.0;
/*3rd RHS term*/
C_UDMI(c,t,22)=(2*C_K_L(c,t)/(pow(C_T(c,t),2)))*((C_T_G(c,t)[0]*C_T_G(c,t)[0]
))+C_T_G
(c,t)[1]*C_T_G(c,t)[1]));
/*4th RHS term*/
/*4a*/
C_UDMI(c,t,23)=(C_K_L(c,t)/C_T(c,t))*((C_UDSI_G(c,t,11)[0]*C_UDSI_G(c,t,1)[
0]))+(
C_UDSI_G(c,t,11)[1]*C_UDSI_G(c,t,1)[1]));
/*4b*/
C_UDMI(c,t,24)=(C_K_L(c,t)/(C_T(c,t)*C_T(c,t)))*((C_UDSI_G(c,t,30)[0]-
(2*(C_R(c,t)*
C_CP(c,t)/C_K_L(c,t))*C_UDSI(c,t,1)*C_T_G(c,t)[0])-
((C_R(c,t)*C_CP(c,t)/C_K_L(c,t))*
C_U(c,t)*C_UDSI_G(c,t,0)[0]))+(C_UDSI_G(c,t,31)[1]-
(2*(C_R(c,t)*C_CP(c,t)/C_K_L(c,t
)))*C_UDSI(c,t,2)*C_T_G(c,t)[1]-
((C_R(c,t)*C_CP(c,t)/C_K_L(c,t))*C_V(c,t)*C_UDSI_G(c,
t,0)[1]]));
/*5th RHS term*/
C_UDMI(c,t,25)=(C_MU_L(c,t)/C_T(c,t))*((C_DUDY(c,t)*(C_DUDY(c,t)+C_DV
DX(c,t)))+(
C_DVDX(c,t)*(C_DVDX(c,t)+C_DUDY(c,t)))+(2*C_DUDX(c,t)*C_DUDX(c,t)))+(
2*C_DVDY(c,t)*
C_DVDY(c,t)));
/*6th RHS term*/

```

```

C_UDMI(c,t,26)=4*C_R(c,t)*(C_D(c,t)/C_T(c,t));
/*7th RHS term*/
C_UDMI(c,t,27)=(-
2*(C_R(c,t)*C_CP(c,t)/C_T(c,t))*(((C_U(c,t)/(2*C_T(c,t)))*C_UDSI_G(
c,t,0)[0])+(C_UDSI(c,t,0)*C_UDSI_G(c,t,11)[0])+(C_V(c,t)/(2*C_T(c,t)))*C_UDS
I_G(c,t,
0)[1])+(C_UDSI(c,t,0)*C_UDSI_G(c,t,11)[1]));
/*8th RHS term*/
C_UDMI(c,t,28)=(-
2*(C_R(c,t)*C_CP(c,t)/C_T(c,t))*(((C_UDSI(c,t,3)*C_UDSI_G(c,t,11)[0
])+(0.5/C_T(c,t)*C_UDSI_G(c,t,3)[0]))+(C_UDSI(c,t,4)*C_UDSI_G(c,t,11)[1])+(
(0.5/C_T
(c,t)*C_UDSI_G(c,t,4)[1]));
/*9th RHS term*/
/*C_UDMI(c,t,29)=((C_K_L(c,t)/(C_T(c,t)*C_T(c,t)))*C_UDSI_G(c,t,0)[0])+(2*C
_K_L(c,t)/
C_T(c,t)*C_UDSI(c,t,0)*C_UDSI_G(c,t,11)[0])+(C_K_L(c,t)/(C_T(c,t)*C_T(c,t))
*C_UDSI_
G(c,t,0)[1])+(2*C_K_L(c,t)/C_T(c,t)*C_UDSI(c,t,0)*C_UDSI_G(c,t,11)[1]);
*/
C_UDMI(c,t,29)=0.0;
C_UDMI(c,t,30)=C_UDMI(c,t,20)+C_UDMI(c,t,21)+C_UDMI(c,t,22)+C_UDMI(c,
t,23)+C_UDMI(c,t
,24)+C_UDMI(c,t,25)+C_UDMI(c,t,26)+C_UDMI(c,t,27)+C_UDMI(c,t,28)+C_UD
MI(c,t,29);
/*C_UDMI(c,t,5)=150000000; */
source=C_UDMI(c,t,30);
dS[eqn]=0.0;
return source;
}
/*direct entropy diffusivity*/
DEFINE_ANISOTROPIC_DIFFUSIVITY(entropy_diff,c,t,i,entropy_aniso)

```

```

{
real prt=0.7;
entropy_aniso[0][0]=(C_K_T(c,t,prt)+C_K_L(c,t))/C_CP(c,t);
entropy_aniso[1][1]=(C_K_T(c,t,prt)+C_K_L(c,t))/C_CP(c,t);
entropy_aniso[0][1]=entropy_aniso[1][0]=0.0;
}
/*DEFINE_DIFFUSIVITY(entropy_diff,c,t,i)
{
real prt=0.7;
return (C_K_T(c,t,prt)+C_K_L(c,t))/C_CP(c,t);
}
*/
/*indirect entropy source*/
DEFINE_SOURCE(indir_entropy_src,c,t,dS,eqn)
{
real source;
/*3rd RHS term*/
C_UDMI(c,t,31)=(2*C_K_L(c,t)/(pow(C_T(c,t),2))*((C_T_G(c,t)[0]*C_T_G(c,t)[0]
)+C_T_G(c,t)[1]
]*C_T_G(c,t)[1]));
/*5th RHS term*/
C_UDMI(c,t,32)=(C_MU_L(c,t)/C_T(c,t))*((C_DUDY(c,t)*(C_DUDY(c,t)+C_DV
DX(c,t)))+(C_DVDX(c,t)*(
C_DVDX(c,t)+C_DUDY(c,t)))+(2*C_DUDX(c,t)*C_DUDX(c,t))+(2*C_DVDY(c,t
)*C_DVDY(c,t)));
C_UDMI(c,t,33)=C_UDMI(c,t,31)+C_UDMI(c,t,32);
source=C_UDMI(c,t,33);
dS[eqn]=0.0;
return source;
}
/*indirect entropy diffisuvity*/
DEFINE_ANISOTROPIC_DIFFUSIVITY(indir_entropy_diff,c,t,i,indir_entropy_ani

```

```

so)
{
/*real prt=0.7;*/
/*
indir_entropy_aniso[0][0]=(C_K_T(c,t,prt)+C_K_L(c,t))/C_CP(c,t);
indir_entropy_aniso[1][1]=(C_K_T(c,t,prt)+C_K_L(c,t))/C_CP(c,t);
*/
indir_entropy_aniso[0][0]=C_K_L(c,t)/C_CP(c,t);
indir_entropy_aniso[1][1]=C_K_L(c,t)/C_CP(c,t);
indir_entropy_aniso[0][1]=indir_entropy_aniso[1][0]=0.0;
}
/*
DEFINE_DIFFUSIVITY(indir_entropy_diff,c,t,i)
{
real prt=0.7;
return (C_K_T(c,t,prt)+C_K_L(c,t))/C_CP(c,t);
}
*/

```

CURRICULUM VITAE

PERSONAL INFORMATION

Surname, Name: Orhan, Ömer Emre

Nationality: Turkish (TC)

Date and Place of Birth: 28 February 1981, Ankara

Marital Status: Single

Phone: +90 532 587 60 38

email: omer.emreorhan@gmail.com

EDUCATION

Degree	Institution	Year of Graduation
MS METU	Mechanical Engineering	2007
BS METU	Mechanical Engineering	2004
High School	Eskişehir Science High School	1999

WORK EXPERIENCE

Year	Place	Enrollment
2012- Present	Borusan EnBW Energy	Wind Engineering Man.
2010-2012	Fichtner GmbH	Wind Team Leader
2007-2009	Alstom Hydro Power	Tendering Engineer
2004-2007	Aselsan MGEO	Design Engineer

FOREIGN LANGUAGES

Advanced English, Spanish; Intermediate German

PUBLICATIONS

1. Orhan, Ö.E., Uzol O., "Direct Calculation of Entropy Generation by Solving Reynolds-Averaged Entropy Transport Equation in an Air-Cooled Turbine Cascade", ASME Turbo Expo, June 11-15, 2012, Copenhagen, Denmark.
2. Orhan, Ö.E., Uzol O., " Comparison of entropy generation figures using entropy maps and entropy transport equation for an air cooled gas turbine blade", ECOS Conference, June 26-29, 2012, Perugia, Italy.

HOBBIES

Tennis, Motorcycles, Outdoor sports